

**HABILITATIONSSCHRIFT**

**Philosophisch–naturwissenschaftliche Fakultät  
der Universität Bern**

**Global Navigation Satellite Systems:  
A Tool to Observe the System Earth**

Rolf Dach

Oktober 2010

Astronomisches Institut der Universität Bern



# Contents

<b>1</b>	<b>Introduction</b>	<b>1</b>
1.1	Activities at GNSS–Research Group of AIUB . . . . .	2
1.2	Overview at the <i>Habilitationsschrift</i> . . . . .	3
1.3	Acknowledgments . . . . .	6
1.4	References . . . . .	7
<b>2</b>	<b>Analysis of GPS data from an Antarctic Ice Stream</b>	<b>9</b>
2.1	Introduction . . . . .	9
2.2	Description of the Dataset . . . . .	10
2.3	GPS Data Processing . . . . .	13
2.3.1	Connection to the ITRF . . . . .	13
2.3.2	Local Network on the Ice Stream . . . . .	14
2.4	Intercomparison of Kinematic Solutions . . . . .	15
2.4.1	Expectation from Theory . . . . .	15
2.4.2	Differences in the Results . . . . .	15
2.4.3	Day Boundary Discontinuities . . . . .	16
2.4.4	Allan Deviation . . . . .	17
2.4.5	Investigating the Vertical Component . . . . .	19
2.5	Summary . . . . .	21
2.6	References . . . . .	22
<b>3</b>	<b>GNSS Processing at CODE: Status Report</b>	<b>25</b>
3.1	Introduction . . . . .	26
3.2	GNSS Orbit Determination . . . . .	27
3.2.1	The GNSS Subnetwork of the IGS . . . . .	27
3.2.2	Radiation Pressure Modelling . . . . .	29
3.2.3	GLONASS Orbit Determination . . . . .	32
3.2.4	Handling of GPS Repositioning Events . . . . .	34
3.3	Comparing GPS–only and multi–GNSS Solutions . . . . .	35
3.3.1	GPS and GLONASS Orbit Characteristics . . . . .	35
3.3.2	Benefit of the Combined GNSS Products on Navigation and Rapid Positioning . . . . .	37
3.3.3	Impact of GLONASS on the CODE Global Products . . . . .	42
3.4	GNSS Applications using the Swiss AGNES Network . . . . .	43
3.5	Summary . . . . .	45
3.6	References . . . . .	47
<b>4</b>	<b>Improved antenna phase center models for GLONASS</b>	<b>49</b>
4.1	Introduction . . . . .	50

4.2	Reprocessing of GLONASS data at CODE . . . . .	51
4.3	GNSS-specific receiver antenna phase center modeling . . . . .	53
4.3.1	Update of the igs05.atx phase center model . . . . .	55
4.3.2	Use of GNSS-specific phase center corrections . . . . .	56
4.4	Satellite antenna phase center modeling . . . . .	59
4.4.1	Motivation . . . . .	59
4.4.2	Computation of the satellite antenna model update . . . . .	60
4.4.3	Update of the satellite antenna phase center offsets . . . . .	60
4.4.4	Update of the satellite antenna phase center variations . . . . .	63
4.5	Validation of the satellite antenna phase center models . . . . .	66
4.5.1	Impact of the updated antenna phase center model on the GLONASS satellite orbits . . . . .	66
4.5.2	Validating the GLONASS orbits using SLR data . . . . .	68
4.5.3	Impact of the updated satellite antenna phase center model on station coordinates . . . . .	69
4.5.4	Impact of the updated antenna phase center model on kinematic positioning . . . . .	69
4.6	Summary and conclusions . . . . .	73
4.7	References . . . . .	74
<b>5</b>	<b>Combining the Observations from Different GNSS</b>	<b>77</b>
5.1	Introduction and Motivation . . . . .	78
5.2	Analysis strategy and receiver statistics . . . . .	80
5.3	Inter-system biases and their impact on the solution . . . . .	81
5.3.1	Stability of the inter-system bias in time . . . . .	81
5.3.2	Inter-system bias in the RMS of the post-fit residuals . . . . .	83
5.3.3	Influence of inter-system bias on station coordinate solutions . . . . .	85
5.3.4	Influence of inter-system bias on rapid-static positioning . . . . .	87
5.4	Impact of the inter-system bias on ambiguity resolution . . . . .	87
5.5	Summary . . . . .	91
5.6	References . . . . .	92
<b>6</b>	<b>Evaluation of the Impact of Atmospheric Pressure Loading Modeling on GNSS Data Analysis</b>	<b>93</b>
6.1	Introduction . . . . .	94
6.2	Data sets . . . . .	96
6.2.1	GNSS solution . . . . .	96
6.2.2	Time series of atmospheric pressure loading corrections . . . . .	97
6.3	Atmospheric pressure loading and coordinate time series . . . . .	100
6.3.1	Comparisons based on weekly GNSS solutions . . . . .	100
6.3.2	Comparisons by direct estimation of scaling factors . . . . .	101
6.4	Atmospheric pressure loading corrections based on local pressure time series . . . . .	106
6.4.1	Comparison of APL corrections with local pressure data . . . . .	107
6.4.2	Regression factors from GNSS data analysis . . . . .	110
6.5	Effects seen in the repeatability of station coordinates . . . . .	112
6.6	Influence of APL on Global Parameters . . . . .	114

6.6.1	Influence on Geodetic Datum Definition . . . . .	114
6.6.2	Influence on GNSS-Satellite Orbits . . . . .	115
6.7	Summary . . . . .	117
6.8	References . . . . .	118
<b>7</b>	<b>Continuous Geodetic Time Transfer Analysis Methods</b>	<b>123</b>
7.1	Introduction . . . . .	124
7.2	Theoretical Background . . . . .	125
7.3	Preprocessing: code and phase consistency . . . . .	127
7.3.1	Detection and Corrective Action . . . . .	127
7.3.2	Multipath Effects . . . . .	128
7.3.3	Classification and Example . . . . .	128
7.3.4	Consequences for GPS CP Time and Frequency Transfer . . . . .	130
7.4	Methods for Continuous Time Transfer Series . . . . .	131
7.4.1	Clock Hand-over . . . . .	132
7.4.2	Ambiguity Stacking . . . . .	134
7.4.3	Comparison . . . . .	136
7.5	Summary and Conclusions . . . . .	139
7.6	References . . . . .	140



# 1 Introduction

In 1980 the US Department of Defense successfully launched the first Block I satellite of the Global Positioning System (GPS). Nobody thought at that time that this was also the starting point for one of the biggest revolutions in space geodesy. Thanks to the open use of GPS for civilian purpose and the development in the receiving and analysis technology the user community — even with high accuracy requirements — is continuously growing.

Apart from the American system a corresponding Global Navigation Satellite System (GNSS) has been developed by the Soviet Union and it is now maintained by the Russian Federation: GLONASS, ГЛОБАЛЬНАЯ НАВИГАЦИОННАЯ СПУТНИКОВАЯ СИСТЕМА (Russian for “Global Navigation Satellite System”). Currently, the European Space Agency (ESA) together with the European Union (EU) is building up an independent European system, named Galileo. The Peoples Republic of China also develops a GNSS called Beidou (Compass). These global systems will be complemented by regional systems, the Japanese QZSS (Quasi-Zenith Satellite System) being best known and most advanced example.

Because the two established GNSS, GPS and GLONASS, are modernizing their systems, many new signals and new systems are expected in near future. Today we are stepping from a single dual-frequency system to a multi-GNSS world with many frequencies and signals. It is a challenging task for the future to get the optimal benefit from this variety of GNSS-signals.

This *Habilitationsschrift* reflects the current situation with two operational GNSS supporting each two frequencies. This situation allows already for many high-end applications. The already achieved performance of GNSS analysis on the centimeter level or better asks for a continuous improvement of the processing models and equipment calibration, which are the limiting factors today.

The work was performed in the environment of the GNSS research group of the Astronomical Institute of the University of Bern. the maintenance and development of CODE, the Center for Orbit Determination in Europe, one of the global analysis centers of the International GNSS Service (IGS) is a core activity of the group. CODE is a joint venture of the Astronomical Institute of the University of Bern (AIUB, Bern, Switzerland), the Swiss Federal Office of Topography (swisstopo, Wabern, Switzerland), the Federal Agency for Cartography and Geodesy (BKG, Frankfurt am Main, Germany), and the Institut für Astronomische und Physikalische Geodäsie of the Technische Universität München (IAPG/TUM, Munich, Germany). The operational computations of CODE are performed at the AIUB since the first IGS test campaign in June 1992.

The IGS is a service of the International Association of Geodesy (IAG) to support the scientific use of GNSS. More than 200 international institutions provide GNSS tracking data on the best effort basis, which are collected in regional and global data centers. Analysis centers, like CODE, use these data to generate numerous of products, which are compared and combined to official IGS products and made available to the interested user community free of charge. It is important to note that the results presented in this *Habilitationsschrift* could not have been generated without the IGS infrastructure, the data from the global IGS tracking network, and the IGS products (generated to a significant extend by CODE).

## 1.1 Activities at GNSS–Research Group of AIUB

The activities of the GNSS research group of the AIUB are based on four pillars, which are closely connected:

### **Activities in the frame of CODE for the IGS:**

Chapter 3 provides a status report on the multi–GNSS activities at CODE. For many years CODE was the only analysis center of the IGS applying a rigorously combined processing of GPS and GLONASS measurements to generate operational products. More and more analysis centers follow this approach today (Springer and Dach, 2010).

CODE does not only contribute to the operational products of the IGS but also to “auxiliary” products, like the estimation of GNSS antenna calibration models (presented in Chapter 4) or the determination and maintenance of several GNSS measurement biases (Dach et al., 2010; Schaer and Dach, 2010).

*Selected references:* Dach et al. (2008); Bock et al. (2009); Dach et al. (2006)

These IGS–related activities allow the group to contribute to other projects based on the experience in multi–GNSS processing (e.g., GGSP, Galileo Geodetic Service Provider Prototype, to build up the geodetic basement for Galileo in a consortium of seven international partners, Gendt et al., 2010) or to support other user communities with the knowledge on precise and operational GNSS analysis for their applications (e.g., to provide very precise geodetic time and frequency transfer to the timing community, Bauch et al., 2006).

### **Precise orbit determination for LEO satellites and gravity field recovery:**

Many Low Earth Orbiting satellites (LEO) are equipped with GPS receivers. This allows for a reduced–dynamic or even a purely kinematic determination of the satellite orbit. The kinematic solution is of particular interest for gravity field recovery by analyzing the satellites trajectory, because it is free of any a priori gravity fields.

*Selected references:* Jäggi et al. (2009); Prange et al. (2010)

**Analysis of SLR measurements to GNSS and geodetic satellites:**

The capability to process microwave and optical (SLR, Satellite Laser Ranging) measurements to GNSS satellites within one and the same analysis environment offers an unique opportunity to tie the two space geodetic techniques not only on ground stations via local ties at a limited number of sites supporting both techniques. The orbit parameters for the GNSS satellites observed by SLR are common parameters connecting solutions from both techniques. These common orbit parameters help to transfer the scale from the SLR to the GNSS solution. The combined analysis is also interesting for assessing the center of mass by a combined processing of the GNSS satellites with geodetic SLR satellites (like LAGEOS).

*Selected reference:* Thaller et al. (2010)

**Development of the Bernese GPS Software:**

This software package is used for all activities mentioned and is therefore the connecting link between all activities. It is maintained and developed in the GNSS research group of the AIUB since 25 years.

*Selected references:* Dach et al. (2007); Ostini et al. (2008); Meindl et al. (2008)

Most of the results and studies presented subsequently are related to the multi-GNSS activities from CODE (first of the four pillars). This is a consequence of the author's main research activities in the preceding ten years. The position as the head of the GNSS research group implies least contributions (supervision and consulting) to the other GNSS-related research topics at the AIUB as well.

## 1.2 Overview at the *Habilitationsschrift*

The *Habilitationsschrift* consists of six research contributions published in refereed international journals (all are accepted, two of them are still "in print") and symposium series (one).

Chapter 2 devoted to an investigation of the influence of different analysis methods of GNSS data on the results. It analyzes kinematic GPS data from a station located on an Antarctic ice stream. Kinematic positions are very sensitive to processing strategies, because of the low redundancy of the estimated parameters. The results demonstrate the equivalence of the double-difference (with correctly considered correlations) processing strategy and the processing of the original, undifferenced measurements (zero-difference processing). The analysis also shows the differences between a zero-difference network solution and the Precise Point Positioning (PPP) approach. The expected degradation of the PPP solution by switching from an internally (from the fully consistent zero-difference) to an externally (e.g., from the IGS) generated set of satellite orbit and clock corrections is confirmed. It is a key conclusion of this

study that resolving phase ambiguities to their correct integer values is beneficial for the GNSS solution. The epoch-to-epoch (short term) stability of the obtained kinematic trajectory is, on the other hand, dominated by the noise characteristics of the observations and cannot profit from the ambiguity resolution.

Chapter 3 provides a general overview of the multi-GNSS activities at the CODE analysis center for the IGS. It consists of three parts. The first part reviews important orbit modeling aspects at the CODE analysis center: an update of the radiation pressure model parameters (as initially defined by Springer et al., 1999) and the extension of the model for GLONASS satellites. It also describes the handling of the repositioning events of GPS satellites in the operational CODE processing. The focus of this part is on the development of the GLONASS tracking capability of the IGS network and its impact on the GLONASS orbit quality. The second part of the Chapter compares the orbit characteristics of the GPS and GLONASS constellations and studies the impact of adding the GLONASS measurements to a GPS-only solution. The conclusion is that kinematic positions and other parameters with a short validity interval in the GNSS solution can benefit from the additional observations provided by the alternative GNSS. Global parameters with a long validity interval (e.g., reference frame parameters) are not affected by adding GLONASS to a GPS-only solution. Multi-GNSS solutions are, nevertheless, preferable because both GNSS have different implicit orbital/constellation frequencies. The third part discusses the extension from a GPS-only to a combined GPS/GLONASS processing scheme from the perspective of a local network processing as it is done, e.g., for the AGNES (Automated GNSS Network for Switzerland) at swisstopo.

To get the optimum benefit from the inclusion of GLONASS to a GNSS solution, the system-specific calibration values for GLONASS need to be known with the same accuracy as for GPS. Chapter 4 discusses the aspect of GNSS receiver and satellite antenna phase center modeling. Because GPS and GLONASS have different signal structures and frequencies, the behavior of the receiver antenna is expected to be different for each GNSS. Geo++ is a private company in Germany supporting the IGS with receiver antenna models from robot calibrations. For this study, the IGS standard receiver antenna model has updated the standard GPS-derived calibration results by system-specific corrections. Their impact on a global multi-GNSS solution is discussed in the first part of Ch. 4. In the second part a satellite antenna phase center model for GLONASS is developed which should be fully consistent with the well-established GPS satellite phase center model used within the IGS. Last but not least the influence the updated antenna phase center modeling for receiver and satellite antennas on different products is validated. The result of Ch. 4 represents the work is the CODE contribution to the igs08.atx antenna model. Dilssner et al. (2010) published a comparison with independently generated results (by the CODE and ESOC AC groups) showing a high consistency level for the GLONASS satellite antenna phase center model.

Chapter 5 discusses a general problem when combining the observations from different GNSS. Due to the different structure and frequencies of the signals from the individual systems one expects an inter-system bias in the receiver. Depending on the stabil-

ity of this bias in time different assumptions are necessary in the multi-GNSS data processing:

- Independent receiver clocks for each GNSS do not pose any requirements on the stability of the inter-system bias, but this approach introduces a big number of additional parameters weakening the solution.
- One inter-system bias per processing interval requires the stability of the bias on the noise level of the phase measurements ( $1 \text{ mm} \approx 3 \text{ ps}$ ). It is an advantage that only one parameter needs to be added to the solution.

The behavior of different currently used receiver types is assessed by using a limited number of local networks within the IGS consisting of two or three stations each. It turns out that a compromise between the two mentioned strategies provides the best results: piece-wise linear inter-system bias parameter for the phase measurements allow for a certain variation in time of the bias but introduce only a limited number of additional parameters. Many of the stations analyzed did, however, not require a high resolution in time.

Chapter 6 represents a mixture of application and improvement of GNSS modeling. The time series of station coordinates from the CODE reprocessing effort (Steigenberger et al., 2009) is compared to displacement corrections provided by a geophysical atmospheric pressure loading model. The strategy to apply the corrections to the weekly mean coordinates after the data processing was compared to that of directly correcting the measurements during the GNSS data analysis. Scaling factors between the geophysical model and the variation of the station position as additional “validation parameter” in the GNSS analysis have been estimated and interpreted. Using these scaling factors the atmospheric loading model has been confirmed by the GNSS solution within the expected uncertainty level. The conclusion of this study is that it is necessary to include this geophysical phenomenon in the GNSS data processing scheme. There are several arguments to apply the corrections for atmospheric pressure loading directly to the observations during the data processing — even if the corrections cannot be removed or exchanged anymore after the analysis.

Chapter 7 is related to an activity of the author before he became the head of the GNSS research group, namely geodetic time and frequency transfer. Solving for the receiver clock in a GNSS carrier phase analysis introduces an one-by-one correlation of the simultaneous estimation of the receiver clock corrections and ambiguity parameters (both are linear dependent parameters). The problem arises if the ambiguities of all satellites in view are interrupted either due to a loss of lock of the signal, a receiver problem, or due to creation a processing batches. If only the phase measurements are used in the processing, the time series of clock differences start with new initial offsets after each interrupt. If the pseudorange observations are included in the processing, the size of the discontinuities depends on the noise behavior of these measurements caused by the quality of the equipment and the environmental conditions. Chapter 7 proposes two methods to mitigate discontinuities on the normal equation level:

- *Clock Hand-Over*: includes a common epoch in two consecutive solutions

- *Ambiguity Stacking*: re-connects the ambiguity parameter between independently processed data pieces

The first approach is simple but depends on the availability of the observations of one single epoch. The second approach is the natural one, because the ambiguity parameter from the continuously tracked satellites was artificially interrupted by introducing processing batches — but the implementation of this algorithm is much more involved than for the first one. Both algorithms lead to continuous series of clock comparisons. Any data problem related to the consistency of the code and phase measurements will thus propagate into the complete solution time series. Therefore, an extensive comparison of the internal receiver clock corrections computed from the code and the phase observations respectively is included.

The six chapters of this *Habilitationsschrift* provide an overview on the wide range of state-of-the-art GNSS processing activities from the principle of data processing algorithms (Chapter 2) to modeling (Chapter 3) and calibration (Chapters 4 and 5). It also includes the aspects of combined processing of GNSS measurements from different systems (Chapters 3 to 5). From the wide range of scientific GNSS-based high-end applications two examples from geodynamics (Chapter 6) and for geodetic time and frequency transfer (Chapter 7) are presented.

### 1.3 Acknowledgments

First of all I would like to thank my wife and children for their patience and for tolerating many absences. It should not be seen as granted that the husband and father is allowed to spend so much time on an *Habilitationsschrift*.

I would like to thank all my colleagues from the GNSS research group at the AIUB and at other institutions for the valuable contributions. This aspect is acknowledged by including the complete list of authors for each chapter.

I am very grateful for the continuous support of Prof. Gerhard Beutler. He tried to allow me and my team the biggest possible freedom in the scientific work.

Last but not least I would like to thank all my excellent colleagues of the GNSS research group of the AIUB for their outstanding daily work for CODE and many other research activities of the group. The gratitude includes also the external partners of the CODE consortium for the very fruitful collaboration going much behind a pure financial support of the activities in the frame of CODE.

## 1.4 References

- Bauch, A., J. Achkar, S. Bize, D. Calonico, R. Dach, R. Hlavac, L. Lorini, T. Parker, G. Petit, D. Piester, K. Szymaniec, and P. Urich (2006). Comparison between frequency standards in Europe and the USA at the  $10^{-15}$  uncertainty level. *Metrologia*, 43(1):109–120, DOI 10.1088/0026-1394/43/1/016.
- Bock, H., R. Dach, A. Jäggi, and G. Beutler (2009). High-rate GPS clock corrections from CODE: support of 1 Hz applications. *Journal of Geodesy*, 83(11):1083–1094, DOI 10.1007/s00190-009-0326-1.
- Dach, R., S. Schaer, U. Hugentobler, and T. Schildknecht (2006). Combined Multi-System GNSS Analysis for Time and Frequency Transfer. In *Proceedings 20<sup>th</sup> European Frequency and Time Forum (EFTF)*, Braunschweig, Germany, March 27–30, 2006.
- Dach, R., U. Hugentobler, P. Fridez, and M. Meindl (editors, 2007). *Bernese GPS Software, Version 5.0*. User Manual, Astronomical Institute, University of Bern, Switzerland.
- Dach, R., S. Schaer, T. Springer, G. Beutler, F. Perosanz, and U. Hugentobler (2008). Multi-GNSS Processing, Position Paper. In: *International GNSS Service: Analysis Center Workshop*, June 2–6, 2008, Miami Beach, Florida, USA.
- Dach, R., S. Schaer, H. Bock, S. Lutz, and G. Beutler (2010). CODE’s new combined GPS/GLONASS clock product. In: *International GNSS Service: Analysis Center Workshop*, June 28–July 2, 2010, Newcastle upon Tyne, United Kingdom.
- Dilssner, F., R. Dach, R. Schmid, T. Springer, and J. Dow (2010). Update of the IGS antenna phase center model: new GLONASS satellite antenna corrections from CODE and ESOC. In: *International GNSS Service: Analysis Center Workshop*, June 28–July 2, 2010, Newcastle upon Tyne, United Kingdom.
- Gendt, G., Z. Altamimi, R. Dach, W. Söhne, T. Springer, and the GGSP Prototype Team (2010). GGSP: Realisation and maintenance of the Galileo Terrestrial Reference Frame. *Advances in Space Research* DOI 10.1016/j.asr.2010.02.001, in press.
- Jäggi, A., R. Dach, O. Montenbruck, U. Hugentobler, H. Bock, and G. Beutler (2009). Phase center modeling for LEO GPS receiver antennas and its impact on precise orbit determination. *Journal of Geodesy*, 83(12):1145–1162, DOI 10.1007/s00190-009-0333-2.
- Meindl, M., R. Dach, S. Schaer, U. Hugentobler, and G. Beutler (2008). Developing a Generic Multi-GNSS Software Package. In: *International GNSS Service: Analysis Center Workshop*, June 2–6, 2008, Miami Beach, Florida, USA.
- Ostini, L., R. Dach, M. Meindl, S. Schaer, and U. Hugentobler (2008). FODITS: a new tool of the Bernese GPS Software. In Ihde, J. and H. Hornik, editors, *EUREF Publication, No. 18*, EUREF Symposium, June 18–20, 2008, Brussels, Belgium, in press.

- Prange, L., A. Jäggi, R. Dach, H. Bock, G. Beutler, and L. Mervart (2010). AIUB-CHAMP02S: The influence of GNSS model changes for gravity field recovery using spaceborne GPS. *Advances in Space Research*, 45(2):215–224, DOI 10.1016/j.asr.2009.09.020.
- Schaer, S. and R. Dach (2010). Biases in GNSS analysis. In: *International GNSS Service: Analysis Center Workshop*, June 28–July 2, 2010, Newcastle upon Tyne, United Kingdom.
- Springer, T. and R. Dach (2010). GPS, GLONASS, and more. *GPS World*, 21(6):48–58.
- Springer, T. A., G. Beutler, and M. Rothacher (1999). A new Solar Radiation Pressure Model for the GPS Satellites. *GPS Solutions*, 3(2):50–62, DOI 10.1007/PL00012757.
- Steigenberger, P., S. Schaer, S. Lutz, R. Dach, L. Ostini, U. Hugentobler, H. Bock, A. Jäggi, M. Meindl, and D. Thaller (2009). CODE contribution to IGS reprocessing: status and perspectives. In: *EGU General Assembly*, April 19–24, 2009, Vienna, Austria.
- Thaller, D., R. Dach, M. Seitz, G. Beutler, M. Mareyen, and B. Richter (2010). Combination of GNSS and SLR observations using satellite co-locations. *Journal of Geodesy*. in review.

# 2 Analysis of GPS data from an Antarctic Ice Stream

Rolf Dach<sup>1</sup>, Gerhard Beutler<sup>1</sup>, G. Hilmar Gudmundsson<sup>2</sup>

<sup>1</sup> Astronomical Institute, University of Bern  
Sidlerstrasse 5, 3012 Bern; Switzerland

<sup>2</sup> British Antarctic Survey  
High Cross, Madingley Road, Cambridge, CB3 0ET, United Kingdom

Published in *Observing our Changing Earth*, edited by M. Sideris, vol. 133, pp. 569-579, DOI 10.1007/978-3-540-85426-5\_67, Springer, Berlin Heidelberg, ISBN 978-3-540-85425-8.

## Abstract

*Temporal variations in the flow of an active ice stream are analyzed using GPS data collected over a period of two months at six different locations. The diameter of the network is about 60 km. The ice stream moves with a velocity of about one meter per day. The kinematic data are processed using three different strategies: zero-difference network solution, Precise Point Positioning, and double-difference network solution with resolved carrier phase ambiguities.*

*The solutions are compared with regard to the quality of the resulting coordinate time series. Special attention is paid to the positional accuracy as a function of temporal frequency for these different analysis methods as the overall aim of the measurements is to estimate temporal variability in ice flow.*

## 2.1 Introduction

To process GNSS data we usual distinguish zero-difference and double-difference processing schemes. Both are mathematically equivalent. The zero-difference method allows to solve for the receiver and satellite clock corrections, in the double-difference approach we have access to the integer nature of the carrier phase ambiguities. Integer carrier phase ambiguities may also be introduced as conditions of sum (or by adequate technologies) to a zero-difference solution.

Resolving the integer phase ambiguity parameters is essential for obtaining optimal results (e.g., in the repeatability of station coordinate estimation). Recent studies at the AIUB (Jäggi et al., 2008) concerning the gravity field recovery have shown that not all GNSS applications benefit from the introduced integer ambiguities. In that study, the orbits of the two GRACE satellites were generated once with real valued ambiguities and once with resolved integer ambiguities. On one hand, the relative validation of the orbits using K-band measurements between the two satellites clearly demonstrated the benefit of introducing the integer ambiguities. On the other hand, the gravity fields obtained from both orbits were nearly identical. For a more detailed description of this experiment we refer to Jäggi et al. (2008).

This result may be surprising at first sight, but can be explained by the fact that the epoch-to-epoch coordinate differences are dominated by the noise of the carrier phase measurements, which is identical for both solutions. Hence, only the long-term characteristics become more stable as the carrier phase ambiguities are fixed. Here we focus on the impact that resolving the carrier phase ambiguities has on the accuracy as a function of temporal frequency.

## 2.2 Description of the Dataset

Six GPS stations were installed on the Rutford Ice Stream, West Antarctica, from end of December 2003 until February 2004 (see Fig. 2.1):

- One of the receivers, C-20, was located on the (freely floating) ice shelf some 20 km downstream from the grounding line.
- A second one, station C+00, was at the grounding line marking the division between the grounded ice stream and the floating ice shelf.
- Four more stations C+10, C+20, C+30, and C+40 were located at increasing distances of 10, 20, 30, and 40 km, respectively, upstream from the grounding line.

Yet another receiver (FLET) was placed at the top of a nearby ice dome (Fletcher Promontory) where little ice movement is to be expected. The nearest tracking station of the International GNSS Service (IGS) with coordinates available in the IGS05 reference frame — the IGS realization of the ITRF2005 considering the corrections between relative and absolute antenna phase center variation modeling (Schmid and Rothacher, 2003; Ferland, 2006) — is O’Higgins (station ID’s OHI2 and OHI3).

Most of the sites were equipped with LEICA SR530 receivers and LEIAT502 antennas. The station C+30 on the ice stream was occupied with a TRIMBLE 4000SSE receiver and a TRM22020.00+GP antenna. None of the antennas were covered by a radome. The two IGS stations in O’Higgins (OHI2/OHI3) are equipped with an AOA SNR-8000 ACT receiver with an AOAD/M\_T antenna (radome DOME) respective with an ASHTECH Z18 receiver with an ASH701941.B antenna (radome SNOW).

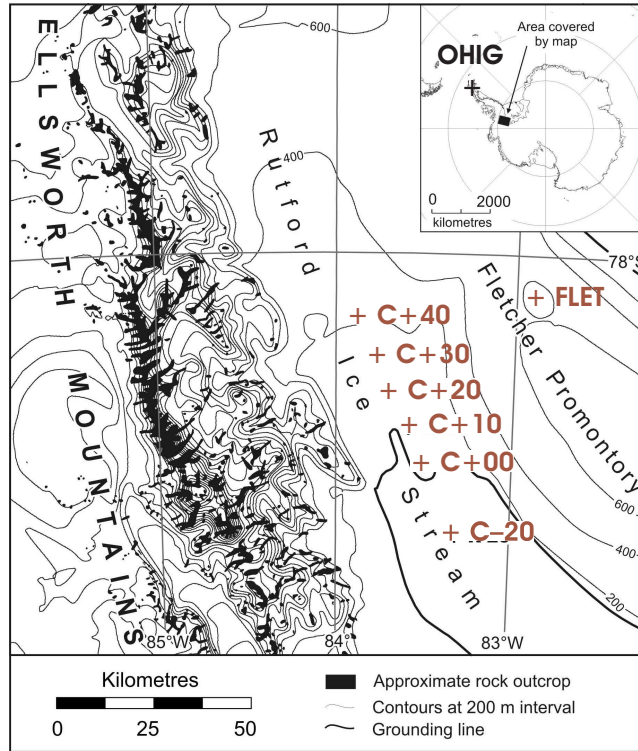


Figure 2.1: Location of the GPS sites on the Rutford Ice Stream.

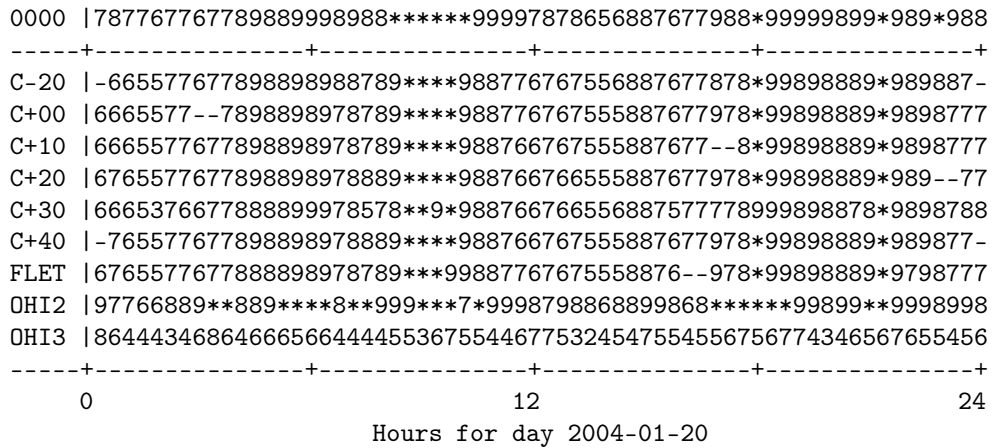


Figure 2.2: Number of GPS satellites contained in the RINEX observation files for the 9 stations in the campaign.

A – character indicates incomplete observations in the bin,  
 a \* character is printed in a bin where more than 9 satellites are observed.  
 In the first line (0000) the number of maximum observable GPS satellites above an elevation angle of 14° are listed.

In Fig. 2.2 the number of satellites observed by the nine GPS stations is plotted for one day. The measurements to GLONASS satellites at stations OHI3 are not considered. This day is typical for all other days of observation. Note that there are intervals with only 5 GPS satellites in view, which limits the quality of a kinematic solution (where we have to solve for 4 parameters per epoch).

Unfortunately, the elevation mask was set to  $14^\circ$  during the measurement campaign. Fig. 2.2 contains in the first line an artificial station with all GPS satellites in view considering the same elevation cut-off. Comparing the number of observed satellites for this artificial station with the content of the RINEX files there are many intervals with one or two missing satellites (PRN 23 was unhealthy for this day from midnight until 23:00UT). To increase the number of available observations significantly it is necessary to decrease the elevation mask considerably during the measurement campaign. With an elevation mask of  $3^\circ$ , for example, at least 8 satellites would have been visible over the entire day.

### Glaciological Background

The experimental setup was designed to study tidally induced temporal variations in the flow of Rutford Icestream. Fig. 2.3 shows linearly detrended stake positions

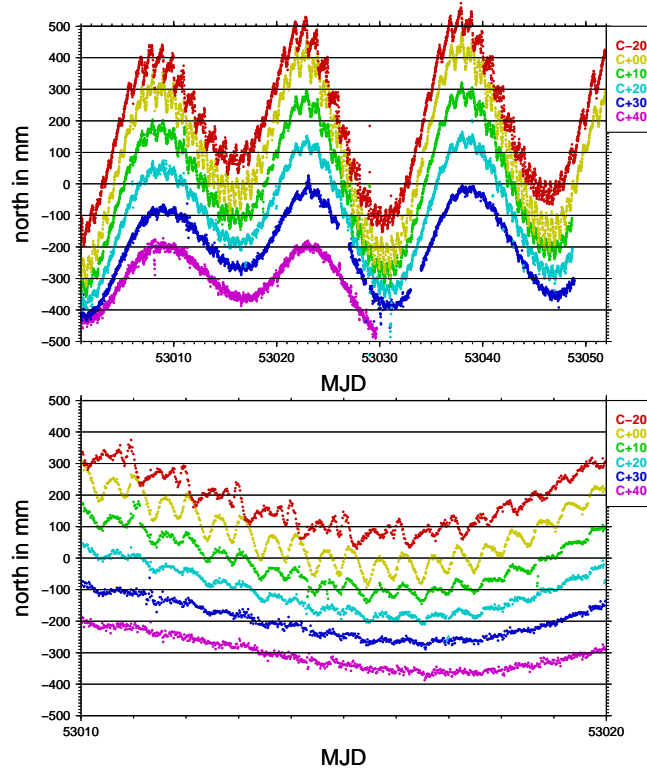


**Figure 2.3:** North component of the kinematic double-difference network solution with resolved ambiguities for the GPS stations on the Rutford ice stream (shifted by 100 mm; top: complete time series; bottom: extraction of 10 days).

in north direction as functions of time. The most surprising aspect of the results is the temporal variation in horizontal movement with a period of about two weeks Gudmundsson (2006). This is clearly seen in the top part of Fig. 2.3. Superimposed on this long-period component are smaller diurnal and semidiurnal components (Fig. 2.3, bottom). The biggest diurnal and semi-diurnal variation in horizontal position results for the station on the grounding line. The size of the amplitude is decreasing rapidly for the stations located inland (becoming effectively zero at a distance of 30 km from the grounding line). Further details of the variation of different tidal constituents with distance are given in Gudmundsson (2006).

## 2.3 GPS Data Processing

The analysis was performed with the Bernese GPS Software, Version 5.0, which is available to the user community (Dach et al., 2007).

### 2.3.1 Connection to the ITRF

In a first step the 2000 km baseline from O'Higgins to the station on the Fletcher Promontory was processed assuming that both stations are static within each daily solution. These daily solutions were then combined to a common solution considering the full covariance information and by introducing the coordinates and velocities from the IGS05 realization of the ITRF2005 for OH12 as known, and a linear velocity for station FLET within this interval.

From these two months of data we obtained a velocity for the Fletcher Promontory station of  $-0.1721$  m/year for the North and  $0.2579$  m/year for the East component. This corresponds to  $0.8$  mm horizontal movement per day. As expected given the fact that

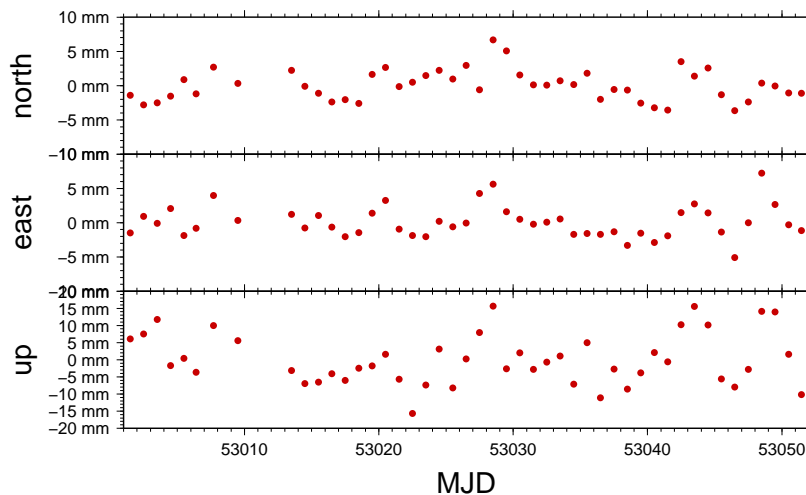


**Figure 2.4:** Repeatability of the 2000 km baseline from O'Higgins to Fletcher Promontory after considering a linear movement.

this station was located at the top of an ice dome with a snow accumulation of about 0.5 m water equivalent, the vertical velocity component was the largest one, or  $-0.8957 \text{ m/year}$  ( $-2.5 \text{ mm/day}$ ).

Figure 2.4 shows the residuals of the daily solutions after the linear station movements for FLET have been removed. In the North and East component the RMS are 2.2 mm and 2.3 mm, respectively, whereas for the vertical component the RMS is 7.6 mm. These values are achieved after the resolution of about 80% of the carrier phase ambiguities.

### 2.3.2 Local Network on the Ice Stream

In a second step the coordinates for the station on the Fletcher Promontory were fixed for each day using the coordinates and velocities obtained in the previous step. One independent set of coordinates was estimated for each epoch (sampling 30 s) for each of the six moving receivers on the ice stream. The troposphere for these six sites was modeled by estimating corresponding parameters every two hours for each of the stations except for FLET because of the small extension of the network.

Based on these assumptions the following solutions were computed using only the carrier phase measurements:

1. a zero-difference network solution<sup>1</sup> where satellite and receiver clock corrections are independently computed as additional parameters for each epoch,
2. a PPP (precise point positioning) solution<sup>1</sup> for each of the six stations on the ice stream introducing the satellite clock corrections obtained in step 1.,
3. a double-difference network solution from six baselines between the FLET station and the receivers on the ice stream with real valued carrier phase ambiguities, and
4. a double-difference network solution using the same baselines as in 3., but introducing the integer values for about 80% of the carrier phase ambiguities.

All solutions are based on the same set of observations. The preprocessing of the data was carried out only once. The baseline solutions use only observations that were also used to obtain to the zero-difference solution. In this way, the results from the four solutions for the six kinematic sites on the ice stream are comparable.

---

<sup>1</sup>Because no pseudorange data are used one carrier phase ambiguity per station and day has to be constrained to prevent the singularity because of the correlation to the clock parameters. This is the only modification with respect to the officially distributed version 5.0 of the Bernese GPS Software.

## 2.4 Intercomparison of Kinematic Solutions

### 2.4.1 Expectation from Theory

The solutions 1. and 2. are expected to be nearly identical because a perfect consistency of the introduced satellite clock corrections with the satellite orbits and the software models are guaranteed. In addition, the data used for the PPP contributed to the computation of the satellite clocks. The second aspect is usually not met in the case of a PPP.

Mathematically, the solutions 1. and 3. are expected to give the same results, as well, because the double-difference solution can be derived from the zero-difference solution by pre-eliminating the receiver and satellite clock parameters. For practical reasons, in the Bernese GPS Software only an independent set of baselines is considered for the double-difference solution. Due to this simplification a few observations may be lost in the double-difference with respect to the zero-difference solution (two independent baselines between the stations A and B and A and C, respectively, contain common observations between A and B and A and C, but not necessarily all observations between B and C).

Another aspect artificially degrading the double-difference solution is that the ambiguities are simply merged from two zero-difference observation files when forming the baseline observation files. They are not updated according to the new observation scenario in the new double-difference solution. As a consequence, ambiguity parameters with a small number of observations are estimated, even if they weaken the parameter estimation. Such ambiguity parameters are eliminated by excluding the corresponding observations from the processing, when the list of ambiguities is updated for the baselines.

### 2.4.2 Differences in the Results

The differences between the three different kinematic solutions (PPP and double-difference with and without ambiguity resolution) relative to the zero-difference network solution (with estimated receiver and satellite clock corrections) were computed and the RMS values were computed for each station and component (see Tab. 2.1). These results confirm the expectations. Especially for the vertical component (U) the mean differences are larger for the ambiguity-fixed solution w.r.t. the other solutions. The same holds for the two horizontal components — but in some cases to a lesser extent.

This direct comparison by forming differences of the resulting time series only shows that the kinematic positions obtained from all three solutions with real-valued ambiguities (1. zero-difference network, 2. PPP, and 3. double-difference network) are closer to each other than the fourth solution based on resolved integer ambiguities. The comparison does not tell which of the solutions is the best.

**Table 2.1:** RMS of the differences between the kinematic solutions:  
 1. zero-difference network solution  
 2. PPP using the satellite clocks from 1.  
 3. double-difference solution, no ambiguity resolution  
 4. double-difference solution with ambiguity resolution

Station		RMS of difference of the solutions		
		2.-1.	3.-1.	4.-1.
C-20	N	2.0 mm	8.5 mm	9.2 mm
	E	2.3 mm	6.1 mm	7.5 mm
	U	6.0 mm	11.9 mm	27.7 mm
C+00	N	2.6 mm	7.7 mm	10.0 mm
	E	4.2 mm	5.9 mm	10.3 mm
	U	9.6 mm	11.1 mm	22.1 mm
C+10	N	5.5 mm	7.6 mm	9.6 mm
	E	3.3 mm	6.5 mm	8.7 mm
	U	9.6 mm	8.2 mm	16.3 mm
C+20	N	2.7 mm	4.4 mm	8.7 mm
	E	3.1 mm	4.9 mm	9.1 mm
	U	9.2 mm	11.9 mm	25.9 mm
C+30	N	3.3 mm	4.4 mm	8.3 mm
	E	3.2 mm	3.2 mm	8.7 mm
	U	9.5 mm	10.1 mm	20.2 mm
C+40	N	2.7 mm	7.8 mm	9.9 mm
	E	3.2 mm	6.4 mm	9.6 mm
	U	10.6 mm	16.9 mm	37.1 mm

### 2.4.3 Day Boundary Discontinuities

Each day's observations were processed independently. The actual movement of the icestream over each 30 s interval is small or less than about 0.5 mm. The size of this discontinuity with respect to the actual expected movement, and with respect to the individual epoch within each daily solution, gives some indication of the accuracy of the results.

Table 2.2 contains the RMS of these epoch differences between two consecutive daily solutions for two of the six stations of the ice stream. It can be seen that for three of the solutions (1. zero-difference network, 2. PPP, and 3. double-difference network) the RMS values are similar, whereas for the double-difference solution with introduced integer ambiguities (4.) the RMS — at least for the horizontal component — is significantly smaller. This is in accordance with the expectation that resolving the ambiguity parameters improves the GNSS derived results.

For comparison Tab. 2.3 contains the RMS value of the epoch-to-epoch difference within each daily solution. These values are of course obtained from many more data points (nearly 3000 epoch differences more) and have in this way a better statistical certainty. The RMS values from different solutions show no significant difference between the four time series of kinematic positions.

**Table 2.2:** RMS of the day boundary discontinuities for the kinematic solutions (keys for the solutions see Tab. 2.1).

		RMS of day boundary discontinuities			
Station		1.	2.	3.	4.
C+00	N	16.3 mm	13.5 mm	15.0 mm	6.2 mm
	E	12.8 mm	13.9 mm	11.7 mm	4.2 mm
	U	50.1 mm	53.6 mm	54.2 mm	52.9 mm
C+10	N	17.1 mm	11.7 mm	12.1 mm	5.6 mm
	E	16.2 mm	17.0 mm	14.7 mm	5.0 mm
	U	51.8 mm	51.4 mm	50.1 mm	37.7 mm

**Table 2.3:** RMS of the epoch-to-epoch differences within each daily kinematic solution (keys for the solutions see Tab. 2.1).

		RMS of epoch-to-epoch differences			
Station		1.	2.	3.	4.
C+00	N	5.1 mm	5.1 mm	4.9 mm	4.9 mm
	E	4.3 mm	4.2 mm	4.0 mm	4.0 mm
	U	20.8 mm	20.7 mm	20.4 mm	20.4 mm
C+10	N	5.1 mm	5.1 mm	4.9 mm	4.9 mm
	E	4.2 mm	4.2 mm	4.0 mm	4.0 mm
	U	20.3 mm	20.3 mm	19.9 mm	19.9 mm

This result indicates that the noise of the kinematic solutions, as it is reflected in Tab. 2.3, is dominated by the noise of the phase measurements (including multipath effects). It is remarkable that — at least for the horizontal components — the RMS of the epoch-to-epoch differences between consecutive days in Tab. 2.2 for solution 4. (with introduced integer ambiguities) reaches almost the same values. For the vertical component the RMS of the epoch-to-epoch difference between two consecutive days is by a factor of about two larger than the general noise level of the solution as judged from the RMS of the epoch-to-epoch differences within each daily solution.

#### 2.4.4 Allan Deviation

In the timing community the Allan deviation ( $\sigma(\tau)$ , Allan, 1987) is a widely used statistical tool to characterize the stability of atomic clocks for different time intervals  $\tau$  (starting from a few minutes/hours for short-term stability up to several days for long-term stability) from a time series of clock values ( $x_1 \dots x_N$ ). For a perfect clock a constant frequency is expected — meaning that a drift of the obtained time values is permitted. The Allan deviation considers the values referring to three epochs separated by an interval length of  $\tau$ :

$$\sigma(\tau) = \sqrt{\frac{1}{2(N-2)\tau^2} \cdot \sum_{i=1}^{N-2} (x_{i+2} - 2x_{i+1} + x_i)^2}$$

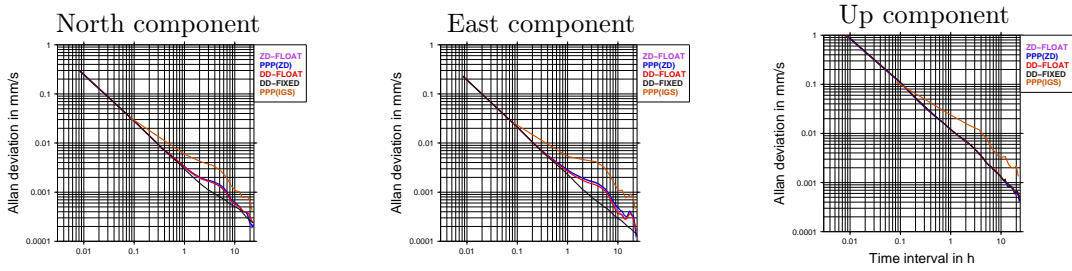


**Figure 2.5:** Allan deviation for station C+30 on the ice stream computed from the time series of kinematic positions obtained from different GNSS processing strategies:

ZD-FLOAT	zero-difference network solution
PPP(ZD)	PPP using the satellite clocks from 1.
DD-FLOAT	double-difference network solution with estimated real valued ambiguities
DD-FIXED	double-difference network solution with introduced integer ambiguities
PPP(IGS)	PPP using the satellite clocks from IGS

We assume parts of the time series separated by more than a five minute data gap to be independent, and, in contrast to the practice in the timing community, do not use a triplet of values to compute the Allan deviation where such a break is found. In particular for long intervals with low number of observed satellites (see Fig. 2.2) this condition reduces the number of triplets of values contributing to the Allan deviation. Nevertheless this assumption is reasonable because some of these independent parts show offsets comparable to the discontinuities between the daily solutions if they are not connected by ambiguity parameters.

Figure 2.5 shows the Allan deviations for one of the stations on the ice stream (C+30) computed from the time series of kinematic positions obtained with the different processing methods. The linear movement of the ice stream is considered by the Allan deviation (analogue to the permitted linear drift of time values from a clock).

For the three processing strategies with real valued ambiguities (1. ZD-FLOAT: zero-difference network, 2. PPP(ZD): PPP with satellite clock corrections from 1., and 3. DD-FLOAT: double-difference network) a similar behavior in the solutions for the horizontal components is observed (see Fig. 2.5). With increasing length of the time interval ( $\tau$ ) the slopes of the curves are at first equal to  $-1$ . This corresponds to the phase noise of the carrier phase measurements itself. For  $1 < \tau < 6$  hours the curves are almost flat indicating that biases existing in the solutions that are constant over these intervals — the carrier phase ambiguity parameters. For longer intervals up to about 12 to 15 hours the slope is again  $-1$  but with a higher noise level than for the intervals shorter than one hour. Note that because of small number of contributing triplets the Allan deviation for intervals longer than 15 hours should be not interpreted.

The fourth solution with resolved ambiguities (4. DD-FIXED) starts for short intervals with the same noise behavior as the other solutions. Up to an interval length of two hours the slope is also  $-1$ . For longer intervals it is only  $0.9$  which can be seen as a

consequence of the discontinuities between the independent daily solutions acting as long-term biases.

For the vertical component a slope of about  $-1$  over the entire interval can be observed for all solutions. The noise level in the kinematic solutions for the vertical component is significantly higher than for the horizontal components, what is to be expected from the general experience in the GNSS data processing (e.g., due to the geometrical coverage of satellites, correlation with other parameters like troposphere or receiver clock corrections) — in particular if no observations to satellites with low elevations are available. (Rothacher and Beutler (1998); Dach et al. (2003))

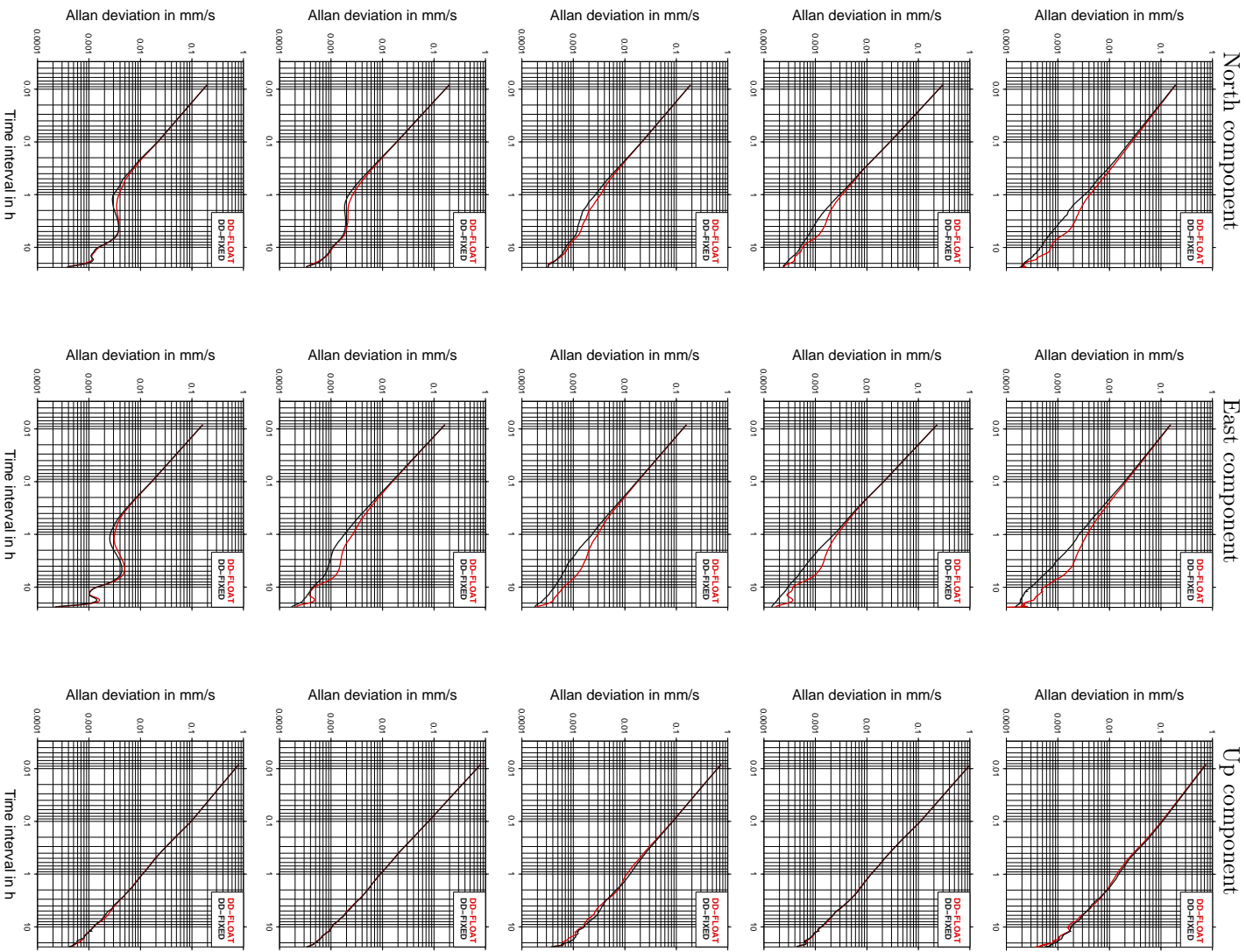
For comparison an alternative PPP solution was added to Fig. 2.5. Instead of using satellite corrections derived from the zero-difference network solution as was done in the PPP (PPP(ZD)) solution described above, the combined satellite clock corrections provided by the IGS were introduced (PPP(IGS)). At first, the IGS provided at that time satellite clock corrections only every 5 minutes with the consequence that the sampling for this solutions has to be adapted accordingly. Secondary, the consistency between all introduced products (satellite orbits and clock corrections as well as Earth orientation parameters) for the combined IGS product cannot be as good as for an internal zero-difference network solution: For the IGS product different analysis centers with different software packages containing different analysis models and individual analysis strategies are mixed with a sophisticated weighting scheme, which cannot be reproduced with one of the processing software packages. The influence of this circumstance is clearly indicated by the Allan deviation for intervals up to 1 hour by a slope of about  $-0.5$  indicating a colored noise. The impact of the unresolved phase ambiguities is observed as well in this solution.

Figure 2.6 shows Allan deviations for two double-difference solutions (with and without resolved integer ambiguities). As the Allan deviations of the zero-difference network solution and the PPP solution are both similar to that of the double-difference solution with real-valued carrier phase ambiguities these are not shown.

The impact of the non-linear movement of the ice stream due to the sub-daily ocean tides — as they are already indicated in Fig. 2.3 — is clearly seen in the Allan deviations of Fig. 2.6 for the horizontal components. The stations closely located to the grounding line (respective to the shelf ice) show a larger peak in the Allan deviation for interval around 6 hours. Because the noise level of the solution with introduced integer ambiguities is in any case lower than the noise level indicated by the Allan deviation for the solution with real-valued ambiguities, the resolution of the ambiguities to their integer value helps to improve the solution and brings out in more detail the sub-daily variations in the movement of the ice stream.

### 2.4.5 Investigating the Vertical Component

Figures 2.5 and 2.6 show no improvement in the Allan deviation for the time series of the kinematic solution with resolved integer ambiguities compared to the solution with real-valued ambiguities for the vertical component. As mentioned above, one



**Figure 2.6:** Allan deviations for the kinematic positions obtained with the double-difference solutions with real-valued (DD-FLOAT) and with introduced integer (DD-FIXED) ambiguities for the stations on the ice stream (from top to bottom: C+40, C+30, C+20, C+10, C+00).

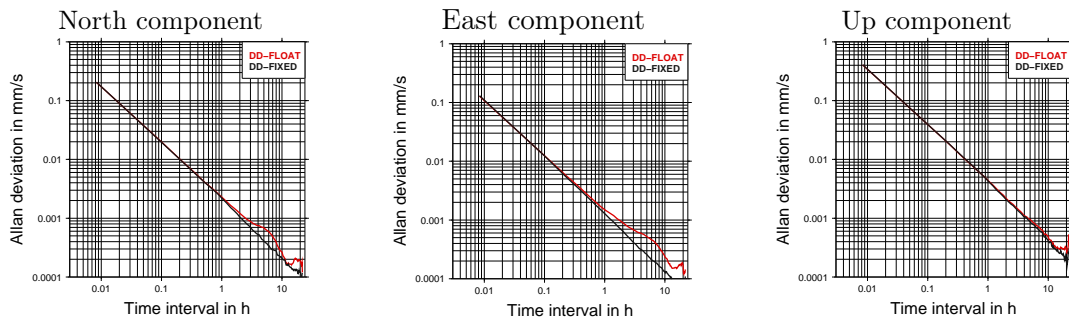


**Figure 2.7:** Allan deviation computed from the time series of kinematic positions obtained from a kinematic short baseline processing with real-valued (DD-FLOAT) and resolved integer (DD-FIXED) ambiguities of the two IGS stations in O’Higgins

possible reason may be the correlation of the vertical component with the troposphere model parameters, which also have to be estimated. For very short baselines with a length of a few meters, no troposphere modeling is needed. A simple analysis of the observations of the phase measurements of the first frequency, where only phase ambiguities and station coordinates have to be solved for, is sufficient. In such a case no correlations can occur.

At the O’Higgins site two receivers, separated by only 3 m, submit data to the IGS. For this short baseline a kinematic solution was calculated for one of the stations, with the coordinates of the other fixed. Two solutions, one with real-valued, and another one with integer ambiguities, were generated. From these two kinematic time series the Allan deviations were computed and displayed in Fig. 2.7.

Interestingly, these solutions show the same Allan deviations for both solution types for the vertical component (as those in the Figs. 2.5 and 2.6). Hence, the correlation of the vertical component with other parameters that had to be solved for cannot explain why the ambiguity resolution does not improve the Allan deviations for the vertical component. The only difference to the local network solutions is a lower noise level of the kinematic solutions, explained by the lower noise level of the L1 phase measurements compared to the ionosphere-free linear combination which was used for the processing of the local network on the ice stream.

## 2.5 Summary

We confirmed by comparing the kinematic coordinate time series computed from GPS data on the Rutford Ice Stream with different processing strategies that the accuracy of a Precise Point Position (PPP) solution is improved by calculating the satellite clock corrections in a initial zero-difference processing step as opposed to using the IGS satellite clock corrections. Double-difference network solution with introduced integer ambiguities improves the accuracy further.

The Allan deviation is well suited to analyze the noise characteristics of kinematic GNSS solutions if the rover receivers follow a linear trajectory. The horizontal com-

ponents of a kinematic solution with resolved ambiguities reveal noise characteristics of the phase measurements in the Allan deviation. For the vertical component we see the same noise behavior in the Allan deviation for solutions with real-valued and resolved ambiguities. Nevertheless, when studying, e.g., the discontinuities at the day boundaries we see the benefit of resolving the ambiguities to their integer values.

Only very short-term characteristics of a kinematic solution (shorter than one hour for terrestrial sites) do not benefit from the ambiguity resolution. The solution is here dominated by the phase noise of the GPS observations.

The analysis of the kinematic solutions for GPS data from Rutford Ice Stream confirms the previously proposed explanation (Jäggi et al., 2008) for the apparent conflict between the improvement of the orbits of the two GRACE satellites due to resolving the ambiguities and the similarity of the derived gravity field from the GRACE orbits without and with ambiguity resolution. The main difference between the Allan deviation for the LEO compared to the terrestrial stations is that the benefit from the ambiguity resolution for the kinematic positions can be seen already for intervals of about 5 minutes for GRACE because of the much shorter mean validity interval for the ambiguities.

## Acknowledgment

The Astronomical Institute at the University of Bern (AIUB) hosts the Center for Orbit Determination in Europe (CODE), which is a joint venture of the AIUB, the Federal Office of Topography (Swisstopo, Switzerland), and the Federal Agency for Cartography and Geodesy (BKG, Germany). The results presented in this paper benefit from the work of the IGS analysis center CODE, (Hugentobler et al., 2008).

## 2.6 References

- Allan, D. W. (1987). Time and Frequency (Time-Domain) Characterization, Estimation, and Prediction of Precision Clocks and Oscillators. *IEEE Transactions on Ultrasonics, Ferroelectrics, and Frequency Control*, 34:647–654.
- Dach, R., G. Beutler, U. Hugentobler, S. Schaer, T. Schildknecht, T. Springer, G. Duddle, and L. Prost (2003). Time transfer using GPS carrier phase: error propagation and results. *Journal of Geodesy*, 77(1–2):1–14, DOI 10.1007/s00190-002-0296-z.
- Dach, R., U. Hugentobler, P. Fridez, and M. Meindl (editors, 2007). *Bernese GPS Software, Version 5.0*. User Manual, Astronomical Institute, University of Bern, Switzerland.
- Ferland, R. (2006). IGS05 Fine Tuning. IGS Mail No. 5455, IGS Central Bureau Information System, URL <http://igs.cb.jpl.nasa.gov/pipermail/igsmail/>.

- Gudmundsson, G.H. (2006). Fortnightly Variation in the Flow Velocity of Rutford Ice Stream, West Antarctica. *Nature*, 444:1063–1064, DOI 10.1038.
- Hugentobler, U., M. Meindl, G. Beutler, H. Bock, R. Dach, A. Jäggi, C. Urschl, L. Mervart, M. Rothacher, S. Schaer, E. Brockmann, D. Ineichen, A. Wiget, U. Wild, G. Weber, H. Habrich, and C. Boucher (2008). CODE IGS Analysis Center Technical Report 2003/2004. In Gowey, K., R. Neilan, and A. Moore, editors, *IGS 2003–2004 Technical Reports*, Jet Propulsion Laboratory, Pasadena, California, USA, pp. 40–50, IGS Central Bureau. URL [http://www.igs.org/igs/scb/resource/pubs/2003-2004\\_IGS\\_Annual\\_Report.pdf](http://www.igs.org/igs/scb/resource/pubs/2003-2004_IGS_Annual_Report.pdf).
- Jäggi, A., G. Beutler, L. Prange, L. Mervart, and R. Dach (2008). Assessment of GPS Observables for Gravity Field Recovery from GRACE. In Sideris, M., editor, *Observing our Changing Earth*, IUGG General Assembly, Perugia, July 2–13, 2007, IAG Symposia, 133:113–123, DOI 10.1007/978-3-540-85426-5\_14, Springer, Berlin Heidelberg, ISBN 978-3-540-85425-8.
- Rothacher, M., and G. Beutler (1998). The Role of GPS in the Study of Global Change. *Physics and Chemistry of the Earth*, 23(9–10):1029–1040, DOI 10.1016/S0079-1946(98)00143-8.
- Schmid, R., and M. Rothacher (2003). Estimation of elevation-dependent satellite antenna phase center variations of GPS satellites. *Journal of Geodesy*, 77(7–8):440–446, DOI 10.1007/s00190-003-0339-0.



# 3 GNSS Processing at CODE: Status Report

Rolf Dach<sup>1</sup>, Elmar Brockmann<sup>2</sup>, Stefan Schaer<sup>2</sup>, Gerhard Beutler<sup>1</sup>, Michael Meindl<sup>1</sup>, Lars Prange<sup>1</sup>, Heike Bock<sup>1</sup>, Adrian Jäggi<sup>1</sup>, Luca Ostini<sup>1</sup>

<sup>1</sup> Astronomical Institute, University of Bern  
Sidlerstrasse 5, 3012 Bern; Switzerland

<sup>2</sup> Swiss Federal Office of Topography swisstopo  
Seftigenstrasse 264; 3084 Wabern; Switzerland

Published in *Journal of Geodesy*, vol. 83(3-4), pp. 353-366, DOI 10.1007/s00190-008-0281-2

Received: 14 May 2008 / Accepted: 14 October 2008

## Abstract

*Since May 2003, the Center for Orbit Determination in Europe (CODE), one of the analysis centers of the International GNSS Service (IGS), has generated GPS and GLONASS products in a rigorous combined multi-system processing scheme, which promises the best possible consistency of the orbits of both systems. The resulting products, in particular the satellite orbits and clocks, are easily accessible by the user community.*

*In the first part of this article, we focus on the generation of the combined global products at CODE, where we put emphasis not only on accuracy, but also on completeness. We study the impact of GLONASS on the CODE products, and the benefit of using them.*

*Last, but not least, we introduce AGNES (Automated GNSS Network for Switzerland), a regional tracking network of small extensions (roughly 400 km East–West, 200 km North–South), which consequently tracks all GNSS satellites and analyzes their measurements using the CODE products.*

### 3.1 Introduction

The Center for Orbit Determination in Europe (CODE) is a joint venture of the Astronomical Institute of the University of Bern (AIUB, Switzerland), the Swiss Federal Office of Topography (swisstopo, Wabern, Switzerland), and the German Federal Office for Cartography and Geodesy (BKG, Frankfurt a. Main, Germany).

CODE started operations on 21 June 1992 and has generated an uninterrupted series of products since that time. All computations are performed at the AIUB using the Bernese GPS Software in its current development version (Dach et al., 2007b). As each of the IGS Analysis Center, CODE aims to provide the “best possible” products also considering the aspects of the demanding user community of Earth sciences and survey institutions. The attribute “best possible” is interpreted by at CODE as follows:

- First, CODE products shall be “state of the art” from the point of view of the products’ accuracy. The IGS Analysis Center Coordinators’ reports since 1994 underline that, in the average over the time span 1994–2004, CODE was successful in this respect.
- Second, CODE products shall be complete to the extent possible. This implies in particular the inclusion of satellites, which are set unhealthy by the operators (including even GPS satellites during repositioning events, since December 2003).
- Third, completeness, in the CODE understanding, also means the inclusion of ephemerides for all GNSS (Global Navigation Satellite Systems) for which the observations are openly available.

In this article, we focus on the second and the third of the above attributes. This paper should be viewed as an intermediary report covering activities and developments initiated about ten years ago and which will eventually (in 5 – 10 years) lead to a CODE processing scheme including all GNSS of interest to the demanding GNSS user community. The decision to proceed in this direction is supported by all partners of CODE.

CODE gained first experience in processing GLONASS data during the IGEX campaign (Ineichen et al., 2003). The processing scheme was a two-step approach, where products like station coordinates, Earth orientation parameters and troposphere parameters were determined by GPS and kept fixed in the second step, where GLONASS was added to the analysis.

In May 2003 CODE started to include the observations of the GLONASS satellites into a fully combined multi-GNSS processing scheme (Schaer et al., 2005) on the level of GPS and GLONASS observations. Due to this strategy all observations may contribute to the generation of the aforementioned products. The rigorous scheme is applied to all product lines of the IGS (final, rapid, and ultra-rapid). Therefore, all CODE-products (apart from the clock corrections) are now multi-system products.

The most important gain of this consequent multi-GNSS processing scheme is the availability of GPS and GLONASS satellites in the same reference frame. It is therefore left to the discretion of the user to select the subset of satellites to be used in a particular analysis. The inclusion of GLONASS into the CODE routine processing is not a trivial step. First we had to make sure that system-specific biases do not contaminate the traditional products. We are now looking back five years in our combined GPS/GLONASS products.

The availability of combined GPS/GLONASS products becomes increasingly more important due to the increasing number of network operators enhancing their permanent networks with GPS/GLONASS combined receivers and antennas. The Swiss Permanent Network AGNES is such an example.

In this paper, we first describe the procedure of our multi-GNSS processing and assess the accuracy of the new and traditional products. In addition, we compare the characteristics of both GNSS and study the use and impact of the combined products.

## 3.2 GNSS Orbit Determination

### 3.2.1 The GNSS Subnetwork of the IGS

The number and distribution of IGS sites providing GPS and GLONASS data has significantly increased and improved since CODE started its combined analysis in Spring 2003. Figure 3.1 shows the number of stations in the IGS network providing GLONASS measurements. The number of GLONASS capable sites grew from about 20 to 30 by the end of the year 2003. The number of stations remained stable for a long time. With the availability of a new generation of combined GPS/GLONASS receivers, produced by several well-known receiver manufacturers in 2006/2007 the number of GLONASS tracking stations in the IGS network increased steadily and still increases today. The CODE final orbits for the GLONASS satellites are now based

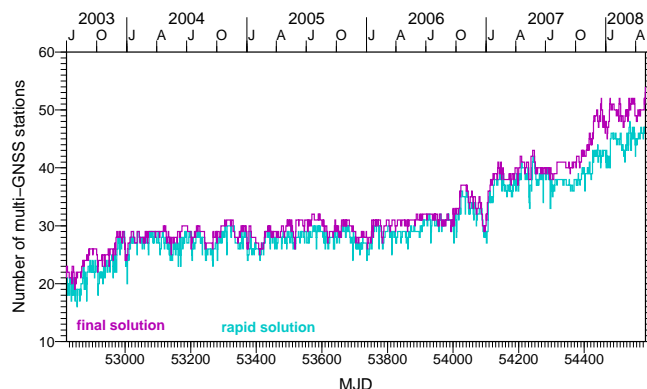
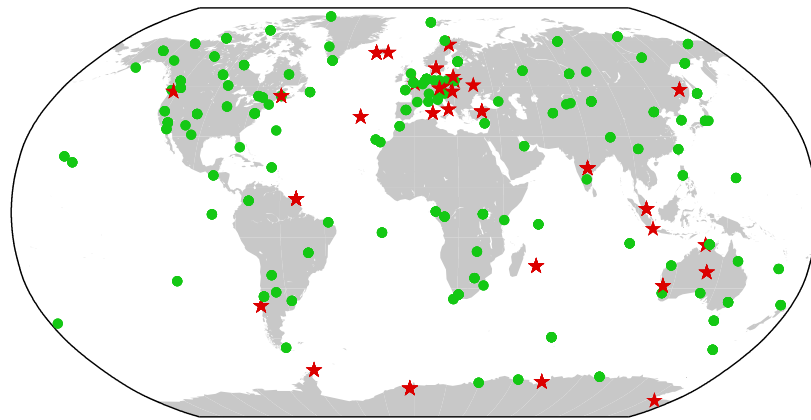
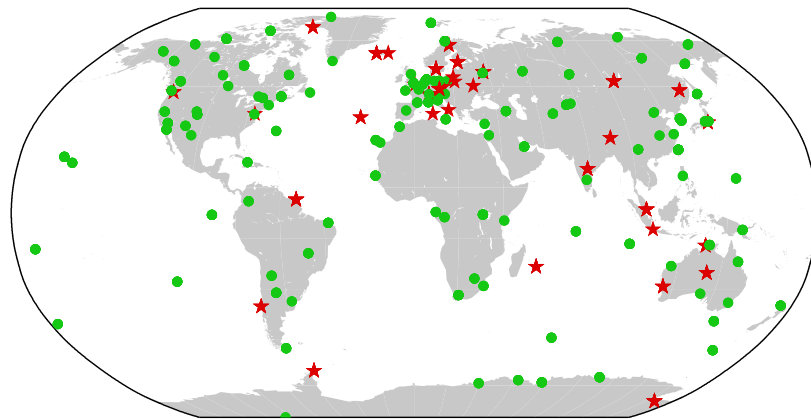


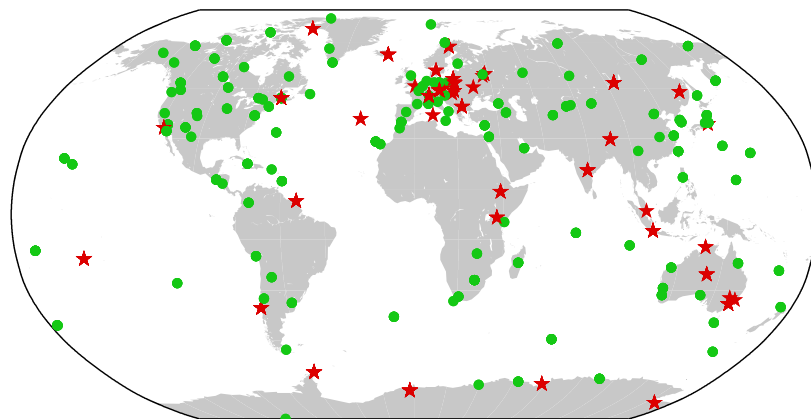
**Figure 3.1:** Number of sites in the IGS network providing GLONASS data, which were used for orbit determination in the CODE rapid (cyan line) and final (magenta line) solution



(a) GNSS subnetwork of the IGS in July 2003 (day of year 182)



(b) GNSS subnetwork of the IGS in March 2005 (day of year 075)



(c) GNSS subnetwork of the IGS in April 2008 (day of year 110)

**Figure 3.2:** Geographical distribution of multi-system GNSS receivers (red stars) and GPS-only receivers (green dots) that are used for the CODE final processing.

on data from 50 tracking stations in the IGS network. For the ultra-rapid solution GLONASS tracking data from about 25 IGS stations are used (the number is limited by the availability of the data). For orbit determination, good global distribution of observing sites is at least as important as their number.

In the summer of 2003, the global coverage of IGS stations tracking GLONASS satellites was highly heterogeneous. Most of the 20 stations with the GLONASS tracking capability were located in Europe (see Fig. 3.2(a)). The 30 stations network available in the time interval 2003–2006 is, in essence, that shown in Fig. 3.2(b). Figure 3.2(c) shows the current network (early 2008). The relation between GPS-only (green dots) and combined GPS/GLONASS (red stars) receivers is now balanced in all regions — except in the American continent, where GPS-only receivers still dominate. In summary, however, we may state that today orbit determination for the GLONASS satellites may be truly based on a global tracking network of geodetic receivers. This significant improvement is due to the efforts of many IGS station managers and their institutions. We acknowledge this significant contribution.

The number of active GLONASS satellites also grew considerably since 2003. Unfortunately, a large number of receivers were unable to track satellites flagged as “unusable”, which reduced the number of receivers tracking these satellites. In 2007, GLONASS moved the frequency range of the system to a new frequency band (announced as a system update already in 2002). The frequencies of the 24 GLONASS satellites of the nominal constellation are no longer computed by the frequency numbers 1 to 12, but by  $-7$  to  $+6$ . When the first satellites with the frequency number  $\leq 0$  became active, several firmware upgrades were necessary to enable the receivers to provide data from these satellites. This (avoidable) receiver problem is responsible that the orbits for some GLONASS satellites had to be computed using the data of only two or three stations for some time periods. For these periods, long arcs of several days were required to guarantee at least a moderate orbit accuracy.

### 3.2.2 Radiation Pressure Modelling

The satellites of all GNSS are orbiting the Earth at rather high altitudes (20000 to 25000 km above the Earth’s surface). Atmospheric drag may thus be neglected and the Earth’s gravity field may be assumed as perfectly known — perhaps with the exception of few low-degree and low-order resonance terms (with Earth rotation).

Radiation pressure is the clearly domination non-gravitational force influencing the GNSS satellites. Unfortunately this force is difficult to take into account in the orbit determination process. One has to make the distinction between the direct radiation pressure (caused by the direct solar radiation) and the albedo radiation pressure, caused by the sunlight reflected from the Earth’s surface, atmosphere, or oceans. As the surface properties (specular and diffuse reflection, absorption) of the satellite and its attitude (orientation of the satellite-fixed coordinate system in the inertial space) are not known with sufficient accuracy, empirical parameters have to be solved for in the orbit determination process. If the orientation were known perfectly, it may

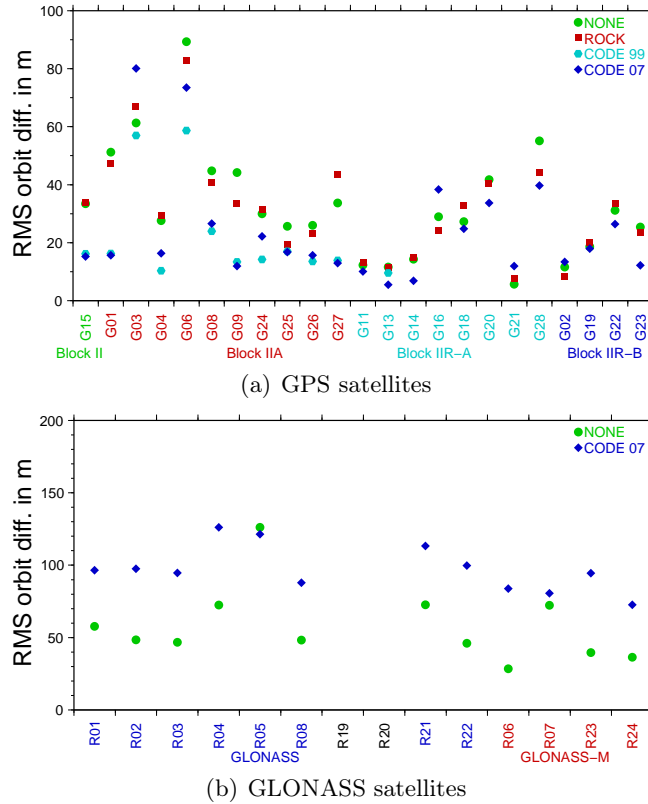


**Figure 3.3:** RMS differences between estimated orbits (“ground truth”) and predicted orbits based on different radiation pressure models. The orbit predictions time span was two weeks. Eclipsing satellites are excluded from the differences.

be sufficient to solve only for a scale factor of a high-quality a priori model. This approach proved to be inadequate for precise orbit determination for GNSS orbits aiming at precision on centimeter level.

The orbit modelling problem may be dealt with in several ways. For example, one may introduce and solve for stochastic accelerations in the satellites’ equations of motion — an avenue followed by the JPL Analysis Center and centers using its software. At CODE the problem is addressed in a different way by the introduction of an empirical force (acceleration) model. These models are in essence based on the theory developed in Beutler et al. (1994).

The empirical model was modified and generalized by Springer et al. (1999) to serve as an a priori model. Since 1998, CODE has used this empirical radiation pressure model containing a set of parameters for each individual satellite or for groups of satellites of a special type. The model contains, in particular, constant, once-per-revolution, twice-per-revolution terms, etc., in the sun-satellite direction ( $D$ ), along the solar panels axes ( $Y$ ), and ( $X$ ), the direction perpendicular to ( $D$ ) and ( $Y$ ). New coefficient sets for this model have been derived recently from the final CODE orbits of the years 2000 to 2006 (the preceding set of coefficient was generated in 1998).

The October 2006 set contains the coefficients for all GPS satellites (including those launched after 1998 for a first time).

The empirical model was, in essence, fine-tuned using the GPS satellites of all types. Given that very little information was available concerning the GLONASS spacecrafts and attitude control, it seemed logical to use the empirical model from Springer et al. (1999) for GLONASS, as well. The corresponding coefficients were derived from data gathered from 2003 through 2007, for which the GLONASS satellites were included into the CODE analysis.

The quality of the new coefficient was assessed by an orbit prediction over two weeks. The prediction is based on three days of observations (from the regular processing at CODE), where each orbit was parameterized by six initial osculating elements and two constant direct radiation pressure components in ( $D$ ) and ( $Y$ ). All the other components were taken over from the October 2006 a priori model. The predicted positions of the 15<sup>th</sup> day are compared to the positions of the final orbit of the same day, where the RMS value for each satellite results from the differences “predicted–final” orbit positions. This prediction procedure was shifted day-by-day over the time interval of three months of the year 2005.

The mean values of all satellite-specific RMS errors for each satellite are provided in Fig. 3.3. The four series of values shown differ only in the a priori radiation pressure model used: One series of values was generated without an a priori model, the second using the ROCK models provided by Fliegel and Gallini (1996), the third using the old set of parameters as published by Springer et al. (1999), and the fourth using the 2006 set of parameters.

From Fig. 3.3, we conclude that the new set of coefficients for the CODE model is of comparable quality to the old one. The CODE models are superior in quality to the ROCK models — this is in particular true for the Block IIA satellites. For GLONASS it is obviously best not to use an a priori model.

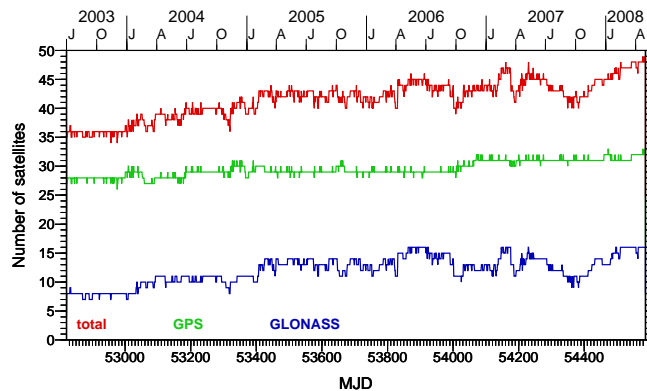


**Figure 3.4:** Number of satellites included in the CODE final orbit product since 2004.

### 3.2.3 GLONASS Orbit Determination

The number of GNSS satellites contained in the CODE final solution is shown in Fig. 3.4. The green curve shows the number of available GPS satellites, which is quite stable around 30 since the year 2000. The number of GLONASS satellites tracked by a sufficient number of sites of the IGS network to allow for precise orbit determination is represented by the blue curve in Fig. 3.4. This number shows much larger variations than the corresponding GPS curve.

This variation is explained by two facts:

1. if an orbital plane is partially eclipsed, the GLONASS satellites were often switched off for a few weeks. When the satellite signals are switched on after such a long time, a new initialization of the orbit determination process is required. Currently, such re-initializations force human interaction in the otherwise highly automated processing scheme.
2. during the maintenance phase a GPS satellite is flagged as unhealthy, but it continues to emit signals; as mentioned, we use such data at CODE for precise orbit determination. GLONASS satellites, however, do not transmit signals for an interval between 1 and 3 days at irregular intervals. The duration and frequency of these events are comparable to the maintenance periods for GPS satellites. These GLONASS maintenance events are usually unannounced. Whereas GPS maintenance periods are often associated with repositioning events, we did not notice any repositioning events for GLONASS. It is thus possible to predict GLONASS orbits over long time intervals for the re-initialization of the orbit determination process, when the satellite is again tracked by the receivers in the IGS network — even if broadcast information is not yet available.

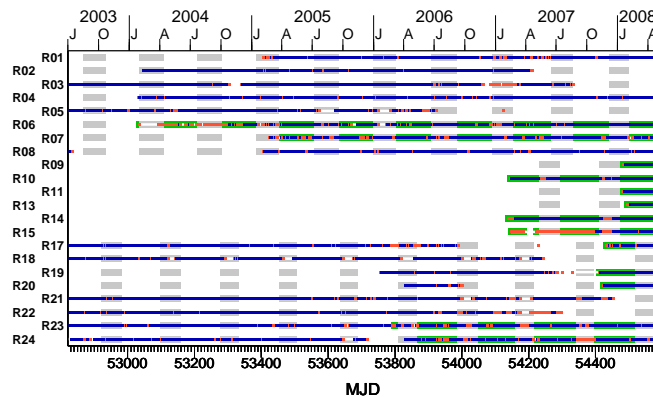


**Figure 3.5:** Days for which orbits of the individual GLONASS satellites are provided by CODE since July 2003 are indicated by blue squares. If the orbit determination was not very reliable because of the lack of tracking data a red square is used instead (in most cases the satellites are flagged as unusable in that time). Green bars indicate intervals where the PRN slot was occupied by a new GLONASS-M satellite. Grey bars indicate eclipsing periods for the satellites at a particular orbital plane.

These system specific outages are summarized in Fig. 3.5: If the CODE final solution contained a GLONASS satellite orbit with the usual accuracy, the day is marked by a blue square. Red squares mark days where orbit determination was of poor quality due to a limited number of receivers tracking the satellite. White squares mark days where no orbit determination was possible, because of missing data (e.g., due to inactive satellites). Many gaps (white squares) occur during the eclipsing phases marked by grey bars. Satellites R05, R18, and R21 illustrate the behavior.

In 2003, the first GLONASS-M satellite — a new generation of GLONASS satellites — was launched (R06 was running in a testing mode over several months in 2004). The replacement of an old-style satellite by a GLONASS-M satellite is indicated by green bars in Fig. 3.5. The current constellation mainly consists of GLONASS-M satellites, because many of the older satellites have been decommissioned. R01 and R08 are the only active old generation satellites. The new satellites continue operating during eclipse phases, which is a big advantage for orbit determination. Also the lifetime of the new generation satellites seems to be longer than for the old ones. The short lifetime of old generation GLONASS satellites is another factor for the bigger variability in the GLONASS satellites constellation displayed in Fig. 3.4.

Let us attempt to assess the precision of the GLONASS (and GPS) orbits. For this purpose we use the ephemerides of our final orbit series of three consecutive days. The positions from the daily (independent) solutions, at 15-minute intervals, are used as pseudo-observations in an orbit determination process, where only six initial osculating elements and nine empirical parameters (three constant and six once-per-revolution parameters in  $D$ -,  $Y$ -, and  $X$ -directions) were determined. The RMS error of one satellite coordinate (hereafter simply referred to as RMS) is used as a precision indicator.

We do not want to include problems of marginally observed satellites and therefore display the median of the RMS over all GLONASS satellites for each day (shown with blue dots in Fig. 3.6). For reference the corresponding values for the GPS satellites are given in green. There is a clear correlation of the RMS with the number of stations

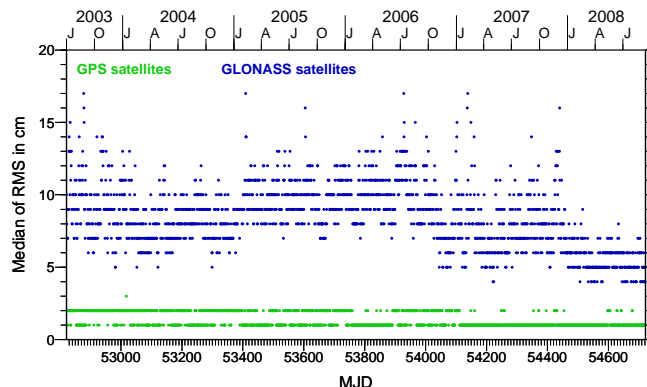


**Figure 3.6:** Median of the RMS for the fit of a three-day arc through the daily independent orbit solutions for the GPS (green) and GLONASS (blue) satellites obtained in the combined GPS/GLONASS processing at CODE since 2003.

tracking GLONASS satellites (see Fig. 3.1): For a long time interval the median of the RMS for the GLONASS satellites was of the order of 8 to 10 cm. With the significantly increased number of GLONASS tracking stations in the IGS network this value was recently reduced to about 5 cm. Note that the median of the RMS error is much larger than the corresponding value for the GPS satellites. This mainly reflects the smaller number of tracking stations and the less than optimal global distribution (compared to GPS). It is, however, remarkable that a long time series of GLONASS ephemerides with sub-decimeter precision are now available. This precision is sufficient for many purposes of “everyday surveys”.

### 3.2.4 Handling of GPS Repositioning Events

Because GPS satellites are in deep 2 : 1 resonance with Earth rotation, i.e., the revolution period of GPS satellites is precisely half a sidereal day, the satellites within the same orbital plane have to be frequently repositioned to maintain a more or less regular satellite constellation. A repositioning is performed by a short thrust in along-track direction. Such a thrust may be approximated by a pulse, an instantaneous velocity change  $\Delta V$  in the along-track direction. Since January 2004, CODE estimates the epochs and the sizes  $\Delta V$  of these pulses using the data from the IGS network (Hugentobler et al., 2008).

The following procedure is applied: Already during the station-specific synchronization of the receiver clocks to GPS system time using the GPS code measurements, the measurement values after the pulse epoch are identified as outliers. Using this information as the starting point, the correct epoch of the pulse is obtained iteratively. Two independent arcs (separated by the pulse epoch) are introduced for the processing of the data of the corresponding satellite. The parameters for both orbital arcs are estimated in several iteration steps. The epoch, where both arcs have the smallest distance, is assumed to be the pulse epoch. This epoch is essential for the successful estimation of the repositioning event since it decides to which of the two arcs an observation contributes. The size,  $\Delta V$ , is simply the velocity difference at the pulse epoch as computed from the two arcs. Figure 3.7 shows the detected repositioning events since January 2004. Most of them have a size of about 200 mm/s.

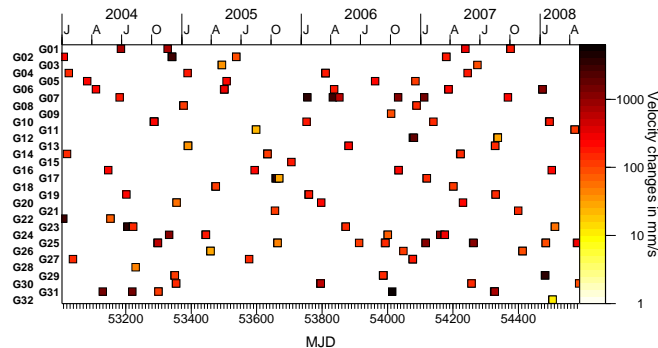


**Figure 3.7:** Repositioning events of the GPS satellites since January 2004 as they are derived by CODE.

A user of the CODE orbits can independently introduce the orbit information before and after the event. In this way, the time where a satellite cannot be used during a repositioning event is minimized. Only few epochs during “very heavy” repositioning events must be excluded, because the thrust lasts for a certain amount of time.

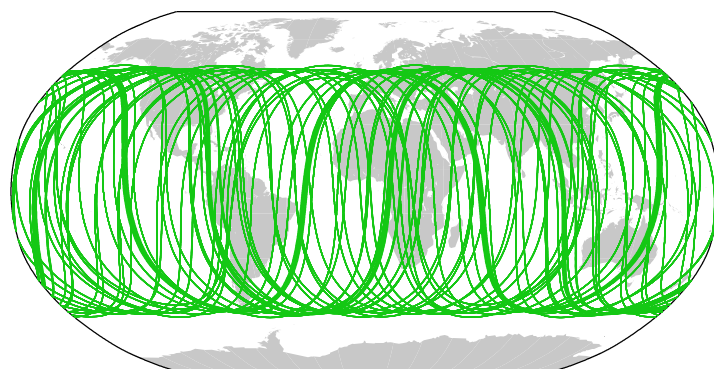
No repositioning events were detected for the GLONASS satellites even if a satellite was inactive for several months. This is only possible because the GLONASS satellites are not in deep, but only shallow 2:1 resonance with Earth rotation (17 revolutions within 8 sidereal days; for comparison a GPS satellite carries out 16 revolutions within 8 sidereal days).

## 3.3 Comparing GPS-only and multi-GNSS Solutions

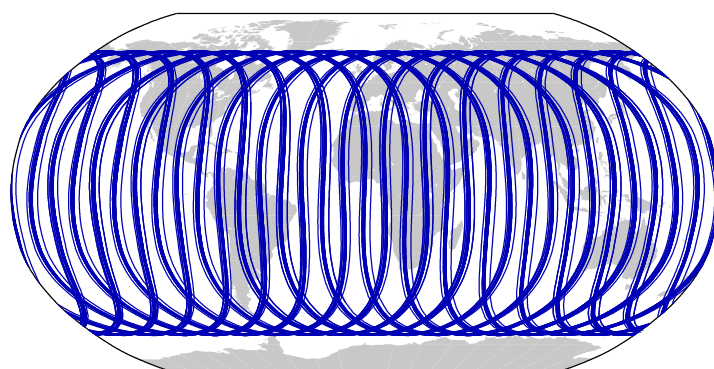
### 3.3.1 GPS and GLONASS Orbit Characteristics

The sub-satellite track of one particular GPS satellite is repeated every day. It is therefore possible to show all sub-satellite tracks for the entire GPS constellation using one day as an example. As long as the satellites are not moved to a different position within the orbital plane, the same ground tracks result for each day. Figure 3.8(a) shows the ground tracks for all GPS satellites during ten days in February 2008. The GPS-specific ground tracks imply that a particular satellite follows the same azimuth-elevation paths (at maximum two visibility intervals per day) for one and the same site. This implies in particular that the observation scenarios of particular GPS satellites are — for a given latitude — longitude-dependent. As the IGS network is not really global and homogeneous, this fact implies that different GPS satellites are most likely not observed with the same “intensity” and with the same quality. Figure 3.9(a) shows an example for the site Zimmerwald at a Northern latitude of about  $45^\circ$ . Note that the ground track actually corresponds to 10 days, which proves that the particular GPS satellite follows the same track day after day. Only one GPS track, culminating almost at  $90^\circ$  elevation results in this case. A site situated at the same latitude as Zimmerwald, but separated in longitude by  $\pm 90^\circ$  would observe two tracks of the same GPS satellite per day, culminating at lower elevations, one in the East and one in the West.

GLONASS ground tracks are repeated after 8 sidereal days (which corresponds to a deep 17 : 8 resonance with Earth rotation). The ground tracks of all 16 GLONASS satellites active on the same days in 2008 are shown in Fig. 3.8(b). The ground track of a particular satellite is shifted by  $45^\circ$  in longitude per day. As the satellites in one and the same orbital plane are separated by  $45^\circ$  in the full nominal constellation, the ground track generated by one particular satellite on day  $i$  is the same as the ground track of its two neighbors on days  $i \pm 1$ . Therefore, one orbital plane of the GLONASS, in essence, generates one ground track, where all ground tracks are much steeper than the GPS ground tracks as a consequence of the 8 sidereal day repeat cycle. From the scientific perspective it is unfortunate that the arguments of latitude of the satellites

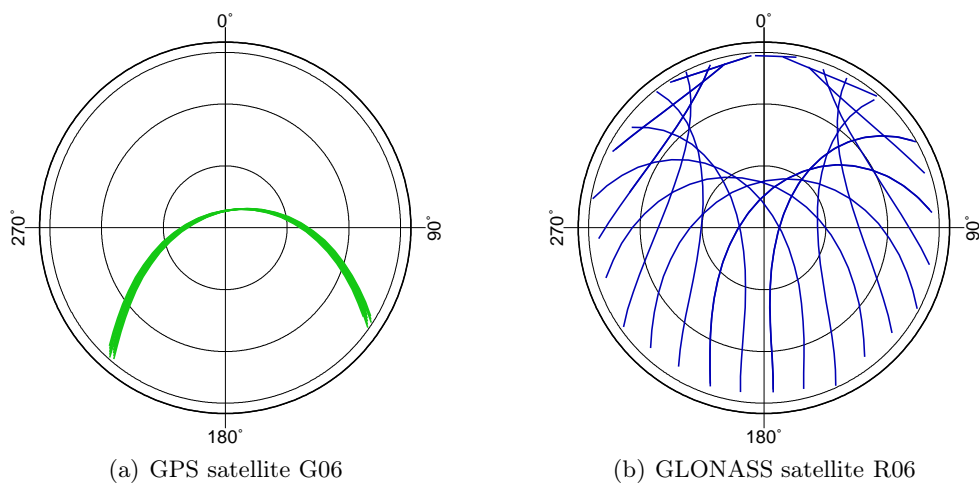


(a) Ground track of the GPS satellites



(b) Ground track of the GLONASS satellites

**Figure 3.8:** Ground track of the GPS (top) and GLONASS (bottom) constellation during 10 days (day 60 to 69 of year 2008) in February 2008.



(a) GPS satellite G06

(b) GLONASS satellite R06

**Figure 3.9:** Elevation-azimuth-diagram for one GPS (left) and one GLONASS (right) satellite at the location of Zimmerwald, Switzerland, accumulated during 10 days (day 60 to 69 of year 2008) in February 2008.

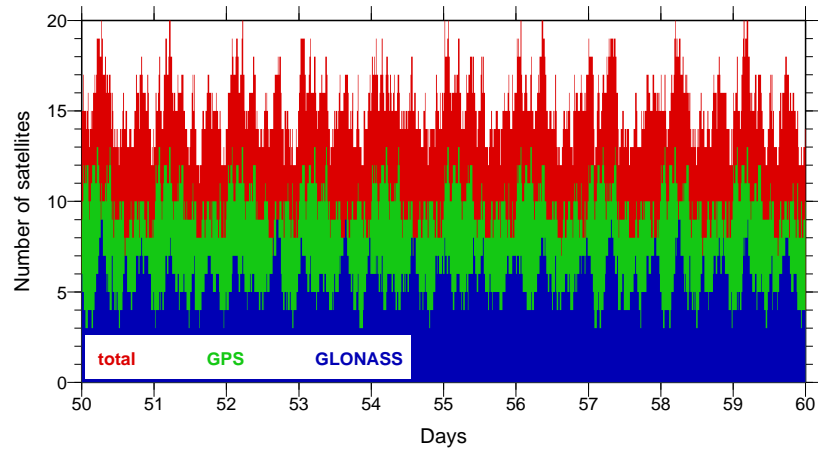
in the three orbital planes are defined in such a way that the satellites in the three orbital planes all generate one and the same ground track. This characteristic may be attractive for the system operators (it reduces the number of necessary control stations) but it would be better from the scientific point of view to have a less regular pattern.

Be this as it may: It is an important difference of the GLONASS with respect to the GPS constellation that, in the average over 8 sidereal days, all sites at one and the same latitude observe each GLONASS satellite in essence in the same way (shifted only by a time offset governed by the longitude difference). Figure 3.9(b), which was generated in the same way as Fig. 3.9(a) covering the time interval of 10 days, illustrates this behavior. One GLONASS satellite in essence fills the entire azimuth–elevation plot (except for the hole in the North, caused by the satellites’ inclination). Due to the special selection of the arguments of latitude in the three orbital planes, Fig. 3.9(b) also characterizes the ground tracks of all GLONASS satellites. As a matter of fact this leads to an eight–hour repeat cycle in the satellite geometry for the stations.

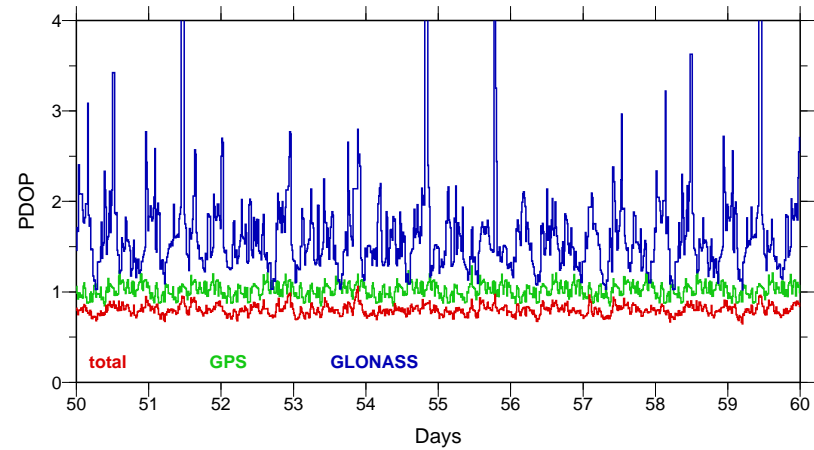
As each GLONASS satellite transmits its signal on an individual frequency the impact of frequency–dependent effects such as multipath on station–specific parameters (such as coordinates and troposphere) should be reduced for this constellation. For such issues we expect a period of four sidereal days (as opposed to one sidereal day for the GPS), because GLONASS satellites separated by  $180^\circ$  in the orbital plane use the same frequencies.

### 3.3.2 Benefit of the Combined GNSS Products on Navigation and Rapid Positioning

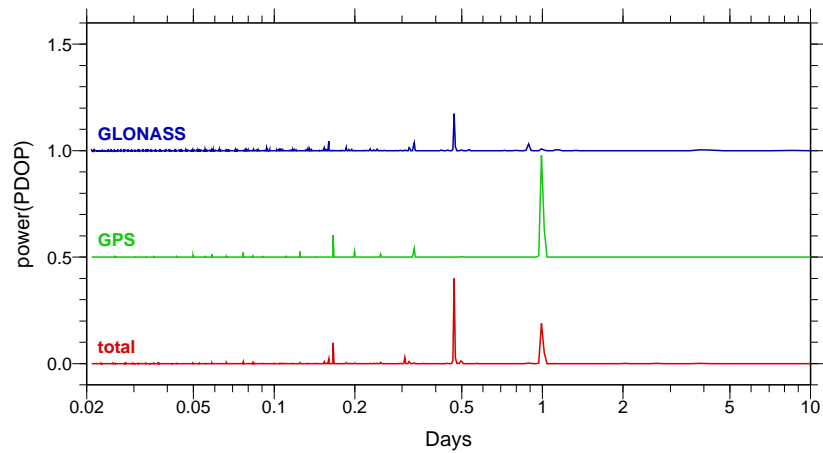
31 GPS satellites and 16 GLONASS were active in the first quarter of the year 2008. A combined GPS/GLONASS receiver thus tracks on average 50% more satellites than a GPS-only receiver. Fig. 3.10(a) shows these numbers for the Zimmerwald site, where one can see that, on average, about 15 GNSS satellites may be observed simultaneously, as opposed to 10 GPS satellites and five GLONASS satellites, individually. As the current GLONASS constellation consists of only 16 out of the 24 satellites of the full constellation, there are short periods where only three or fewer GLONASS satellites are in view. Nevertheless, we may expect an accuracy gain of the combined system for navigation and for positioning using short (few minutes) time spans of about  $\sqrt{31/16} \approx \sqrt{1.5} \approx 1.22 = 122\%$  in a least square adjustment. This expectation is confirmed by Fig. 3.10(b) showing the PDOP values for the GPS, GLONASS, and the multi-GNSS constellation. The PDOP value in essence gives the average of the mean errors in the three orthogonal directions North, East, Up of a position determination assuming code observations of the accuracy of one meter (remember that smaller PDOP values correspond to better satellite geometry). The same PDOP may be used for phase observations with resolved ambiguities, where the unit would be mm. The expected accuracy gain is not dramatic. With the full 24 satellite constellation the gain will be  $\sqrt{55/32} \approx 1.31 = 131\%$ . More important, but more difficult to illustrate, is the gain in robustness of the solution.



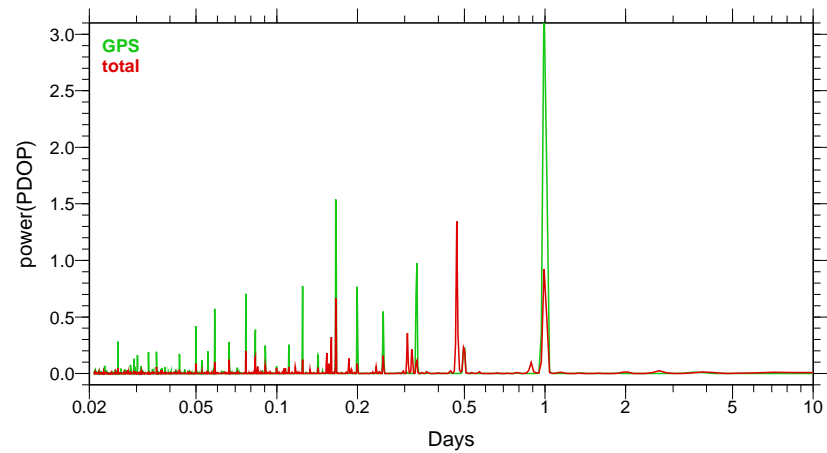
(a) Number of satellites for station Zimmerwald for 10 days in 2008.



(b) PDOP for station Zimmerwald for 10 days in 2008.



(c) Normalized power spectra of the PDOP time series for station Zimmerwald for two months (day 20 to 79 of year 2008). The three curves are shifted by 0.5 for plotting.



(d) Power spectra of the PDOP time series for station Zimmerwald for two months (day 20 to 79 of year 2008). The curve for the GLONASS-only PDOP values was not plotted because it is much more noisier than the other ones because of the incomplete GLONASS constellation.

**Figure 3.10:** Comparison of the satellite geometry for IGS stations Zimmerwald for the GPS (green), GLONASS (blue), and combined (red) satellite constellation. An elevation cut-off of  $5^\circ$  is assumed.

The normalized power spectra of the GPS, the GLONASS, and the combined PDOP series in Fig. 3.10(c) differ considerably: The main feature of the PDOP spectrum for GPS is the signal at  $23^h56^m$ , corresponding to one sidereal day and to the repetition of the satellite geometry at a ground station after two revolutions of the GPS satellites. The main feature of the GLONASS PDOP spectrum is the signal at  $11^h16^m$ , corresponding to the GLONASS revolution period. As expected, the power spectrum of the GNSS signal contains both prominent spectral lines. At least with the current incomplete GLONASS constellation the spectral line at  $11^h16^m$  is stronger than that at  $23^h56^m$ . Regarding the big reduction of the amplitude at  $23^h56^m$  due to adding the GLONASS measurements to the GPS observations — as shown in the non-normalized power spectra of Fig. 3.10(d) — this additional spectral line in the PDOP series of the combined GPS/GLONASS processing (red line) with respect to a GPS-only series (green line) seems to be acceptable.

The difference of the PDOP spectra may have an important consequence when studying the coordinate repeatability based on daily coordinate sets (solar day) using time spans of one to two weeks: In case of a GPS-only solution, the satellite constellation is repeated one-by-one in every daily solution. This may lead to too optimistic results, e.g., in case of a satellite-dependent error source. Because of the higher variation in the satellite geometry within a daily solution, the repeatability of daily coordinate solution in a GLONASS-only or a combined GPS/GLONASS processing may therefore slightly worse than in a GPS-only analysis but it gives a more realistic measure of the accuracy.

From the deliberations in this subsection we may conclude that the user of the combined products has the following advantages when processing data gathered in time spans of several minutes:

- With more satellites, the solutions are much more robust, at least in the sense of a better redundancy. Outlier detection and bias identification and removal (in particular cycle slip identification and correction) are much easier. Also the success rate of ambiguity resolution within short time intervals is expected to be improved.
- The accuracy of results (point positioning, differential positioning) should be improved by the statistical  $\sqrt{n}$ -law, where  $n$  is the number of observations. As the number of observations is proportional to the number of satellites, we expect the results to follow the same law, where  $n$  is the number of simultaneously observed satellites.

In order to check the second expectation, the following test was performed: The European network solution, the CODE contribution to the EPN (European Permanent Network, Bruyninx and Roosbeek, 2009), was processed in daily batches, for a two month interval. The orbits and the coordinates of the reference stations were introduced from the official CODE contribution to the IGS (final solution) respective to the EPN. The coordinates of the other sites and the troposphere parameters were adjusted in the experiment. The combined GPS/GLONASS receiver at Zimmerwald observatory (ZIM2) was considered as “mildly kinematic”, i.e., coordinates were estimated at 3-minute intervals whereas, the ambiguities were re-introduced as known from the

standard network processing. Only the GPS observations were used for all stations in the solution in the first part of the test. All observations (GPS and GLONASS) were used in the second part of the test. It would have been most thorough to generate a third solution using only the GLONASS measurements. However, in view of the limited number of simultaneously visible GLONASS satellites (at times there are only 3 satellites, see Fig. 3.10(a)), such a solution makes little sense.

The obtained time series of kinematic positions for Zimmerwald station with a sampling of three minutes (all in all 30'240 data points within 63 days) was analyzed in two different ways: At first the Allan deviation (see Allan, 1987) is generated to assess the impact of the additionally used GLONASS measurements on the obtained “kinematic trajectory”. In a second analysis the time series was divided into subintervals to compute the standard deviation for the mean value of the interval. The length of these subintervals was varied to study the influence of the additional observations on a fictive coordinate solution obtained from the different intervals of measurements.

In Fig. 3.11 the *Allan deviations* is displayed generated with the two sets of three minutes solutions for Zimmerwald station. The Allan deviations referring to a spacing of  $\tau$  between data points are given by

$$\sigma(\tau) = \sqrt{\frac{1}{2(N-2)\tau^2} \cdot \sum_{i=1}^{N-2} (x_i - 2x_{i+1} + x_{i+2})^2},$$

where the data values  $x_k$ ,  $k = i, i + 1, i + 2$  refer to epochs separated by  $\tau$ .

The red line in Fig. 3.11 refers to the combined processing of GPS and GLONASS measurements, whereas the green line is obtained from the GPS-only solution. For short time intervals (up to a few minutes) the Allan deviation is dominated by the noise of the carrier phase (see also Dach et al., 2007a). In this domain the additional GLONASS measurements help according to the  $\sqrt{n}$ -law to reduce the noise of the kinematic positions by 20 to 25%. For longer intervals — let us say half an hour or more — the improvement becomes very small. For intervals of one hour and longer the difference of both curves is even smaller. It means that the additional GLONASS measurements help to improve mainly the epoch-to-epoch stability of the obtained kinematic trajectory.

An alternative analysis of the three-minutes series of the kinematic positions for the Zimmerwald station is presented in Fig. 3.12. The time series has been divided into intervals, each with  $N$  3-minute epochs. The positions estimated from all the observations within an interval may be approximated by forming an arithmetic mean from the 3-minute kinematic positions of this interval. Then the quality of such a mean interval positions can be assessed from the *standard deviation of the mean* computed by

$$\sigma = \sqrt{\frac{1}{N \cdot (N - 1)} \cdot \sum_{i=1}^N (x_i - \bar{x})^2} \quad \text{with} \quad \bar{x} = \frac{1}{N} \cdot \sum_{i=1}^N x_i.$$

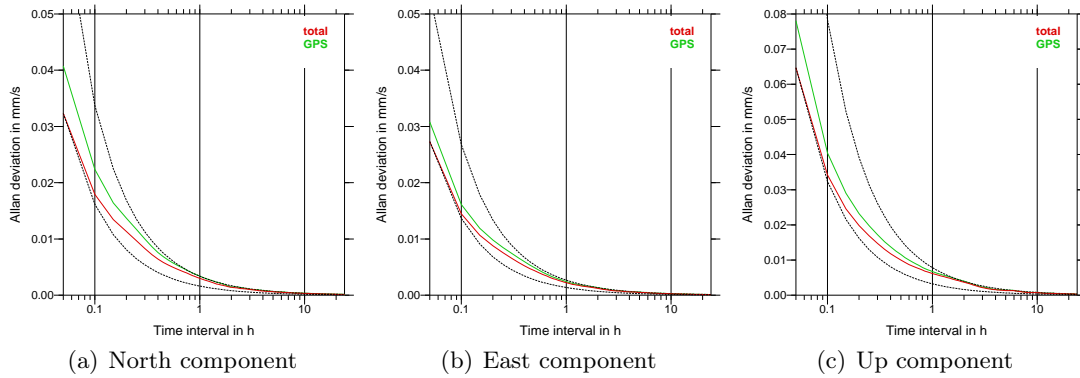


**Figure 3.11:** Allan deviations of the kinematic positions (at 3-minute intervals over 60 days) of the combined GPS/GLONASS receiver in Zimmerwald (ZIM2) using only GPS measurements (green line) and observations from both GNSS (red line), respectively.

The unusual non-logarithmic scale was used to show the differences between the two curves more clearly. The dotted lines indicate the slope of  $-1$  for a white noise behaviour.

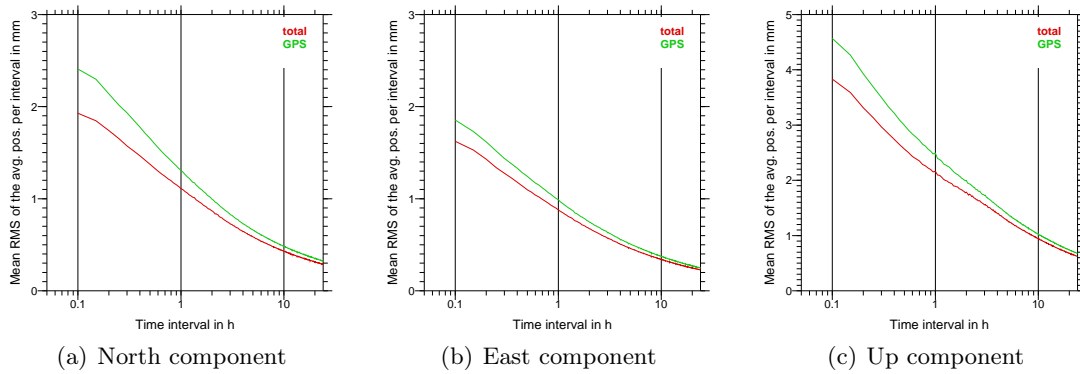


**Figure 3.12:** Standard deviation of the mean position computed over a certain time interval — derived from the kinematic positions (at 3-minute intervals over 60 days) of the combined GPS/GLONASS receiver in Zimmerwald (ZIM2) using only GPS measurements (green line) and observations from both GNSS (red line), respectively.

The length of the interval to compute the fictive mean coordinate has been varied from a few epochs over several hours up to one day.

The green line in Fig. 3.12 represents the results derived from the GPS-only solution whereas the red line refers to the combined GPS/GLONASS solution. The benefit for the short intervals (e.g., 6 minutes or 0.1 hour) is again 20 to 25% — as it was found in the Allan deviation. For an hourly processing the analysis still promises a benefit of 5 to 10% due to the additionally processed measurements — for longer interval lengths the benefit decreases rapidly, but the red curve (GPS/GLONASS solution) remains slightly below the green line (GPS-only solution).

The decreasing benefit due to adding the GLONASS to the GPS observations in the kinematic solution for time intervals longer than one hour may need a further discussion: Beside the  $\sqrt{n}$ -law, one should also not forget the general modelling aspects in the GNSS processing (e.g., troposphere) acting in the same (or at least very similar) way on the measurements of each GNSS. Concerning GLONASS in this particular case it must be stated, that less ambiguities<sup>1</sup> are resolved than for GPS. A degradation of the benefit from the GLONASS measurements for the combined solution is expected according to the experience with ambiguity resolutions in the GPS-only environment. On the other hand, even an ambiguity resolution rate of 85 to 95% in the Swiss national network (see Section 3.4) gives very similar Allan deviation plots when the stations are processed in a kinematic mode. This might indicate that beside the ambiguity resolution there seem to be other effects that are not adequately modelled in the processing (e.g., the antenna phase center models for GLONASS receiver and satellite antennas).

### 3.3.3 Impact of GLONASS on the CODE Global Products

Based on the findings of the previous paragraph we cannot expect major improvements by adding the GLONASS measurements to the GPS data in the coordinate series

<sup>1</sup>In the CODE IGS-processing the GLONASS ambiguity resolution is only enabled for baselines shorter than 20 km since August 2007 (success-rate is close to 100%) whereas for the European solution the GLONASS ambiguities are only allowed between satellites using the same frequencies for test purposes when using the QIF-ambiguity strategy for baselines up to 2000 km length (success-rate is about 30% with respect to all ambiguities). A detailed description of the ambiguity resolution strategies in the Bernese GPS Software is given in Mervart (1995).

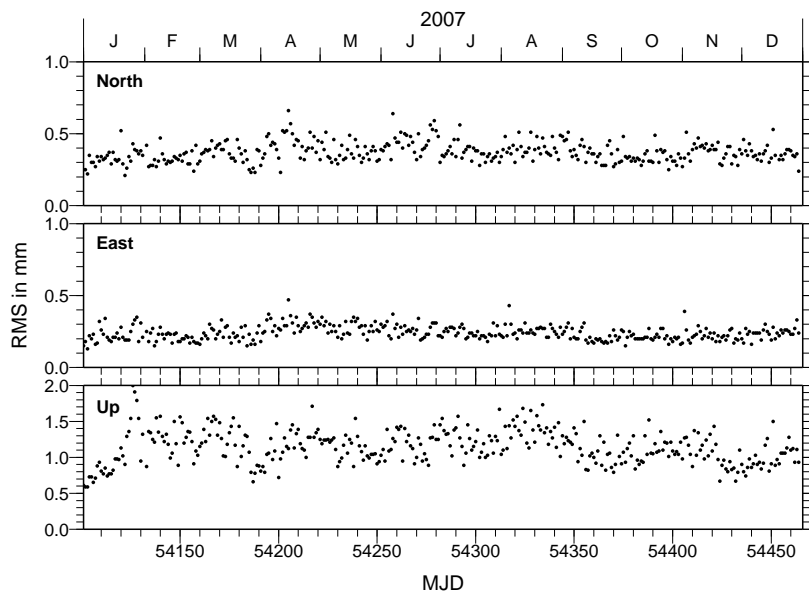


**Figure 3.13:** RMS of the coordinate differences obtained in daily GPS-only respective combined GPS/GLONASS solutions in a global network during the year 2007

estimated in the CODE routine processing — the coordinates are only available in daily batches.

Figure 3.13 shows the daily RMS values in North, East and Up components of the coordinate differences between two solutions with and without using the GLONASS observations in the processing. About 150 sites are included in the global analysis corresponding very closely to the CODE IGS analysis (i.e., solving for all relevant parameters, including orbit, coordinates, troposphere, and ambiguities that are not resolved to their integer values). Figure 3.13 has a simple message: The global reference frame is only marginally changed when adding or leaving out GLONASS measurements in the processing.

The comparison of the GPS orbits in a GPS-only and a in a combined GPS/GLONASS processing shows differences in the order of  $\approx 1$  cm (up to 2 cm for some cases). These are small values, which correspond to the mm-differences in the station coordinates. We conclude that the addition of GLONASS into the analysis currently has no significant impact on the GPS orbits, i.e., including GLONASS does not help nor hurt the determination of global parameters from GPS data.

The same conclusion can be drawn for the Earth rotation parameters. The differences in the results with and without using GLONASS data are insignificant.

### 3.4 GNSS Applications using the Swiss AGNES Network

The Automated GNSS Network for Switzerland (AGNES) and the Swiss Positioning Service (swipos) constitute an important part of the geodetic infrastructure of Switzerland. Since AGNES is a multifunctional reference network not only for applications in national surveying but also for scientific studies and positioning services, swisstopo had to find a compromise between the continuity of the observations and the rapid alignment to the demands and developments of the market: All major manufacturers of GNSS receivers have been designing combined receivers for both, GPS and GLONASS, since 2006. The greater number of satellites does bring about improvements in the positioning service swipos because the availability and performance of the service has increased in difficult terrain (built up areas, narrow valleys, etc.). In order to keep up with this development, swisstopo adapted its network AGNES, consisting of 31 permanently operating stations, to the new technical demands.

During summer 2007 the first 11 AGNES stations was converted from GPS-only to new combined GPS/GLONASS receivers. Until April 2008 nearly all AGNES sites have been equipped with the new receivers. The present status of the network is given in Fig. 3.14 — red circles indicate the location of the combined GPS/GLONASS receivers. To assure continuity, the old GPS-only receivers are planned to be operated simultaneously with the new GPS/GLONASS receivers on ten AGNES stations (Brockmann et al., 2009; Ineichen et al., 2009). Six of these double-sites are currently (April 2008) installed (yellow circles in Fig. 3.14).

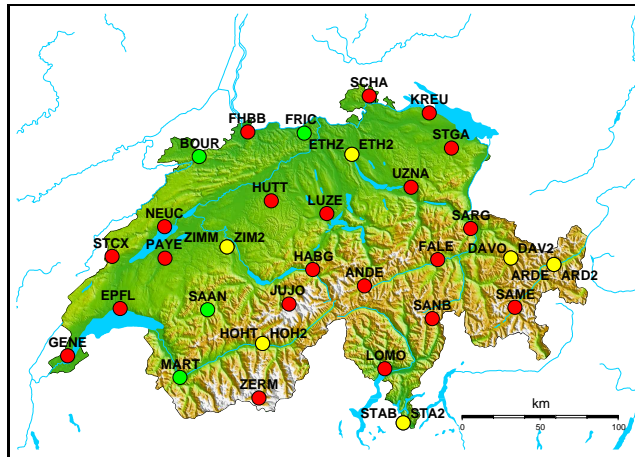


**Figure 3.14:** Status of the AGNES network (April 2008): red circles indicate new GPS/GLONASS receivers, green circles show the locations of stations with a GPS-only tracking receivers, yellow circles represent stations where a GPS-only and a GPS/GLONASS receiver are operating simultaneously.

The monitoring of the stability of site coordinates is an important part of AGNES to guarantee reference frame maintenance. To fulfill this demand, the complete AGNES network is analyzed with about 40 other EPN/IGS sites on an hourly and daily basis using the Bernese GPS Software, Version 5.0. The ultra-rapid and the final orbit products from the CODE analysis center of the IGS are used to process these stations, because combined multi-system products are not available through the IGS.

To guarantee highest precision, all of the new GNSS antennas were first calibrated by the company Geo++ in Germany, which is specialized to perform such calibrations, e.g., Wübbena et al. (2006). Absolute elevation- and azimuth-dependent antenna phase center variations were derived for GPS (individual corrections for each antenna) and for GLONASS (one set of group corrections). Discontinuities in the coordinate time series, which occurred due to the change of the antenna, were below several millimeters for the horizontal direction and at maximum 3 centimeters for the vertical direction (see Fig. 3.15). Another consequence of the interruption is the reduced accuracy of the velocity estimation. An analogue process is currently ongoing within the IGS network (see Fig. 3.1). It may be expected in a much shorter interval when the Galileo system and the corresponding hardware is in place.

Ambiguity resolution of GPS/GLONASS combined observations was not possible using Bernese GPS Software beginning of 2007 (Schaer, 2009). In close cooperation with the University of Bern, swisstopo developed several improvements (optimization of the generation of short GNSS-baselines, improved preprocessing, improved GNSS ambiguity resolution). With these modifications it became possible to successfully implement ambiguity resolution since June 2007 for the post-processing solutions and since September 2007 for the near real-time processing. No double-difference ambiguities in between GPS and GLONASS are solved for. Also, the QIF ambiguity resolution strategy (Mervart, 1995) only allows it to solve ambiguities referring to

the same frequencies. For all baselines between Swiss stations (on average separated by 50 km) and for all GNSS-baselines shorter than 200 km, the combined widelane and narrowlane ambiguity resolution strategy enables a successful ambiguity resolution of 85–95%, which is comparable to the success rate when analyzing GPS data, only.

Similar to the findings in Section 3.3.2, the results presented in Ineichen et al. (2008) for station-depending parameters (coordinates and troposphere) are also very comparable. This is true for daily results as well as for results derived from a near real-time processing of the data in hourly sliding batches of 8 hours. These solutions are finished and submitted within 30 minutes. The main reason for enhancing the AGNES network with GLONASS is therefore the increasing availability of the Swiss Positioning Service (swipos) for surveyors measuring positions on centimeter level in real-time and in difficult environments — about 60% of the swipos users indicate to use both available GNSS in combination.

### 3.5 Summary

Since May 2003 CODE offers in its products GPS and GLONASS ephemerides referring to one and the same reference frame (in essence a realization of the most recent ITRF release(s)). According to the weekly reports of the IGS Analysis Coordinator, the GPS ephemerides are consistent on the 1–2 cm level with the IGS combined products. From the combination of the GLONASS orbits, a consistency level of 3–5 cm between the contributing ACs<sup>2</sup> may be derived.

In this article we assessed the precision of the GLONASS orbits to be of the order of 8 cm RMS per coordinate, initially, (in 2004) and 5 cm, today. These figures will get closer to the GPS figures (a) with the completion of the full GLONASS configuration and (b) with the increase of the number and the improvement of the global distribution of state of the art combined GPS/GLONASS receivers.

<sup>2</sup>Please note that only four centers provide GLONASS orbits but only two of them contribute also to the traditional IGS products.

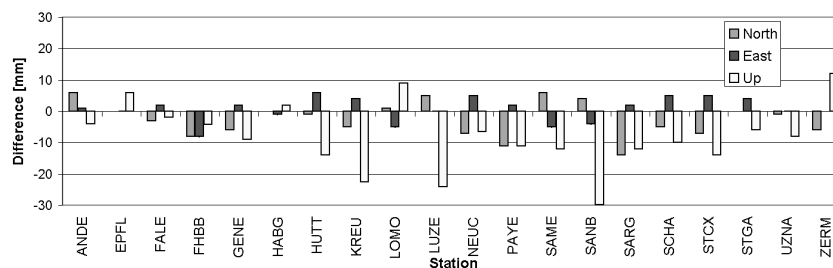


**Figure 3.15:** Discontinuities in the coordinate time series due to the replacement of the antennas at 20 AGNES sites.

We have pointed out important differences between the GPS and the GLONASS observation geometries: The observation geometry (expressed by the PDOP) shows a strong once-per-revolution signal for GLONASS, whereas there is a prominent daily signal (sidereal day) in the GPS PDOP. The observation geometry of the combined GPS/GLONASS PDOP contains, as expected, both signals.

The power spectrum of the GPS-only PDOP shows a prominent signal at one sidereal day. This has to be expected, as the entire configuration is repeated after one sidereal day. Two aspects are important in this context:

- The solar day is very close to the sidereal day (difference of about four minutes). Using the solar day as sampling interval, e.g., for coordinate time series may lead to an over-estimation of GPS accuracies derived from the repeatability of the daily positions.
- The sampling of a signal over a period which is slightly different from the prominent period in the GPS PDOP spectrum (in the GPS case one sidereal day) may generate spurious beat signals — which were, as a matter of fact, described by Ray et al. (2008).

The power spectrum of the GLONASS-only PDOP in essence has one prominent spectral line corresponding to the revolution period of  $11^h 16^m$  of the GLONASS satellites. There is almost no power in the daily or quasi-daily domain. If we would have the same number of satellites in both constellations we would, therefore, expect for GLONASS-only solutions to have

- a slightly reduced (solar) daily coordinate repeatability as compared to GPS
- but a reduced quasi-annual beat signal — the current GLONASS does not allow it to study this aspect with sufficient precision.

We have shown that the statistical expectation (improvement of the results of GNSS surveys with  $\sqrt{n}$ , where  $n$  is the number of (simultaneously available) satellites, roughly holds when analyzing GNSS observations from short (few minutes) data spans. This is an important benefit for many users of GNSS products, in particular for the surveying and (potentially) the navigation communities. For longer data spans, the advantages soon become much smaller, or even marginal. This means that (unmodelled) systematic effects in the data analysis dominate with respect to the pure noise of the observations.

Currently the contribution of GLONASS to the global products, in particular to the reference frame (set of station coordinates) and the Earth rotation parameters cannot be clearly identified. We are confident that this situation will change with the deployment of the full GLONASS constellation and the improvement of the global tracking network equipped with combined receivers.

The Swiss Permanent Network AGNES, which was enhanced from GPS to GPS/GLONASS in 2007 as one of the first networks consequently gathers and analyzes GPS and GLONASS observations and makes the combined products available to its user community. AGNES uses the CODE/IGS products (including the GLONASS

orbits) for its analyses and provides a good example for the link from the GNSS activities within the IGS to daily surveying activities. It demonstrates the IGS is not just an “academic environment” to study GNSS phenomena. The IGS products are very central for the daily work of a very big user community. Their needs and wishes should be kept in mind in all scientific activities within the IGS. The CODE consortium as a joint venture between the scientific (AIUB) and application (swisstopo and BKG) part stands for both sides.

### 3.6 References

- Allan, D. W. (1987). Time and Frequency (Time-Domain) Characterization, Estimation, and Prediction of Precision Clocks and Oscillators. *IEEE Transactions on Ultrasonics, Ferroelectrics, and Frequency Control*, 34:647–654.
- Beutler, G., E. Brockmann, W. Gurtner, U. Hugentobler, L. Mervart, M. Rothacher, and A. Verdun (1994). Extended Orbit Modeling Techniques at the CODE Processing Center of the International GPS Service for Geodynamics (IGS): Theory and Initial Results. *Manuscripta Geodetica*, 19(6):367–386.
- Brockmann, E., M. Kistler, U. Marti, B. V. Schlatter, A. Wiget, and U. Wild (2009). National Report of Switzerland: New Developments in Swiss National Geodetic Surveying. In Torres, J., J. Ihde. and H. Hornik, editors, *EUREF Publication, No. 17*, EUREF Symposium, June 04–06, 2007, London, United Kingdom, Mitteilungen des BKG, volume 42, ISBN 978-3-89888-916-2.
- Bruyninx, C. and F. Roosbeek (2009). EPN Status and New Developments. In Torres, J., J. Ihde. and H. Hornik, editors, *EUREF Publication, No. 17*, EUREF Symposium, June 04–06, 2007, London, United Kingdom, Mitteilungen des BKG, volume 42, ISBN 978-3-89888-916-2.
- Dach, R., G. Beutler, and G.H. Gudmundson (2007a). Analysis of GPS data from an Antarctic Ice Stream. In Sideris, M., editor, *Observing our Changing Earth*, IUGG General Assembly, Perugia, July 2–13, 2007, IAG Symposia, 133:113–123, DOI DOI10.1007/978-3-540-85426-5\_67, Springer, Berlin Heidelberg, ISBN 978-3-540-85425-8.
- Dach, R., U. Hugentobler, P. Fridez, and M. Meindl (editors, 2007b). *Bernese GPS Software, Version 5.0*. User Manual, Astronomical Institute, University of Bern, Switzerland.
- Fliegel, H.F. and T.E. Gallini (1996). Solar Force Modeling of Block IIR Global Positioning System Satellites. *Journal of Spacecraft and Rockets*, 33(6):863–866.
- Hugentobler, U., M. Meindl, G. Beutler, H. Bock, R. Dach, A. Jäggi, C. Urschl, L. Mervart, M. Rothacher, S. Schaer, E. Brockmann, D. Ineichen, A. Wiget, U. Wild, G. Weber, H. Habrich, and C. Boucher (2008). CODE IGS Analysis Center Technical Report 2003/2004. In Gowey, K., R. Neilan, and A. Moore, editors, *IGS 2003–2004*

- Technical Reports*, Jet Propulsion Laboratory, Pasadena, California, USA, pp. 40–50, IGS Central Bureau. available at [http://www.igs.org/igs/scb/resource/pubs/2003-2004\\_IGS\\_Annual\\_Report.pdf](http://www.igs.org/igs/scb/resource/pubs/2003-2004_IGS_Annual_Report.pdf).
- Ineichen, D., E. Brockmann, and S. Schaer (2009). Enhancing the Swiss Permanent GPS Network (AGNES) for GLONASS. In Torres, J., J. Ihde. and H. Hornik, editors, *EUREF Publication, No. 17*, EUREF Symposium, June 04–06, 2007, London, United Kingdom, Mitteilungen des BKG, volume 42, ISBN 978-3-89888-916-2.
- Ineichen, D., E. Brockmann, and S. Schaer (2008). Processing Combined GPS/GLONASS Data at swisstopo’s Local Analysis Center. In Ihde, J. and H. Hornik, editors, *EUREF Publication, No. 18*, EUREF Symposium, June 18–20, 2008, Brussels, Belgium. in press.
- Ineichen, D., T. Springer, and G. Beutler (2003). Combined Processing of the IGS and the IGEX network. *Journal of Geodesy*, 75(11):575–586, DOI 10.1007/s001900000152.
- Mervart, L. (1995). *Ambiguity Resolution Techniques in Geodetic and Geodynamic Applications of the Global Positioning System*. Geodätisch-geophysikalische Arbeiten in der Schweiz, Band 53. Schweizerische Geodätische Kommission, Institut für Geodäsie und Photogrammetrie, Eidg. Technische Hochschule Zürich, Zürich.
- Ray, J., Z. Altamimi, X. Collilieux, and T. van Dam (2008). Anomalous Harmonics in the Spectra of GPS position Estimates. *GPS Solutions*, 12/(1):55–64, DOI 10.1007/s10291-007-0067-7.
- Schaer, S., E. Brockmann, and D. Ineichen (2009). Inclusion of GLONASS for EPN Analysis at CODE/swisstopo. In Torres, J., J. Ihde. and H. Hornik, editors, *EUREF Publication, No. 17*, EUREF Symposium, June 04–06, 2007, London, United Kingdom, Mitteilungen des BKG, volume 42:86–94, ISBN 978-3-89888-916-2.
- Schaer, S., U. Hugentobler, R. Dach, M. Meindl, H. Bock, C. Urschl, and G. Beutler (2005). GNSS Analysis at CODE. In Meindl, M., editor, *Celebrating a Decade of the International GPS Service - Workshop and Symposium*, 2004, Bern, Switzerland, March 1-15, 2004.
- Springer, T. A., G. Beutler, and M. Rothacher (1999). A new Solar Radiation Pressure Model for the GPS Satellites. *GPS Solutions*, 3(2):50–62, DOI 10.1007/PL00012757.
- Wübbena, G., M. Schmits, and G. Boettcher (2006). Absolute GNSS Antenna Calibration with a Robot: Repeatability, GLONASS, and Carrier-to-Noise Pattern. In 10th EUPOS@IGS, November 22–24, Budapest, Hungary.

## 4 Improved antenna phase center models for GLONASS

Rolf Dach<sup>1</sup>, Ralf Schmid<sup>2</sup>, Martin Schmitz<sup>3</sup>, Daniela Thaller<sup>1</sup>, Stefan Schaer<sup>4</sup>, Simon Lutz<sup>1</sup>, Peter Steigenberger<sup>5</sup>, Gerhard Wübbena<sup>3</sup>, Gerhard Beutler<sup>1</sup>

<sup>1</sup> Astronomical Institute, University of Bern  
Sidlerstrasse 5, 3012 Bern; Switzerland

<sup>2</sup> Forschungseinrichtung Satellitengeodäsie, Technische Universität München  
Arcisstraße 21, 80333 München; Germany

<sup>3</sup> Geo++ GmbH  
Steinriede 8, 30827 Garbsen; Germany

<sup>4</sup> Swiss Federal Office of Topography swisstopo  
Seftigenstrasse 264; 3084 Wabern; Switzerland

<sup>5</sup> Institut für Astronomische und Physikalische Geodäsie, Technische Universität München  
Arcisstraße 21, 80333 München; Germany

Published in *GPS Solutions*, DOI 10.1007/d10291-010-0169-5

Received: 12 October 2009 / Accepted: 27 March 2010

### Abstract

*Thanks to the increasing number of active GLONASS satellites and the increasing number of multi-GNSS tracking stations in the network of the International GNSS Service (IGS), the quality of the GLONASS orbits has become significantly better over the last few years. By the end of 2008, the orbit RMS error had reached a level of 3 to 4 cm. Nevertheless, the strategy to process GLONASS observations still has deficiencies.*

*One simplification — as applied within the IGS today — is the use of phase center models for receiver antennas for the GLONASS observations which were derived from GPS measurements only, by ignoring the different frequency range. The antenna phase center model for the GLONASS satellites was derived in early 2006, when the multi-GNSS tracking network of the IGS was much sparser than it is today. Furthermore, many satellites of the constellation at that time have in the meantime been replaced by the latest generation of GLONASS-M satellites.*

*Geo++ GmbH calibrates GNSS receiver antennas using a robot in the field. This procedure yields separate corrections for the receiver antenna phase centers for each navigation satellite system, provided its constellation is sufficiently populated. With a limited set of GLONASS calibrations it is possible to assess the impact of GNSS-specific receiver antenna corrections that are ignored within the IGS so far.*

*This paper provides an update and extension of the presently used correction tables for the GLONASS satellite antenna phase centers for the current constellation of GLONASS satellites. The updated GLONASS antenna phase center model helps to improve the orbit quality.*

### 4.1 Introduction

The Globalnaya Navigatsionnaya Sputnikovaya Sistema (GLONASS; Russian for Global Navigation Satellite System) — the Russian counterpart of the American Global Positioning System (GPS) — became important in GNSS (Global Navigation Satellite System) analyses during the last few years. Today (May 2009) twenty GLONASS satellites are active and the satellite constellation has become very stable with the second generation of GLONASS-M satellites. A number of manufacturers provide combined GPS/GLONASS receivers. As the GPS/GLONASS tracking network of the International GNSS Service (IGS, Dow et al., 2009) reached nearly global coverage by the end of 2008, the quality of the GLONASS orbits is now at a level of 3 to 4 cm.

This accuracy level still is about three times lower than that for the GPS orbits. Dach et al. (2009) showed that the improvements due to adding GLONASS to GPS observations are limited to parameters valid for a short time span (one hour and shorter). For parameters with a longer validity interval the uncertainty of the observation modeling absorbs the statistically expected benefit from additional measurements in the analysis model.

The currently available models for the receiver and satellite antenna phase center locations limit the achievable accuracy of GLONASS results. Both categories of antennas will be addressed subsequently, but first of all it is necessary to describe the data processing strategy used as the basis for all further experiments in Sect. 4.2.

No distinction is made between the GPS and GLONASS frequencies for the receiver antennas within the IGS so far. The GPS-derived corrections are used for the measurements of both GNSS. In Sect. 4.3 the differences between GNSS-specific corrections as well as their impact on coordinate estimates are analyzed.

The phase center corrections (PCC) currently used within the IGS for the GLONASS satellite antennas (igs05.atx model, Schmid et al., 2007) also have several drawbacks. They were computed in early 2006 when the GLONASS-capable receivers in the IGS network were mainly located in Europe and when the first two GLONASS-M satellites were in space only for a short time span. Since then almost all GLONASS satellites

have been replaced by new generation satellites. Both the number and the global distribution of GLONASS tracking stations have been improved significantly since 2006. The number of different antenna types has also grown significantly. These developments indicate that an update of the satellite antenna phase center models for the GLONASS satellites is badly needed. Section 4.4 describes the generation of such models.

The updated receiver and satellite antenna phase center models are validated in Sect. 4.5.

## 4.2 Reprocessing of GLONASS data at CODE

CODE, the Center for Orbit Determination in Europe, is a joint venture of the Astronomical Institute of the University of Bern (AIUB, Bern, Switzerland), the Swiss Federal Office of Topography (swissjtopo, Wabern, Switzerland), the Federal Agency for Cartography and Geodesy (BKG, Frankfurt am Main, Germany), and the Institut für Astronomische und Physikalische Geodäsie of the Technische Universität München (IAPG/TUM, Munich, Germany). CODE has been one of the global analysis centers of the IGS since the start of IGS test campaign operations on June 21, 1992. All operational computations are performed at the AIUB using the development version of the Bernese GPS Software (Dach et al., 2007). Since May 2003, CODE has been analyzing GPS and GLONASS data in a combined analysis to achieve the best possible consistency of the GPS and GLONASS orbit products. This strategy is not only applied to the CODE contributions to the IGS final products, but also to its rapid and ultra-rapid products.

CODE also participates in the first reprocessing campaign of the IGS. The IGS decided to limit this activity to a GPS-only solution. The corresponding computations of CODE were performed at IAPG/TUM between summer 2008 and spring 2009 (Steigenberger et al., 2009). The processing strategy of the operational CODE solution from August 2008 was used for this effort (except that the reprocessing was limited to GPS). In this way a consistent time series of GPS-derived CODE products from January 1994 up to December 2008 could be generated.

The reprocessed GPS-only products were extended to GLONASS by introducing GLONASS tracking data gathered after May 2003 in addition to the GPS data. The GPS/GLONASS tracking data were processed using the strategy applied to the IGS reprocessing. Finally, the additional observations were combined with the GPS-only part on the observation level to generate a fully consistent multi-system time series of products.

For the GLONASS extension of the reprocessed solutions more GLONASS tracking stations could be included than in the operational processing (see Fig. 4.1). Even though most of the stations were still located in Europe (at least till the end of 2007), the quality of the GLONASS orbits could be improved by a factor of about two. It reached a level of about 5 – 6 cm at the end of 2007 and improved to 3 – 4 cm by

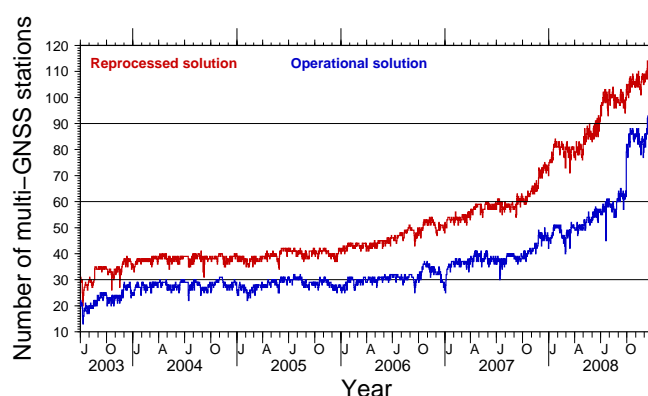


**Figure 4.1:** Number of sites in the IGS network providing GLONASS data which were used for orbit determination in the CODE operational (blue) and reprocessed (red) solutions.

the end of 2008 (see Fig. 4.2). For comparison, the corresponding values for the GPS satellites are 1 – 2 cm. This quality measure is based on an orbit determination process: apart from the six initial osculating orbital elements, nine empirical parameters in the Sun-oriented coordinate system at the satellite consisting of a component ( $D$ ) pointing from the satellite to the Sun, of a ( $Y$ ) component along the solar panel axis of the satellite, and the ( $X$ ) component completing the right-hand system (three constant and six once-per-revolution parameters, Beutler et al., 1994) were determined introducing the satellite positions every 15 min from three independent consecutive daily solutions.

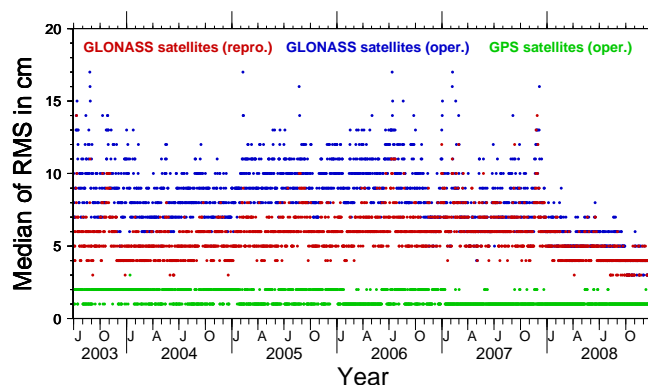


**Figure 4.2:** Median of the RMS for the fit of a three-day arc of the operational (blue) and reprocessed (red) CODE orbits for the GLONASS satellites as well as of the operational GPS orbits (green).

### 4.3 GNSS-specific receiver antenna phase center modeling

The PCC model as it is used within the IGS consists of two components. The so-called phase center offset (PCO) is a vector pointing from a mechanical marker at the antenna (antenna reference point, ARP) to a mean phase center. Additional azimuth- and elevation-dependent phase center variations (PCV) are usually provided in grids. Any change in the PCO can be compensated by the PCV. In consequence the PCO can be freely defined (e.g., to have no PCV correction in zenith direction) as long as the PCV are consistently used.

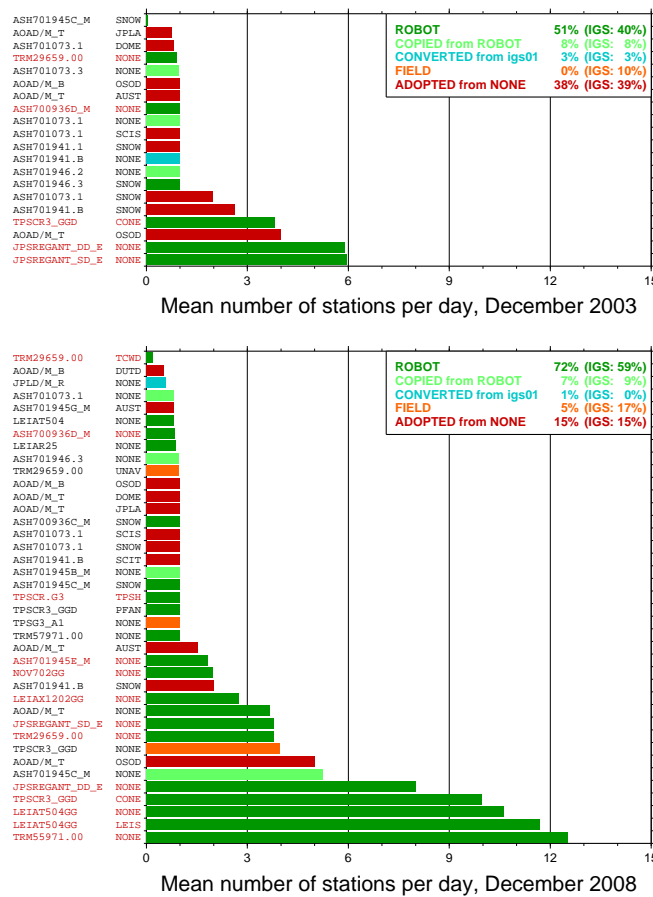


**Figure 4.3:** Number of combined GPS/GLONASS tracking stations in the processed network equipped with a specific antenna/radome combination (top: average over all days in December 2003, bottom: average over all days in December 2008). The colors characterize the calibration types (Rothacher and Schmid, 2006). The percentage of the different calibration types is given in the legend for igs05(upd).atx and in parentheses for the original igs05.atx model. Antenna types with red labels got updated PCC in igs05(upd).atx.

**Table 4.1:** Antenna/radome combinations with updated antenna PCC in igs05(upd).atx. A statistics on how many antennas and calibration runs did contribute to the “type-mean” values for GPS and GLONASS is provided. The number of stations provides an overview on the usage of the antenna/radome combination within the processed network (on reference frame stations, combined GPS/GLONASS tracking stations, and on GPS-only tracking stations).

Antenna	Radome	“Type-mean” values are derived from				Number of stations			Calibration type in igs05.atx	also used for
		GPS: No. of antennas	GPS: No. of calibrations	GLO: No. of antennas	GLO: No. of calibrations	Reference	GNSS	GPS-only		
ASH700936D_M	NONE	2	27	3	6	3	2	1	ROBOT	DOME, JPLA JPLA
ASH701945E_M	NONE	2	4	1	2	7	2	9	COPIED	
JPSREGANT_DD_E	NONE	24	153	1	6	0	8	0	ROBOT	
JPSREGANT_SD_E	NONE	15	74	1	5	1	7	0	ROBOT	
LEIAT504GG	NONE	25	49	21	41	2	8	0	ROBOT	
LEIAT504GG	LEIS	79	157	70	136	1	11	0	ROBOT	
LEIAX1202GG	NONE	14	28	14	28	0	1	0	FIELD	
NOV702GG	NONE	2	4	2	4	0	1	0	ROBOT	
TPSCR.G3	TPSH	60	120	58	113	1	4	0	ROBOT	
TPSCR3_GGD	CONE	159	385	47	94	1	13	0	FIELD	
TRM29659.00	NONE	18	36	16	31	13	2	12	ROBOT	DOME
TRM29659.00	TCWD	6	57	1	2	1	1	2	ROBOT	
TRM55971.00	NONE	59	116	59	116	2	11	2	ROBOT	

### 4.3.1 Update of the igs05.atx phase center model

The set of antenna PCC (contained in the file igs05.atx, maintained by the IGS) currently used by the IGS was compiled in 2005/06 when the absolute antenna phase center model was introduced (Schmid et al., 2007). According to the rules for the maintenance of that file (Gendt, 2006; Schmid, 2008) generally only new antenna/radome combinations are added. Therefore many corrections are up to four years old. Many additional antennas were calibrated since that time, which could help to improve the “type-mean” corrections of the corresponding antenna types. The calibration values contained in igs05.atx are based on GPS measurements only. GLONASS observations were not included due to the weak GLONASS constellation at that time. This is why the GPS-derived antenna PCC are also used for the GLONASS observations made on different frequencies.

More GLONASS satellites are active today than in 2005/06. Therefore, system-specific corrections for GPS and GLONASS can be determined using a robot (Wübbena et al., 2006). Table 4.1 lists all antenna/radome combinations contained in the reprocessed network, for which GNSS-specific PCC were available. The calibration values resulted in an updated version of igs05.atx, called from now on igs05(upd).atx, which was used for this study. Note that the new calibration values for GPS replace the existing values in the IGS file igs05.atx.

As a consequence, all reference frame stations using one of these antenna types have to be excluded from the datum definition because an offset in the estimated station coordinates is expected (see Sect. 4.3.2). Therefore, 35 out of 96 IGS reference frame sites were omitted for the datum definition. This results in a dilemma: one would like to have the most recent antenna PCC tables with as many individual calibrations for the “type-mean” values as possible, and one would like to maintain a stable geodetic reference frame at the same time.

The number of individual antennas and calibration runs used to obtain the updated GPS-specific antenna “type-mean” corrections for igs05(upd).atx reveals a strong imbalance between the different antenna/radome combinations (see Tab. 4.1). The “type-mean” values for the Ashtech and NovAtel antennas are both based on only two individual antennas. Thus, the redundancy is small. Fortunately these antenna types did not find widespread use in the IGS network (except for ASH701945E\_M NONE). Therefore it is expected this problem to have only marginal impact on the general results of this study.

There are several antennas with a limited number of individual antennas contributing to the GLONASS-specific antenna “type-mean” PCC (see Tab. 4.1). The conclusions emerging from this study may be in particular problematic for the two Javad Regant types, because they dominated the GLONASS tracking network prior to 2006 (about one third of the network was equipped with this combination).

Figure 4.3 (top), showing the number of stations in the reprocessed GLONASS tracking network of December 2003 equipped with a specific antenna/radome combination, illustrates the situation. About 50% of the stations are equipped with antenna

types for which robot calibrations are available (for the original `igs05.atx` model before the update the percentage is only 40%). `igs05(upd).atx` includes GLONASS-specific antenna PCC for about half of the stations (indicated by red-labeled antenna names in Fig. 4.3). This situation is more or less stable till the second half of 2006.

Figure 4.3 (bottom) illustrates the situation in December 2008, which is very close to the current state of the GLONASS tracking network used in the operational CODE processing. Note that there are new antenna types (in particular from Trimble and Leica) dominating the network. Most of these antenna types were calibrated with a robot. By updating the robot calibrations from `igs05.atx` to `igs05(upd).atx` the percentage of receiver/antenna combinations with a robot calibration grows from 59% to 72%. About two thirds of the GLONASS tracking stations available in December 2008 can be processed with GNSS-specific antenna PCC in this study (red labels in Fig. 4.3, bottom).

#### 4.3.2 Use of GNSS-specific phase center corrections

Before studying the impact of GNSS-specific antenna PCC it is possible to check the impact of the updated GPS corrections on the resulting station coordinates. Coordinate estimates from a solution using the original `igs05.atx` antenna PCC tables are compared to a solution using the updated `igs05(upd).atx` values. In both cases the GPS-derived corrections are used for the GPS and GLONASS measurements. The differences in the up component are shown in Fig. 4.4. They reach values of up to 5 mm, even though both solutions use the same set of reference stations for the no-rotation (NNR) condition in a minimum constraint solution for the datum definition. As expected the differences show systematics for the individual antenna types, regardless of whether the antenna was used at a GPS-only or a combined GPS/GLONASS tracking station (dark blue and red bars). Surprisingly, there are also a few stations that show differences of more than 1 mm, although the same antenna PCC are used in

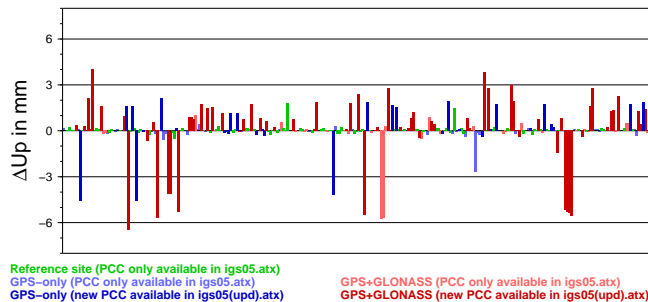


**Figure 4.4:** Differences of the station heights between solutions using the original `igs05.atx` and the updated `igs05(upd).atx` antenna PCC. The GPS-derived corrections are used for the GPS and the GLONASS measurements. The stations are sorted alphabetically, but they are not labeled. Both coordinate sets are computed from the entire interval of 6.5 years of the GLONASS extension of the CODE reprocessing as described in Sect. 4.2.

both computations (light blue and red bars). Most of these stations only observed for a limited number of days within the entire period of 6.5 years.

The differences between the elevation- and azimuth-dependent PCV for the GPS and GLONASS frequencies are in the range of a few mm for L1 and L2, respectively. According to Wübbena et al. (2006) these values are reproducible to within 0.3 to 0.4 mm. The differences between individual antennas of the same type have absolute values in the range of 2 – 3 mm for low elevations. Thus, the differences between GNSS-specific antenna PCC are significant, at least for those with a “type-mean” value derived from a suitable number of individual antennas.

When converting the elevation- and azimuth-dependent PCV for the L1 and L2 frequencies into the ionosphere-free linear combination (as they are needed for a global network analysis), the differences between the GPS- and GLONASS-specific corrections may reach 10 mm in absolute value. The differences for one of the Ashtech antennas are shown as a typical example in Fig. 4.5. Note that the mean difference between the GPS- and GLONASS-specific PCV corresponds to a time bias between the GPS and GLONASS measurements. Thus it is absorbed by the inter-system bias, which has to be taken into account in the multi-GNSS processing for each station at least as a constant bias between the receiver hardware delays of the individual GNSS.

In order to analyze the impact of the GNSS-specific antenna PCC on the mean station coordinates, the entire interval of the GLONASS extension of the CODE reprocessing (6.5 years) has been analyzed with the updated antenna PCC table. In a first run the GPS-derived corrections were used for both GPS and GLONASS measurements, whereas in the second run the GNSS-specific corrections were used. Two cumulative solutions have been derived considering mean station coordinates and velocities. The resulting time series of station positions have been analyzed with FODITS, a new component of the Bernese GPS Software. FODITS stands for “Find Outliers and Discontinuities in Time Series” (Ostini et al., 2008). The new tool was used to detect outliers and significant discontinuities in the station coordinate time series. The differences between the two coordinate sets (introducing identical outlier and discontinuity

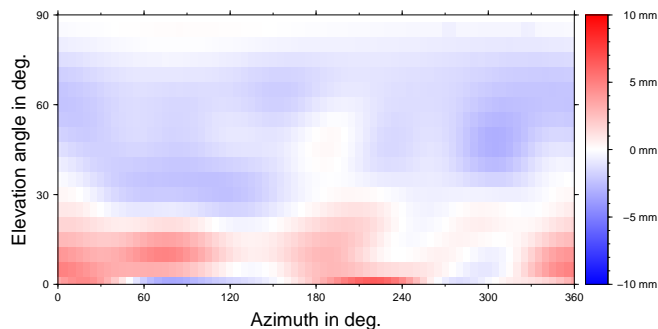


**Figure 4.5:** Differences between the PCV for GLONASS and GPS from GNSS-specific calibrations as a function of azimuth and elevation for the ASH701945E\_M NONE (the antenna phase center offset is identical for both GNSS). The influence on the ionosphere-free linear combination is shown.

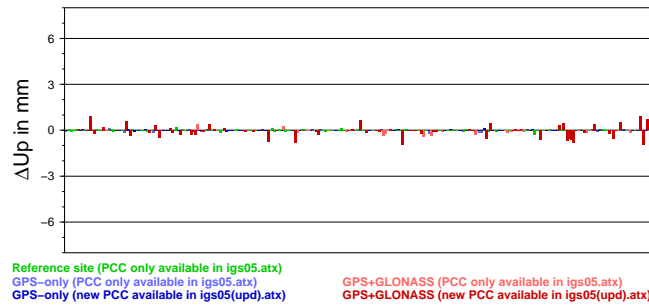


**Figure 4.6:** Differences of the station heights between solutions considering and ignoring GLONASS-specific PCC, respectively. Both coordinate sets are computed from the entire interval of 6.5 years of the GLONASS extension of the CODE reprocessing. (Same scale as in Fig. 4.4 has been used for comparison.)

definition) in the vertical component are provided in Fig. 4.6. They are very small and reach values of 1 mm at maximum. These differences show, not unexpectedly, systematic effects as a function of the antenna type.

The small absolute value of the differences is surprising in view of the fact that the differences between GLONASS- and GPS-specific PCV (as, e.g., shown in Fig. 4.5) are about twice as large as the PCV differences causing the coordinate differences in Fig. 4.4. It was already mentioned that the average of the difference between GNSS-specific antenna PCC is absorbed by the inter-system bias. There are, however, several other reasons for the marginal impact of GNSS-specific PCC on the estimated station coordinates:

1. The GLONASS constellation consists only of half of the number of satellites in the GPS constellation during the analyzed time span (slowly increasing to about two thirds towards the end of 2008).
2. A much smaller number of GLONASS ambiguities were resolved than in the case of GPS, because ambiguity resolution for GLONASS was only enabled for baselines shorter than 20 km.
3. Schaer et al. (2009) found evidence that the inter-system biases between GPS and GLONASS significantly deviate from a constant. As the current multi-GNSS processing usually implies this behavior the solution cannot benefit in an optimal way from the additional measurements.

These reasons might explain why the averaged station coordinates are so clearly dominated by GPS.

In view of the sizable differences between GPS- and GLONASS-specific antenna PCC and of the continuously increasing number of available GLONASS satellites, which enhances the impact of GLONASS on the combined solution, GNSS-specific antenna PCC should be applied whenever processing multi-GNSS data sets.

## 4.4 Satellite antenna phase center modeling

### 4.4.1 Motivation

The currently used `igs05.atx` model includes in addition to the receiver antenna calibrations consistent corrections for the satellite antennas. The nadir-dependent corrections for the satellite antenna phase center are mean values for all satellites of the same type (no azimuth-dependence has been considered so far). The PCO are provided individually for each satellite. The values in `igs05.atx` were determined in 2005 and in early 2006 (Schmid et al., 2007)

Block mean values were defined and used for the satellites launched since that time. The following GPS satellites are affected:

SVN 52/PRN G31 (launched on September 25, 2006),  
 SVN 58/PRN G12 (November 17, 2006),  
 SVN 55/PRN G15 (October 17, 2007),  
 SVN 57/PRN G29 (December 20, 2007),  
 SVN 48/PRN G07 (March 15, 2008), and  
 SVN 49/PRN G01 (March 24, 2009)  
 (Satellites launched after December 2008 are not included because the computations for this paper were started in early 2009.)

This number of satellites corresponds to about 16% of the entire constellation of 32 GPS satellites in May 2009.

The situation is even more dramatic for the GLONASS satellites. Due to the short lifetime of the older GLONASS satellites, in May 2009 there is an almost completely new GLONASS constellation compared to 2005/06 (only three satellites from end of 2005 are still active in May 2009, namely SVNs 701, 712, and 795, see Fig. 4.7).

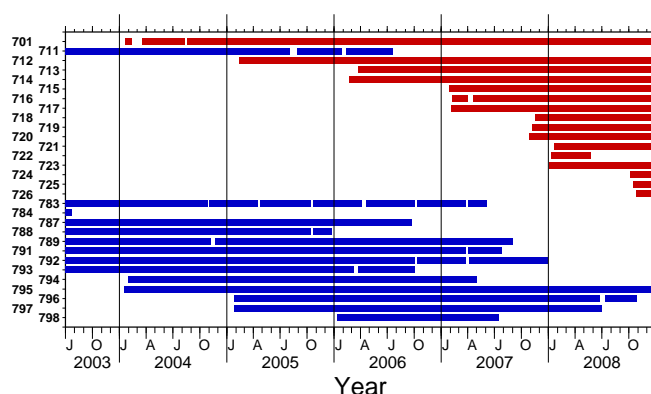


**Figure 4.7:** Development of the GLONASS constellation since June 2003 until end of 2008 (a satellite is indicated as active as soon as an orbit determination was possible in the operational CODE final solution). The blue bars indicate the old style GLONASS satellites whereas red bars are used for the modernized GLONASS-M satellites. SVN 711 is a prototype of the GLONASS-M series.

An update of the satellite antenna phase center model — at least for these newly launched satellites — is therefore badly needed. The following sections discuss the process of updating the satellite antenna phase center model for all GLONASS and for the youngest GPS satellites.

### 4.4.2 Computation of the satellite antenna model update

The satellite antenna PCC were derived from the GLONASS extension of the CODE reprocessing. From the independent one-day solutions, three-day solutions were derived by combining the three corresponding one-day normal equations. As the number of orbit parameters is comparable in the one-day and three-day orbits, the three-day orbits are much better defined than the one-day orbits. This is in particular true for those GLONASS satellites, which were observed mainly over Europe. The step from the one-day to the three-day orbits is essential, because the orbit parameters and the satellite antenna PCC are highly correlated. Six initial osculating orbital elements and nine empirical parameters (three constant and six once-per-revolution parameters in  $D$ -,  $Y$ -, and  $X$ -directions according to the orbit model described in Beutler et al., 1994) are set up for each satellite arc, where the periodic terms of the  $D$ - and  $Y$ -components are constrained to zero. Empirical velocity changes (so called pseudo-stochastic pulses) are set up and solved for at 12 hour intervals.

The three-day solutions (more than 2000) were then combined to generate a cumulative solution. Again FODITS was used to detect outliers and significant discontinuities in the station coordinate time series. The reference frame was aligned with the ITRF2005 using stations provided in the IGS05 (an IGS-specific realization of ITRF2005; Altamimi et al., 2007) together with NNR conditions applied to a minimum constraint solution. The station coordinates and velocities resulting from this step were introduced as known when computing the satellite antenna PCC. The `igs05.atx` values for all satellite antennas were kept fixed for datum definition. Different sets of coordinates and velocities were computed using the different scenarios for handling the receiver antenna PCC, but using the same set of reference stations together with the same list of outliers and discontinuities.

### 4.4.3 Update of the satellite antenna phase center offsets

To keep the updated satellite antenna model consistent (in scale) with `igs05.atx`, the PCO of the GPS satellites launched before 2005 were fixed to their `igs05.atx` values. Only the  $Z$ -offsets for the five new GPS satellites (see the Sect. 4.4.1) and for the GPS satellite SVN 53, PRN G17 (launched on September 26, 2005) were estimated, because no or only a very limited amount of data contributed to the `igs05.atx` values for these satellites. The  $Z$ -offsets for all GLONASS satellites were recomputed because of the high uncertainty of these values in `igs05.atx`, which was caused by the sparse GLONASS network of about 30 stations (located moreover mainly in Europe at that time).

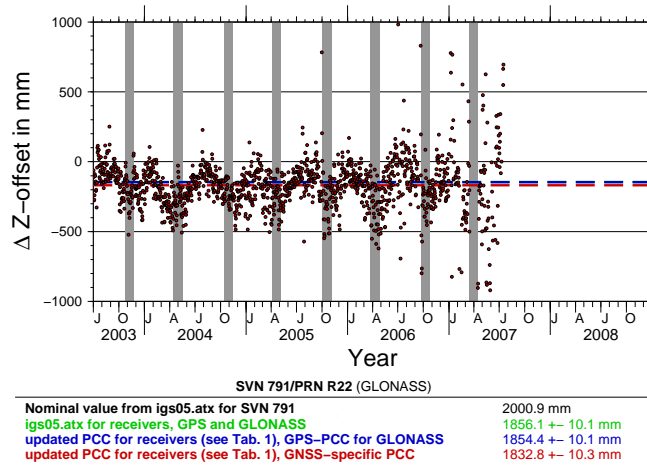


**Figure 4.8:** Differences between satellite antenna phase center  $Z$ -offset for GLONASS satellite SVN 791 (PRN R22) from three-day solutions of the GLONASS extension of the CODE reprocessing and the values in igs05.atx. The shaded periods indicate the eclipse periods. The dashed lines indicate the mean values of the three scenarios for handling the receiver antenna PCC, see text (note, the green line is located behind the blue one).

The time series of estimates for the satellite antenna PCO ( $Z$ -component) from the three-day solutions with respect to the corresponding igs05.atx value is shown for one of the GLONASS satellites (SVN 791, PRN R22) in Fig. 4.8. The shaded areas indicate the eclipse periods. A correlation between the noise pattern of the estimated antenna PCO and the eclipse periods is clearly visible. This observation indicates that the  $Z$ -offset is correlated with the orientation of the orbital plane with respect to the Sun, which in turn influences the correlation between the  $Z$ -offset and the radiation pressure parameters. The noise of the  $Z$ -offsets increases towards the end of the time series, when the satellite was no longer reliably tracked by the stations.

The mean satellite antenna PCO computed from this time series is also plotted in Fig. 4.8. Three options for handling the receiver antenna PCC (mainly for the GLONASS observations) were used for comparison purposes:

- Green: The original igs05.atx receiver antenna PCC were applied, implying that the GPS-derived values are also used for the GLONASS measurements.
- Blue: Updated GPS receiver antenna PCC igs05(upd).atx where applied where available (see Tab. 4.1), whereas the igs05.atx corrections were introduced for the other antennas. The GPS-derived corrections were used for both the GPS and the GLONASS data.
- Red: Updated receiver antenna PCC igs05(upd).atx are used (see Tab. 4.1). GNSS-specific corrections were applied for the GPS and the GLONASS data.

The three mean  $Z$ -offsets were estimated using the full covariance information by combining the corresponding normal equations. The stated uncertainty is the standard deviation of the mean offset derived from the time series. The three  $Z$ -offsets significantly differ by about 150 mm from the currently used igs05.atx value. On the

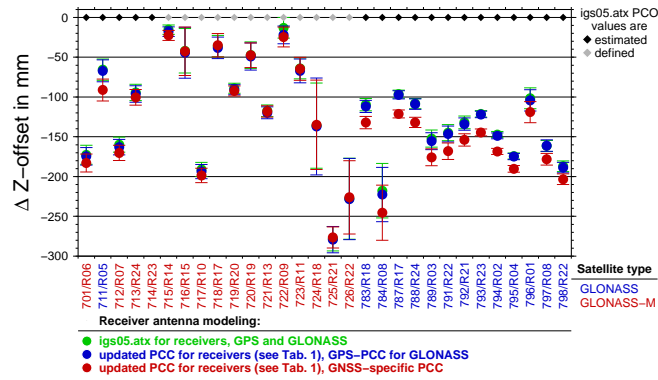


**Figure 4.9:** Differences of the new mean satellite antenna phase center  $Z$ -offsets for the GLONASS satellites with respect to igs05.atx (diamonds). The receiver antenna phase centers: original igs05.atx corrections (green); igs05(upd).atx with GPS-derived corrections for GLONASS (blue); igs05(upd).atx with GNSS-specific corrections for GPS and GLONASS observations (red). The error bars indicate the uncertainty of the mean offset as derived from the entire time series of three-day solutions. (SVN 711 is a prototype of the GLONASS-M series; SVN 714 outside of the diagram).

one hand, the two solutions based on GPS-derived receiver antenna corrections for GLONASS (“Green” and “Blue”) agree very well. The  $Z$ -offset emerging from solution “Red” using GNSS-specific corrections, on the other hand, differs by 22 mm from these two solutions.

Figure 4.9 gives an overview of the corresponding values for the complete GLONASS constellation active in the time span of 6.5 years, where only satellites observed for at least 90 days are included. The difference of about 20 mm between using GNSS-specific receiver antenna PCC (“Red”) and the other two solutions is approximately the same for all older GLONASS satellites. The difference is smaller for the GLONASS-M satellites. For the youngest satellites SVN 718 up to 726 (SVN 716 might also belong to this group, but only few observations were available till summer 2007, because many receivers needed a firmware upgrade to enable tracking of this satellite with frequency channel zero), it even vanishes. These GLONASS-M satellites were launched in 2007 or 2008 when most of the older GLONASS satellites were already inactive. In the same time period the number of different GNSS receiver antenna types in the tracking network grew. Therefore, either the characteristics of the two satellite antenna types are different or some of the systematic differences between GNSS-specific receiver antenna PCC are absorbed by the satellite antenna  $Z$ -offsets. Note that the GLONASS tracking network was dominated by two Javad Regant types in the early days, see Fig. 4.3 (top). A full consistency of the receiver and satellite antenna corrections is, in any case, a requirement to achieve high-quality results.

#### 4.4.4 Update of the satellite antenna phase center variations

Using the previously estimated satellite antenna PCO as known, consistent nadir-dependent satellite antenna PCV can now be established. For this purpose, a zero-mean condition was imposed for the estimated PCV of each satellite antenna, which is why corrections for all GPS and GLONASS satellites could be estimated simultaneously.

The nadir-dependent satellite antenna PCV are not sensitive to the three different scenarios for handling the receiver antenna PCC. Therefore only the most sophisticated solution with GNSS-specific receiver antenna PCC (“Red”) is subsequently discussed.

Figure 4.10 compares the yearly solutions for the nadir-dependent satellite antenna PCV as derived from the GLONASS extension of the CODE reprocessing. Stable solutions were obtained for all GPS and GLONASS satellites. The yearly solutions coincide to within  $\pm 1$  mm. Only for nadir angles of  $0^\circ$  (GPS and GLONASS),  $14^\circ$  (GPS), and  $15^\circ$  (GLONASS) the variations are somewhat larger due to the limited number of observations contributing at these angles. As opposed to GPS, corrections for nadir angles up to  $15^\circ$  can be reliably estimated for GLONASS from ground stations thanks to the lower orbit height of these satellites. `igs05.atx` does, however, only contain corrections up to nadir angles of  $14^\circ$ .

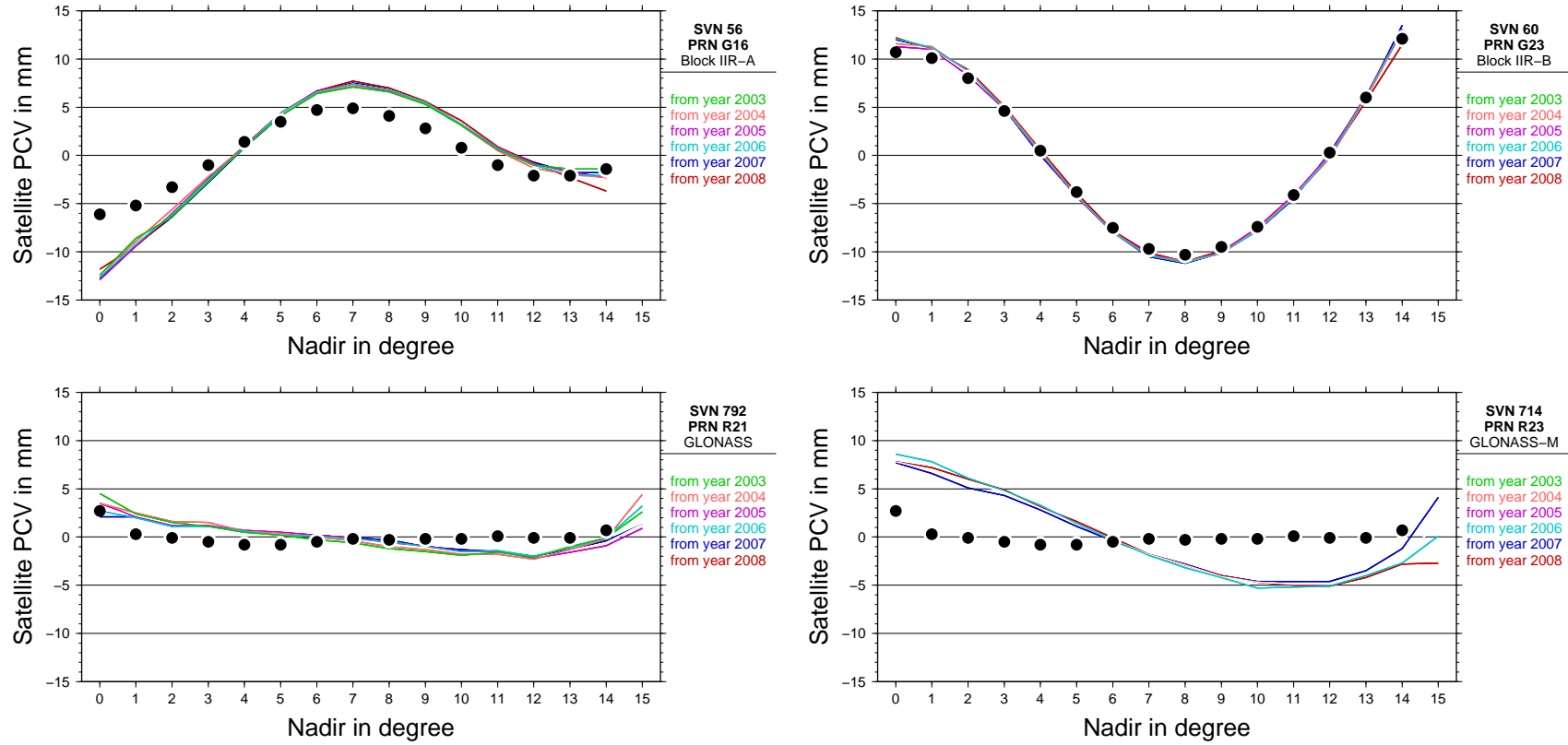
For most of the satellites the nadir-dependent PCV from `igs05.atx` (black dots) and from our estimation were very close (e.g., for SVN 60, PRN G23, Fig. 4.10, top, right). For some GPS and GLONASS satellites, however, the new PCV show small, but significant differences with respect to the values in `igs05.atx` (e.g., for SVN 792, PRN R21, Fig. 4.10, bottom, left). Differences of a few millimeters may be understood because `igs05.atx` only contains block-specific mean PCV (Schmid et al., 2007). The largest differences between our new corrections and those in `igs05.atx` are those for SVN 56 (Fig. 4.10, top, left) for GPS and for SVN 714 (Fig. 4.10, bottom, right) for GLONASS. In both cases the new set of nadir-dependent corrections are almost the same in the available yearly solutions.

Figure 4.11 gives an overview of the consistency of the nadir-dependent satellite antenna PCV for all satellites of each type and compares them to the block-specific `igs05.atx` values.

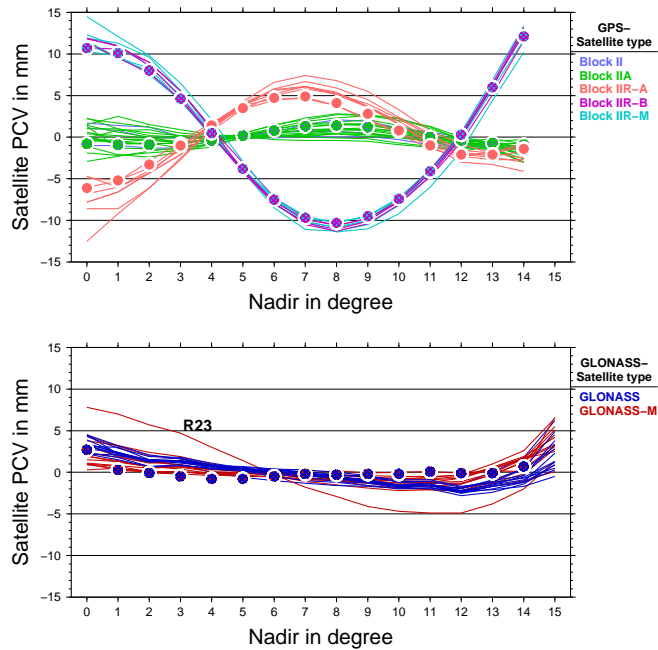
Schmid et al. (2007) distinguish three satellite groups of common antenna behavior for the GPS, namely Block II/IIA, Block IIR-A, and Block IIR-B/IIR-M.

Figure 4.10 says, however, that the differences of the corrections between individual satellites of a group are small, but significant. This results in the proposal that satellite-specific antenna PCV should be considered for future antenna phase center models. There are, however, two important arguments in favor of the current strategy based on a minimum number of parameters:

- Additional parameters might weaken the normal equation system.



**Figure 4.10:** Examples of yearly solutions for the nadir-dependent satellite antenna PCV for individual GPS (top) and GLONASS (bottom) satellites. The colors refer to the individual yearly solutions. The black dots mark the igs05.atx corrections.



**Figure 4.11:** Nadir-dependent satellite antenna PCV for all GPS (top) and GLONASS (bottom) satellites observed for more than 90 days during the GLONASS extension of the CODE reprocessing. The colors indicate the different satellite types, the dots illustrate the corresponding igs05.atx corrections.

- As each GPS satellite follows the same ground track day after day the station-specific observation geometry is repeated day after day, as well. Therefore, station-specific effects may cause systematic satellite-specific errors, e.g., errors in the satellite antenna PCV.

The inclusion of observations from Low Earth Orbiting satellites (LEO) might mitigate this problem. As opposed to a terrestrial site, the LEOs track the GNSS satellites more uniformly. Calibration of the spaceborne GPS antennas is, on the other hand, a challenging task because of local multipath and cross-talk effects (Jäggi et al., 2009).

The impact of station-dependent effects might, e.g., be studied by comparing satellite-specific PCV derived from solutions using different and independent tracking networks.

The older and the modernized GLONASS satellites obviously show a similar behavior. The scatter of the nadir-dependent GLONASS PCV is comparable to that of the two older generations of GPS satellites (see Fig. 4.11).

The satellite-specific PCV for GLONASS show a similar behavior as in the case of GPS. The scatter between the individual satellites in Fig. 4.11 is, on one hand, larger than the scatter between the yearly solutions for the individual satellites (see Block II/II A and Block IIR-A in Fig. 4.10). On the other hand, the GLONASS satellites are not observed as intensely as the GPS satellites (fewer stations, not well globally distributed). The GLONASS constellation has, however, the advantage that

each satellite is observed by the complete tracking network within 17 revolutions corresponding to eight sidereal days. Therefore, the derived GLONASS parameters are less dependent on the tracking network.

One GLONASS–M satellite, namely SVN 714, PRN R23, shows a significantly different behavior in the satellite antenna phase center (PCO in Fig. 4.9 and PCV in Fig. 4.10 and 4.11). The mean  $Z$ -offset is, however, only 3 cm larger than the mean value of all GLONASS–M satellites. As this satellite became active in February 2006, the time slot for computing the corresponding igs05.atx corrections was (in particular in view of the sparse tracking network) not long enough to detect the anomalous behavior of that particular satellite. The assumption that all GLONASS satellites had the same nadir-dependent PCV led to an igs05.atx value for the PCO which was off by about 40 cm. Recently, the value for PRN R23 was corrected (Dilssner et al., 2009).

## 4.5 Validation of the satellite antenna phase center models

In Sect. 4.3.2 it was suggested that GNSS-specific receiver antenna PCC should be used as soon as reliable values would become available. The satellite antenna phase center model for the GLONASS satellites was also updated whereas the igs05.atx values for the old GPS satellites were fixed (see Sect. 4.4).

To validate these two conclusions the following solutions have generated:

- S<sub>1</sub>:** The IGS convention for the GPS-derived receiver antenna PCC for GPS and GLONASS measurements is used. The values in the file igs05.atx are used for the satellite antennas.
- S<sub>2</sub>:** The GNSS-specific PCC for the receiver antennas igs05(upd).atx (as available in Tab. 4.1) and the new satellite antenna PCC are used (derived in Sect. 4.4).

The differences of the results from both solutions are discussed in this section by studying the arc overlaps, the residuals of Satellite Laser Ranging (SLR) measurements, the station coordinates estimated over long time periods, and the results of the kinematic positioning method.

### 4.5.1 Impact of the updated antenna phase center model on the GLONASS satellite orbits

The orbits of two consecutive days  $i$  and  $i + 1$  should provide identical positions for each satellite for the midnight epoch  $t + 1$ :  $\vec{r}_i(t + 1) = \vec{r}_{i+1}(t + 1)$ . The resulting discontinuities  $|\vec{r}_i(t_{i+1}) - \vec{r}_{i+1}(t_{i+1})|$  may serve as quality indicators of a particular series of orbits. In an analogous manner discontinuities may be calculated for the velocity vectors. The orbits  $\vec{r}_i(t)$  actually used here for this purpose are those corresponding to the middle day of three-day arcs, in the way they are generated by the

**Table 4.2:** Sum of differences according to Eq. (4.1) at the day boundaries using the IGS standard and the updated satellite antenna PCC from Sect. 4.4, respectively. Only satellites with at least 400 day boundary values are included. The GLONASS-M satellites are in the upper, the first generation of GLONASS satellites in the lower part.

PRN	SVN	Number of arc boundaries	Differences in the	
			position in mm	velocity in mm/s
R06	701	1518	944	288
R05	711	979	326	75
R07	712	1263	1350	240
R24	713	929	424	59
R23	714	957	1285	197
R14	715	684	47	-15
R15	716	482	97	7
R10	717	682	122	47
R20	719	407	103	13
R19	720	418	276	27
R18	783	1208	671	73
R17	787	1164	658	184
R24	788	827	891	221
R03	789	1428	85	203
R22	791	1399	1644	336
R21	792	1539	2456	343
R23	793	952	871	223
R02	794	1160	680	196
R04	795	1792	1082	264
R01	796	1224	997	238
R08	797	1207	953	163
R19	798	519	448	126

CODE analysis center, see Ineichen et al. (2003). Consecutive three-day arcs are not independent but they are required because of the poor GLONASS tracking geometry outside Europe.

The differences between the solutions  $S_1$  and  $S_2$  at the day boundaries were computed for the position and for the velocity vectors:

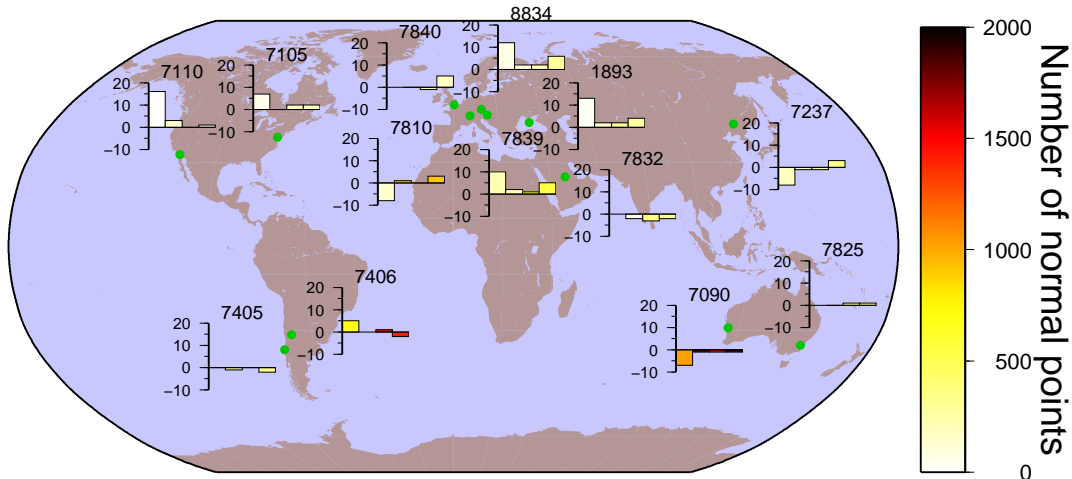
$$\begin{aligned}
 \Delta r_i &= +|\vec{r}_{S_1,i}(t_{i+1}) - \vec{r}_{S_1,i+1}(t_{i+1})| \\
 &\quad - |\vec{r}_{S_2,i}(t_{i+1}) - \vec{r}_{S_2,i+1}(t_{i+1})| \\
 \Delta v_i &= +|\vec{v}_{S_1,i}(t_{i+1}) - \vec{v}_{S_1,i+1}(t_{i+1})| \\
 &\quad - |\vec{v}_{S_2,i}(t_{i+1}) - \vec{v}_{S_2,i+1}(t_{i+1})|
 \end{aligned} \tag{4.1}$$

The differences  $\Delta r_i$  and  $\Delta v_i$  are summed up for each satellite over the entire time span of the comparison. The result for the GLONASS satellites is provided in Tab. 4.2. A positive sum of differences indicates on the average larger discontinuities for the solution  $S_1$ , implying that the more sophisticated GLONASS antenna phase center model from solution  $S_2$  is preferable.

The mean position discontinuity per day, averaged over all GLONASS satellites, is only reduced from 63.8 to 63.0 mm due to the use of updated antenna PCC. For the GLONASS-M satellites the benefit is even smaller (from 62.8 to 62.4 mm). The improvement thus amounts to about 1% for the complete constellation (from 63.3 to 62.7 mm). The benefit is small, but the orbit quality consistently improves for all satellites, except for SVN 715.

#### 4.5.2 Validating the GLONASS orbits using SLR data

The quality of GLONASS orbits may also be validated using the SLR measurements (normal points) provided by the International Laser Ranging Service (ILRS, Pearlman et al., 2002) and the distances between the satellite and the microwave tracking station at the epoch of the SLR measurement. The differences between the two observations are called SLR residuals in this paper. The coordinates of the ILRS sites were taken from the file SLRF2005 (a special reference frame currently used



ILRS ID	Station location	ILRS ID	Station location
7840	Herstmonceux United Kingdom	7090	Yarragadee Australia
8834	Wettzell Germany	7825	Mt. Stromlo Australia
7810	Zimmerwald Switzerland	7110	Monument USA
			Peak
7839	Graz Austria	7105	Greenbelt USA
1893	Katziwely Ukraine	7405	Concepcion Chile
7832	Riyadh Saudi Arabia	7406	San Juan Argentina
7237	Changchun China		

**Figure 4.12:** Mean differences of the absolute values of the SLR residuals between the three-day GLONASS orbits computed with original igs05.atx or updated antenna PCC (Tab. 4.1 and Sect. 4.4) in mm. Only SLR stations (green dots) with at least 400 normal points in 2008 were included. The four bars per tracking station indicate the residual differences for the GLONASS satellites 712 (PRN R07), 723 (PRN R11), 716 (PRN R15), and 713 (PRN R24), respectively. The colors of the bars indicate the number of normal points contributing to this statistics.

within the ILRS) to generate the residuals for the two sets of GLONASS orbits. Four GLONASS satellites were tracked by ILRS stations in 2008: SVN 712/PRN R07 (only from January to May), SVN 723/PRN R11 (only from June to December), SVN 716/PRN R15, and SVN 713/PRN R24 (both throughout the year). Fig. 4.12 shows the mean differences of the absolute values of the residuals between the orbit solutions  $S_1$ – $S_2$ .

Most of the mean differences are positive, implying that the residuals were reduced by the updated antenna phase center model. Satellite SVN 712 is an exception, showing negative differences for some of the SLR stations, namely 7810: Zimmerwald, 7237: Changchun, and 7090: Yarragadee. Stations located in the vicinity of the three sites do, however, show a different behavior. This is in particular true for Zimmerwald (7810) and Wettzell (8834) (for a few time periods) when tracking SVN 712 at the same time. The effect is probably related to station problems, which were not taken into account in our validation procedure, described in Urschl (2007). There was, e.g., not attempt to consider station-specific range biases.

### 4.5.3 Impact of the updated satellite antenna phase center model on station coordinates

In order to study the impact of the updated satellite antenna PCC on the reference frame, the updated PCC for the GLONASS satellites from Sect. 4.4 were used to generate a new set of station coordinates and velocities for the full interval of the GLONASS extension of the CODE reprocessing. The resulting coordinates were compared to the coordinates obtained with the original `igs05.atx` corrections for the GLONASS satellites. Both solutions were based on the same corrections for the GPS satellites and for the receiver antennas (`igs05(upd).atx`). The differences between the vertical components of the two solutions are below the 1 mm limit — the horizontal ones are even smaller.

Obviously, the updated GLONASS satellite antenna PCC do not have a significant influence on the coordinates. This is consistent with the findings in Sect. 4.3.2, where it was already shown that GLONASS has only a small impact on the estimated coordinates. One may also draw the conclusion that the updated satellite antenna corrections do not have a negative impact on the reference frame.

### 4.5.4 Impact of the updated antenna phase center model on kinematic positioning

Dach et al. (2009) and Ineichen et al. (2008) showed that GLONASS observations used in addition to GPS measurements have a significant impact on coordinates estimated in the rapid-static mode (based on short data spans). One may therefore expect that the coordinates calculated in the kinematic mode are also prone to the use of different phase center models.

The global network was processed with a sampling rate of 30 s over ten days in December 2008 (days of year 350 to 359) to study the impact of the antenna phase

**Table 4.3:** Standard deviation of the mean station height over a certain time interval (15 or 60 min) derived from a kinematic coordinate estimation. Different observations were processed (GPS-only, GLONASS-only, and fully combined GPS/GLONASS); in addition, the modeling of the antenna PCC for the receiver and satellite antennas was varied:

igs05.atx for rec. IGS standard receiver antenna PCC from igs05.atx derived from GPS observations are used for both GPS and GLONASS measurements

igs05(upd).atx for rec. igs05.atx was updated with GNSS-specific receiver antenna PCC (see Tab. 4.1)

igs05.atx for sat. IGS standard antenna PCC from igs05.atx are used for all satellites

igs05(upd).atx for sat. IGS standard antenna PCC from igs05.atx are only used for GPS satellites, whereas for the GLONASS satellites the PCC derived in Sect. 4.4 are introduced

The values are given in mm.

Station	Antenna	Radome	GPS-only igs05.atx for rec. igs05.atx for sat.		GPS/GLONASS igs05.atx for rec. igs05.atx for sat.		GPS-only igs05(upd).atx for rec. igs05.atx for sat.		GPS/GLONASS igs05(upd).atx for rec. igs05.atx for sat.		GLONASS-only igs05.atx for rec. igs05.atx for sat.		GLONASS-only igs05(upd).atx for rec. igs05.atx for sat.	
			15 min		15 min		15 min		15 min		60 min		60 min	
MAS1	ASH701945E_M	NONE	1.7	1.5	1.7	1.5	1.5	1.5	7.0	8.0	14.9	16.1		
CAGZ	JPSREGANT_DD_E	NONE	1.3	1.1	1.3	1.1	1.1	1.1	2.9	2.9	3.1	3.2		
CRAR	JPSREGANT_DD_E	NONE	2.5	1.7	2.5	1.7	1.7	1.7	3.6	3.6	2.9	2.9		
UNB3	JPSREGANT_DD_E	NONE	1.1	0.9	1.1	0.9	0.9	0.9	2.0	2.0	2.0	2.0		
IRKJ	JPSREGANT_SD_E	NONE	1.3	1.0	1.3	1.0	1.0	1.0	3.6	3.5	4.2	4.1		
ZIMJ	JPSREGANT_SD_E	NONE	1.2	1.0	1.2	1.0	1.0	1.0	2.7	2.8	2.3	2.4		
BZRG	LEIAT504GG	LEIS	1.4	1.1	1.4	1.1	1.1	1.1	6.8	6.8	14.0	14.0		
RCMN	LEIAT504GG	LEIS	1.7	1.5	1.7	1.5	1.5	1.5	3.8	3.8	3.6	3.6		
TSEA	LEIAT504GG	LEIS	2.1	1.6	2.1	1.6	1.6	1.6	3.3	3.3	3.1	3.0		
HYDE	LEIAT504GG	NONE	1.7	1.5	1.7	1.5	1.5	1.5	4.3	4.4	8.5	8.4		
JOZ2	LEIAT504GG	NONE	1.2	0.9	1.2	0.9	0.9	0.9	2.5	2.4	2.5	2.3		
PDEL	LEIAT504GG	NONE	1.5	1.2	1.5	1.2	1.2	1.2	3.2	3.2	3.3	3.2		
BARH	LEIAX1202GG	NONE	1.8	1.4	1.8	1.4	1.4	1.4	4.3	4.4	7.0	7.2		
REYK	TPSCR.G3	TPSH	1.6	1.3	1.6	1.3	1.3	1.3	2.6	2.5	2.1	2.1		
AZCO	TPSCR3_GGD	CONE	2.7	2.1	2.7	2.1	2.1	2.1	7.0	6.9	10.1	10.6		
CONZ	TPSCR3_GGD	CONE	1.8	1.5	1.8	1.4	1.5	1.5	7.5	7.4	20.3	20.0		
FFMJ	TPSCR3_GGD	CONE	1.2	1.0	1.2	1.0	1.0	1.0	2.2	2.2	1.8	1.8		
WTZJ	TRM29659.00	NONE	1.2	1.1	1.2	1.1	1.1	1.1	2.6	2.6	2.1	2.0		
GANP	TRM55971.00	NONE	1.6	1.2	1.6	1.2	1.2	1.2	3.0	3.1	2.8	2.8		
REUN	TRM55971.00	NONE	3.0	2.4	3.0	2.4	2.4	2.4	14.8	14.3	24.5	22.5		
ROSA	TRM55971.00	NONE	3.0	2.3	3.0	2.4	2.3	2.3	7.0	6.9	9.4	9.1		
ZIM2	TRM55971.00	NONE	1.5	1.2	1.5	1.2	1.2	1.2	3.1	3.1	2.6	2.5		
Mean over all stations			1.7	1.4	1.7	1.4	1.4	1.4	4.5	4.6	6.7	6.6		

centers. A few stations representing the antennas with updated PCC (see Tab. 4.1) on different continents were treated as kinematic. The coordinates of all the remaining stations, the satellite orbits, and the Earth rotation parameters were introduced as known values from the daily processing of the static network.

Approximately 28,800 positions for each of the kinematic stations were assigned to adjacent subintervals with lengths of either 15 or 60 min. The 30 or 120 positions within each interval were used to compute the standard deviation of the mean values of the coordinates. The arithmetic mean of the standard deviations from all 960 or 240 intervals is provided in Tab. 4.3. Four sets of solutions (experiments) are discussed subsequently. The first set is represented by columns 4 and 5, the second by columns 6, 7, and 8, the third by columns 9 and 10, and the fourth by columns 11 and 12.

The first set of solutions in Tab. 4.3, based on 15 min intervals, compares the GPS-only and the combined GPS/GLONASS solution applying identical receiver antenna PCC for the GPS and GLONASS measurements — corresponding to current practice in the IGS. Despite this deficiency the standard deviation of the mean station height for intervals of 15 min is improved. 32 GPS and 16 GLONASS satellites were active in December 2008. Assuming a white noise law, one would expect an improvement by a factor of  $\sqrt{1.5} \approx 1.22$  due to the additional GLONASS observations. This value was achieved for many of the analyzed sites.

The updated GNSS-specific receiver antenna PCC model `igs05(upd).atx` was used for a second set of solutions, also based on 15 min intervals. The GPS-only and the combined GPS/GLONASS solution (first two solutions of the second set) are compared as in the previous experiment and the results are the same. The third of the second set of solutions used the updated satellite antenna PCC from Sect. 4.4 for the GLONASS satellites and was based on a combination of GPS and GLONASS. Compared to the solution using the IGS satellite antenna PCC the differences are below 0.1 mm. This result could be expected, because the satellite geometry does not change substantially during the 15 min intervals. The antenna phase center model therefore has only a systematic influence on the mean value of a rapid-static solution, but does not show up in the standard deviation of the mean coordinates.

The third set of solutions in Tab. 4.3 is based on GLONASS only. The impact of the updated antenna PCC on the standard deviations of the coordinates is slightly larger than in the combined case. It is, on one hand, remarkable that a rapid-static solution is at all possible with the limited number of active GLONASS satellites (16 in December 2008). The noise of these solutions is, on the other hand and not unexpectedly, larger than the corresponding noise of the GPS-only solution, in particular for stations with a weak satellite geometry during a significant part of the day (e.g., CONZ and REUN).

As the effect of the antenna PCC on the 15 min solutions is limited, the fourth set of solutions (corresponding to the last two columns in Tab. 4.3) is fictitious 60 min coordinate solutions. As the satellite geometry changes significantly within 60 min, the antenna phase center model should have more influence on the standard deviations of the hourly solutions. Two GLONASS-only solutions are compared in Tab. 4.3

**Table 4.4:** RMS of the hourly mean coordinates derived from a kinematic positioning considering only GLONASS measurements. Different satellite antenna phase center models were applied (descriptions of the solution IDs are given in Tab. 4.3). The values are given in mm.

Station	GLONASS-only igs05(upd).atx for rec. igs05.atx for sat.			GLONASS-only igs05(upd).atx for rec. igs05(upd).atx for sat.		
	north	east	up	north	east	up
MAS1	1.2	5.6	6.2	0.5	5.1	6.4
CAGZ	5.2	12.7	0.8	4.7	12.3	0.6
CRAR	0.7	1.1	0.7	0.6	1.4	0.0
UNB3	0.7	0.0	0.8	0.4	0.0	0.6
IRKJ	5.5	1.5	5.4	5.4	3.3	5.8
ZIMJ	0.0	0.0	0.3	0.1	0.0	0.1
BZRG	1.2	3.9	3.4	1.3	4.5	3.7
RCMN	1.7	3.7	2.0	1.6	3.7	2.0
TSEA	2.9	3.0	6.2	3.5	1.5	6.8
HYDE	1.3	4.7	16.5	3.5	5.2	19.4
JOZ2	0.5	0.8	0.9	0.5	0.6	0.9
PDEL	0.6	3.1	7.5	0.6	3.0	7.6
BARH	1.8	0.3	0.2	1.6	0.6	1.3
REYK	0.1	0.8	0.9	0.1	0.8	0.6
AZCO	4.0	1.0	28.6	3.1	1.1	27.3
CONZ	66.5	185.4	125.7	61.3	184.8	99.8
FFMJ	0.4	0.8	0.7	0.5	0.7	0.5
WTZJ	0.5	0.7	2.0	0.5	0.7	2.0
GANP	0.7	0.1	3.6	0.7	0.0	3.6
REUN	27.4	104.8	105.5	27.8	114.5	101.2
ROSA	7.6	2.9	1.9	7.7	2.4	1.6
ZIM2	0.0	0.1	0.2	0.1	0.0	0.1
Mean	6.2	15.9	15.6	6.0	16.4	14.2

both using the GLONASS-specific receiver antenna PCC from igs05(upd).atx. The first solution uses the igs05.atx GLONASS satellite antenna corrections, the second one the updated values provided in Sect. 4.4. A small benefit of using the improved antenna phase center model results in the case of the 60 min solution (10 stations have smaller, 5 larger standard deviations, and 7 are on the same level). Note that other effects like near-field multipath also have an impact on these values. Such site-specific issues play a more important role for the 60 min solutions because of the reduced redundancy of the kinematic GLONASS-only solution compared to a GPS-only (double number of satellites) or a combined GPS/GLONASS (triple number of satellites) solution.

For the latter two GLONASS-only solutions the variations of the fictitious hourly solutions were analyzed. For this purpose, the mean coordinates for intervals of 60 min were extracted from the kinematic solutions. The RMS of these time series of hourly coordinates is shown in Tab. 4.4. The updated satellite antenna PCC only cause a minor impact on the hourly coordinate solutions (excluding the stations CONZ and

REUN, the mean of the RMS values of all stations is identical on the sub-mm level). This confirms the conclusions drawn from Tab. 4.3 and Sect. 4.5.3 that the updated satellite antenna phase center model for the GLONASS satellites does not “disturb” the coordinate solution. The solution is dominated by environmental effects which are difficult to be eliminated in the case of a GLONASS-only solution due to the small redundancy.

## 4.6 Summary and conclusions

The CODE reprocessing solution for the IGS based on GPS only, performed at the Technische Universität München, has been expanded to a combined GPS/GLONASS solution for the time period from May 2003 to December 2008. Due to improved modeling and additional tracking sites the GLONASS orbits could be improved by up to a factor of about two compared to the operational solution (in particular prior to 2007) achieved by the CODE Analysis Center. The time series of combined GPS/GLONASS solutions was used as the basis for this study and to update the antenna phase center model.

An updated antenna PCC file, called `igs05(upd).atx`, was generated containing all receiver antenna/radome combinations available with reliably GNSS-specific corrections. Some converted field calibrations could be replaced by robot calibrations in the updated file. These updated corrections affect the station coordinates by up to 5 mm, even if the GPS-derived values are used for both, the GPS and the GLONASS observations. This result underlines the problem of a stable reference frame realization on one hand and the necessity to update the receiver antenna PCC on the other hand.

GNSS-specific receiver antenna corrections became available for many antenna types since 2005/06. The differences between GPS and GLONASS PCV reach values of up to 10 mm for the ionosphere-free linear combination. The introduction of these GNSS-specific corrections has a systematic impact of only up to 1 mm on the estimated station coordinates in a multi-year solution. In some cases the GLONASS-specific “type-mean” values show larger uncertainties than the GPS-specific values, because of the smaller number of calibrated antennas. As soon as the uncertainty is small enough, the GNSS-specific corrections should be used, because the impact of GLONASS on a combined GPS/GLONASS solution currently grows from month to month thanks to the continuous growth of the multi-GNSS tracking sites in the global IGS network and thanks to the growing number of GLONASS satellites. The differences between GPS- and GLONASS-specific receiver antenna PCV are typically twice as large as the difference between `igs05.atx` values and the updated receiver antenna PCC for GPS. The latter differences caused 5 mm changes in the estimated station heights.

An update of the currently used GNSS satellite antenna phase center model is also necessary for at least formal reasons. More or less the complete GLONASS constellation has been replaced since the computation of the currently used `igs05.atx` values. The GLONASS tracking situation has, moreover, dramatically improved since that time.

Today the uncertainties of the GLONASS satellite antenna corrections, as documented here, are comparable to those of the GPS satellites.

Some satellite antennas show significant deviations from the nadir-dependent block-specific PCV. Examples for both GPS- and GLONASS-satellites were provided. Exceptions from the block-specific PCC should therefore be allowed for specific satellites. Satellite-specific corrections should be considered for future satellite antenna phase center models.

The updated satellite antenna phase center model does not degrade the reference frame of combined GPS/GLONASS solutions. GLONASS-only rapid-static or kinematic solutions benefit most from the updated satellite antenna corrections. The new coefficients will be provided as a contribution to the next generation of standard IGS antenna PCC.

### 4.7 References

- Altamimi, Z., X. Collilieux, J. Legrand, B. Garayt, and C. Boucher (2007). ITRF2005: A new release of the International Terrestrial Reference Frame based on time series of station positions and Earth orientation parameters. *Journal of Geophysical Research*, 112(B9):401–419, DOI 10.1029/2007JB004949.
- Beutler, G., E. Brockmann, W. Gurtner, U. Hugentobler, L. Mervart, M. Rothacher, and A. Verdun (1994). Extended Orbit Modeling Techniques at the CODE Processing Center of the International GPS Service for Geodynamics (IGS): Theory and Initial Results. *Manuscripta Geodetica*, 19(6):367–386.
- Dach, R., U. Hugentobler, P. Fridez, and M. Meindl (editors, 2007). *Bernese GPS Software, Version 5.0*. User Manual, Astronomical Institute, University of Bern, Switzerland.
- Dach, R., E. Brockmann, S. Schaer, G. Beutler, M. Meindl, L. Prange, H. Bock, A. Jäggi, and L. Ostini (2009). GNSS processing at CODE: status report. *Journal of Geodesy*, 83(3–4):353–365, DOI 10.1007/s00190-008-0281-2.
- Dilssner, F., R. Dach, and R. Schmid (2009). Z-offset update for R23/R714 planned at the beginning of GPS week 1542. IGS Mail No. 5970, IGS Central Bureau Information System, available at <http://igscb.jpl.nasa.gov/pipermail/igsmail/>.
- Dow, J., R. Neilan, C. Rizos (2009). The International GNSS Service in a changing landscape of Global Navigation Satellite Systems. *Journal of Geodesy*, 83(3–4):191–198, DOI 10.1007/s00190-008-0300-3.
- Gendt, G. (2006). IGS switch to new antenna model — a few remarks. IGS Mail No. 5440, IGS Central Bureau Information System, available at <http://igscb.jpl.nasa.gov/pipermail/igsmail/>.
- Ineichen, D., T. Springer, and G. Beutler (2003). Combined Processing of the IGS and the IGEX network. *Journal of Geodesy*, 75(11):575–586, DOI 10.1007/s001900000152.

- Ineichen, D., E. Brockmann, and S. Schaer (2008). Processing Combined GPS/GLONASS Data at swisstopo's Local Analysis Center. In Ihde, J. and H. Hornik, editors, *EUREF Publication, No. 18*, EUREF Symposium, June 18–20, 2008, Brussels, Belgium. in press.
- Jäggi, A., R. Dach, O. Montenbruck, U. Hugentobler, H. Bock, G. Beutler (2009). Phase center modeling for LEO GPS receiver antennas and its impact on precise orbit determination *Journal of Geodesy*, 83(12):1145–1162, DOI 10.1007/s00190-009-0333-2.
- Ostini, L., R. Dach, M. Meindl, S. Schaer, and U. Hugentobler (2008). FODITS: a new tool of the Bernese GPS Software. In Ihde, J. and H. Hornik, editors, *EUREF Publication, No. 18*, EUREF Symposium, June 18–20, 2008, Brussels, Belgium. in press.
- Pearlman, M., J. Degnan, J. Bosworth (2002). The International Laser Ranging Service. *Advances in Space Research*, 30(2):135–143, DOI 10.1016/S0273-1177(02)00277-6
- Rothacher, M. and R. Schmid (2006). ANTEX: The antenna exchange format, version 1.3. IGS Central Bureau Information System, available at <ftp://ftp.igs.org/pub/station/general/antex13.txt>.
- Schaer, S., E. Brockmann, and D. Ineichen (2009). Inclusion of GLONASS for EPN analysis at CODE/swisstopo. In Torres, J., J. Ihde. and H. Hornik, editors, *EUREF Publication, No. 17*, EUREF Symposium, June 04–06, 2007, London, United Kingdom, *Mitteilungen des BKG*, volume 42:86–94, ISBN 978-3-89888-916-2.
- Schmid, R. (2008). General antenna file information: responsibilities, update requirements, etc.. IGS Central Bureau Information System, available at [ftp://ftp.igs.org/pub/station/general/antenna\\_README.pdf](ftp://ftp.igs.org/pub/station/general/antenna_README.pdf).
- Schmid, R., P. Steigenberger, G. Gendt, M. Ge, and M. Rothacher (2007). Generation of a consistent absolute phase center correction model for GPS receiver and satellite antennas. *Journal of Geodesy*, 81(12):781–798, DOI 10.1007/s00190-007-0148-y.
- Steigenberger, P., S. Schaer, S. Lutz, R. Dach, L. Ostini, U. Hugentobler, H. Bock, A. Jäggi, M. Meindl, and D. Thaller (2009). CODE contribution to IGS reprocessing: status and perspectives. In: EGU General Assembly, April 19–24, 2009, Vienna, Austria.
- Urschl, C. (2007) Center for Orbit Determination in Europe (CODE) Associate Analysis Center. In: Noll, C. and M. Pearlman, editors, *International Laser Ranging Service 2005-2006 Report*, NASA/TP-2007-214153, pp 12/19–12/20.
- Wübbena, G., M. Schmitz, G. Boettcher, and C. Schumann (2006). Absolute GNSS antenna calibration with a robot: repeatability of phase variations, calibration of GLONASS and determination of carrier-to-noise pattern. In: Springer, T., G. Gendt, and J. Dow, editors, *International GNSS Service: Analysis Center Workshop*, May 08–12, 2006, Darmstadt, Germany.



# 5 Combining the Observations from Different GNSS

Rolf Dach<sup>1</sup>, Stefan Schaer<sup>2</sup>, Simon Lutz<sup>1</sup>, Michael Meindl<sup>1</sup>, Gerhard Beutler<sup>1</sup>

<sup>1</sup> Astronomical Institute, University of Bern  
Sidlerstrasse 5, 3012 Bern; Switzerland

<sup>2</sup> Swiss Federal Office of Topography swisstopo  
Seftigenstrasse 264, 3084 Wabern; Switzerland

To be published in *EUREF Publication, No. 20*,  
EUREF Symposium, June 02–05, 2010, Gävle, Sweden

## Abstract

*Until quite recently the precise applications for Global Navigation Satellite Systems (GNSS) were exclusively based on using the American Global Positioning System (GPS). With the much improved stability of the Russian counterpart GLONASS (Global Navigation Satellite System) and the development of alternative systems in Europe (Galileo) or China (Compass) we are facing more and more multi-GNSS applications.*

*The Center for Orbit Determination in Europe (CODE), acting as a global analysis center of the International GNSS Service (IGS), has a long tradition in the combined analysis of data from different GNSS. All CODE contributions to the IGS are in fact generated from a rigorously combined analysis of GPS and GLONASS data — apart from the clock products — for a long time.*

*Inter-system biases are taken into account when generating the procedures to compute multi-GNSS satellite clock corrections. Traditionally, a constant offset between the internal GPS and GLONASS receiver clocks is assumed and set up in the data processing. A detailed analysis revealed on the one hand that this simple approach is not sufficient. It is not necessary, on the other hand, to introduce independent receiver clock parameters for each GNSS. Such an approach would considerably reduce the benefit of the combined processing of observations from different GNSS as opposed to analyzing the measurements of only one GNSS. Finally, a compromise*

*between both strategies seems to be most promising: a piece-wise linear inter-system bias with a resolution of, e.g., one hour.*

## 5.1 Introduction and Motivation

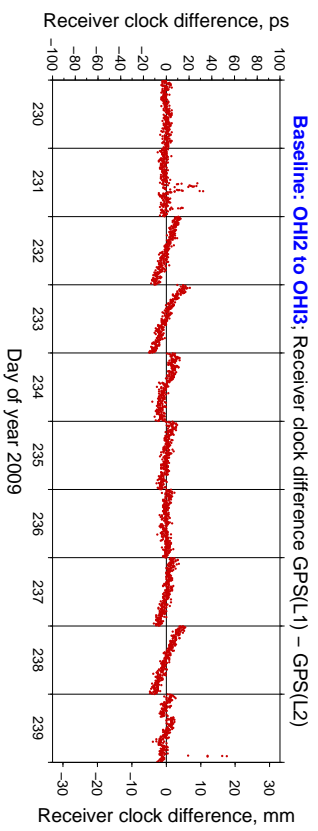
Two Global Navigation Satellite Systems (GNSS) are currently operational, namely GPS, Global Positioning System and GLONASS, GLObalnaya NAvigatsionnaya Sputnikovaya Sistema (Russian for “Global Navigation Satellite System”). Other systems are under development in particular the European Galileo or the Chinese COMPASS. A combined processing of the observations from the different GNSS promises better results than analyzing only the data from a single GNSS constellation.

CODE, the Center for Orbit Determination in Europe, is a joint venture of the Astronomical Institute of the University of Bern (AIUB, Bern, Switzerland), the Swiss Federal Office of Topography (swisstopo, Wabern, Switzerland), the Federal Agency for Cartography and Geodesy (BKG, Frankfurt am Main, Germany), and the Institut für Astronomische und Physikalische Geodäsie of the Technische Universität München (IAPG/TUM, Munich, Germany). It acts as a global analysis center (AC) of the International GNSS Service (IGS, Dow et al., 2009) since the early phase of the first test campaign in June 1992. CODE has started with a rigorously combined analysis of GPS and GLONASS measurements in May 2003 (Dach et al., 2009). For nearly five year, CODE was the only AC submitting products to the IGS generated from a rigorous combination of the GPS and GLONASS observations. Meanwhile, other ACs of the IGS (ESOC, Darmstadt and GFZ, Potsdam, both in Germany) followed this approach (Springer and Dach, 2010).

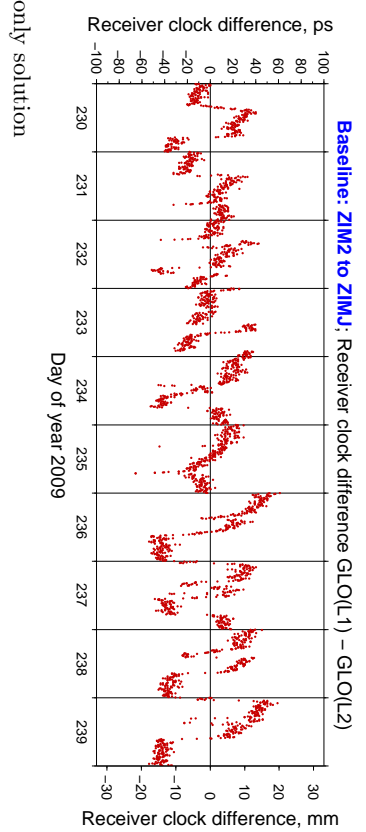
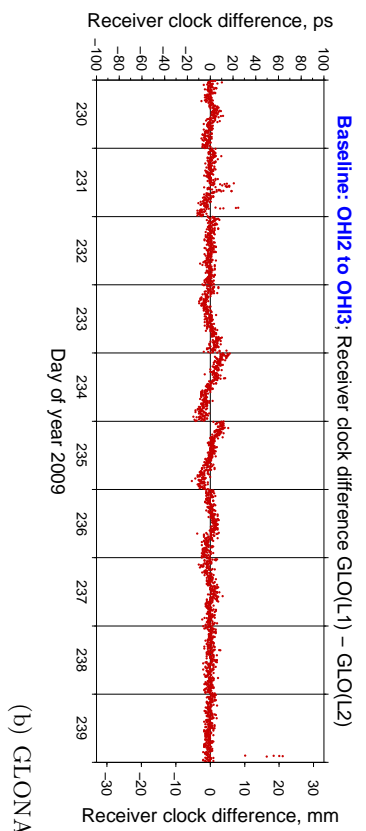
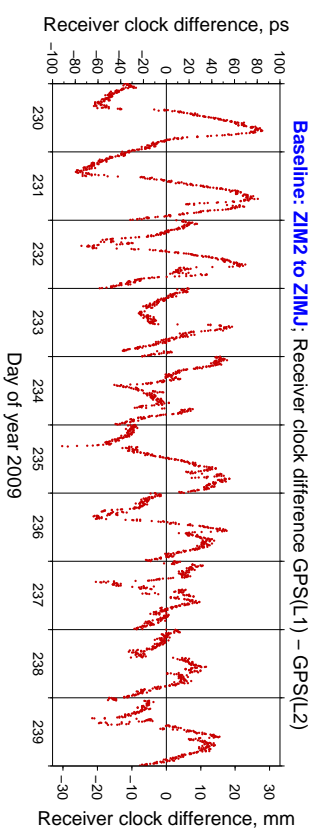
Because of the differences between the signals of different GNSS, the receivers will introduce inter-system biases (ISB) for the pseudorange as well as for carrier phase measurements. The ISB for the pseudorange observations are very stable within the noise level of the data (Dach et al., 2010). Assuming a noise of the phase observations of 1 mm, the corresponding stability requirement for the ISB is on the 3 ps level — which is very challenging. If the receivers cannot meet this high stability level for the ISB we have to cope with the variation of the ISB in time in a multi-GNSS data processing.

The two extreme ways of ISB handling are:

- *Independent receiver clocks per GNSS are introduced:*  
There are no requirements concerning the ISB in the receiver, but one additional parameter per station and epoch has to be added.
- *One constant ISB for the interval of processing (e.g., one day) is set up:*  
The receivers have to preserve the stability of the ISB on the noise level of the phase measurements during the entire processing interval. Only one additional parameter per station is necessary.



(a) GPS-only solution



(b) GLONASS-only solution

Figure 5.1: Differences between the receiver clock corrections computed using only L1 and L2 observations from GPS and GLONASS, respectively.

The three IGS ACs (CODE, ESOC, and GFZ) currently providing multi-GNSS solutions follow the second option.

There are indications that we do not use the full potential of adding GLONASS to the GPS measurements by introducing only a constant ISB. Schaer (2009) demonstrated that the station repeatability is slightly better if independent receiver clocks are assumed for each GNSS. Dach et al. (2009) showed that a benefit from additional GLONASS measurements in a rapid static solution for the estimation of station positions only results for intervals of up to one hour in a network covering Europe.

Even if geodetic GNSS receivers contain only one physical clock there is not only a simple offset between receiver clock differences computed with the L1 and L2 carrier phase data on short baselines. The magnitude of these deviations from the theoretically expected behavior clearly exceeds the general noise of the solution for many receiver types. Two examples are given in Fig. 5.1. The left plots (O’Higgins) are typical for most of the stations in the IGS network — but there are significant exceptions (see, e.g., Zimmerwald in the right plots). Such results raise the question about the stability of the ISB in time. This issue will be studied in detail in the subsequent sections.

## 5.2 Analysis strategy and receiver statistics

Our study has the focus on short baselines of multi-GNSS receivers available in the IGS tracking network to allow for single frequency solutions using only L1 or L2. The stations and their equipment are listed in Tab. 5.1.

The pre-processing (residual screening) has been performed in four independent solutions: use of L1 or L2 in the GPS-only mode and use of L1 or L2 in the GLONASS-only mode. Ten days in August 2009 (day of year 230 to 239) have been processed in small subnetworks consisting of two or three stations (as indicated in Tab. 5.1) without

**Table 5.1:** Stations used for the short baseline/network solutions and their equipment.

Station	Location	Receiver type	Firmware
OHI2 66008M005	O’Higgins	JPS E_GGD	2.6.1 Jan10,2008
OHI3 66008M006	Antarctica	TPS E_GGD	2.6.1 Jan10,2008
STR1 50119M002	Canberra Australia	LEICA CRX1200GGPRO	7.50
STR2 50119M001		TRIMBLE NETR5	3.84
TID1 50119M108		TRIMBLE NETR8	3.80
UNBJ 40146M002	Fredericton Canada	TPS LEGACY	2.6.1 Jan10,2008
UNBN 40146M002		NOV OEM3	3.260
UNBT 40146M002		TPS NET-G3	3.4 Feb,25,2009 t3
WTZJ 14201M012	Wetzell Germany	JPS LEGACY	2.6.0 Oct24,2007 O
WTZR 14201M010		LEICA GRX1200GGPRO	7.53/3.017
WTZZ 14201M014		TPS E_GGD	2.7.0 Mar31,2008
ZIM2 14001M008	Zimmerwald	TRIMBLE NETR5	Nav 4.03/Boot 3
ZIMJ 14001M006	Switzerland	JPS LEGACY	2.6.1 Jan10,2008

estimating any parameters for the troposphere (the GPT/GMF standard corrections were applied, Böhm et al., 2006).

The three receivers UNBJ, UNBN, and UNBT are connected to the same antenna, which results in a lower noise level. The baseline in O'Higgins (OHI2/OHI3) provides an example for stable ISB conditions whereas the baseline in Zimmerwald (ZIM2/ZIMJ) represents the worst case in this study. The results at the other baselines are typical for most of the examples.

## 5.3 Inter-system biases and their impact on the solution

### 5.3.1 Stability of the inter-system bias in time

Similar experiments to that underlying Fig. 5.1 can be carried out when comparing receiver clock estimates derived only from GPS or GLONASS measurements gathered by multi-GNSS receivers. Figure 5.2 shows the differences between the GPS- and GLONASS-derived receiver clock corrections computed from the L1 (left) and L2 (right) observations. The L1-based series are more stable in time than the L2-based values, a fact also observed for other baselines.

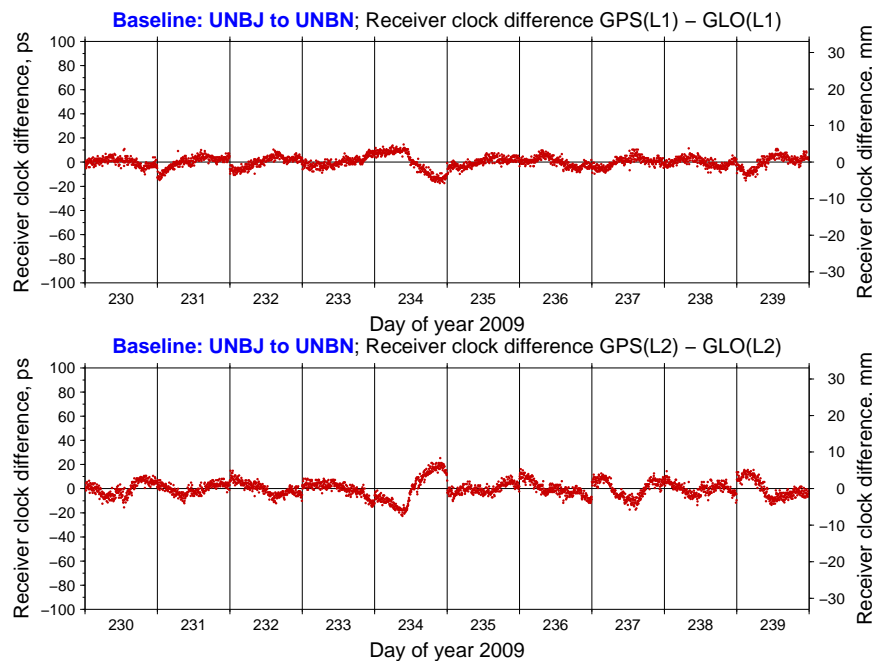


**Figure 5.2:** Differences between the receiver clock corrections computed using only L1 or L2 observations from GPS and GLONASS.

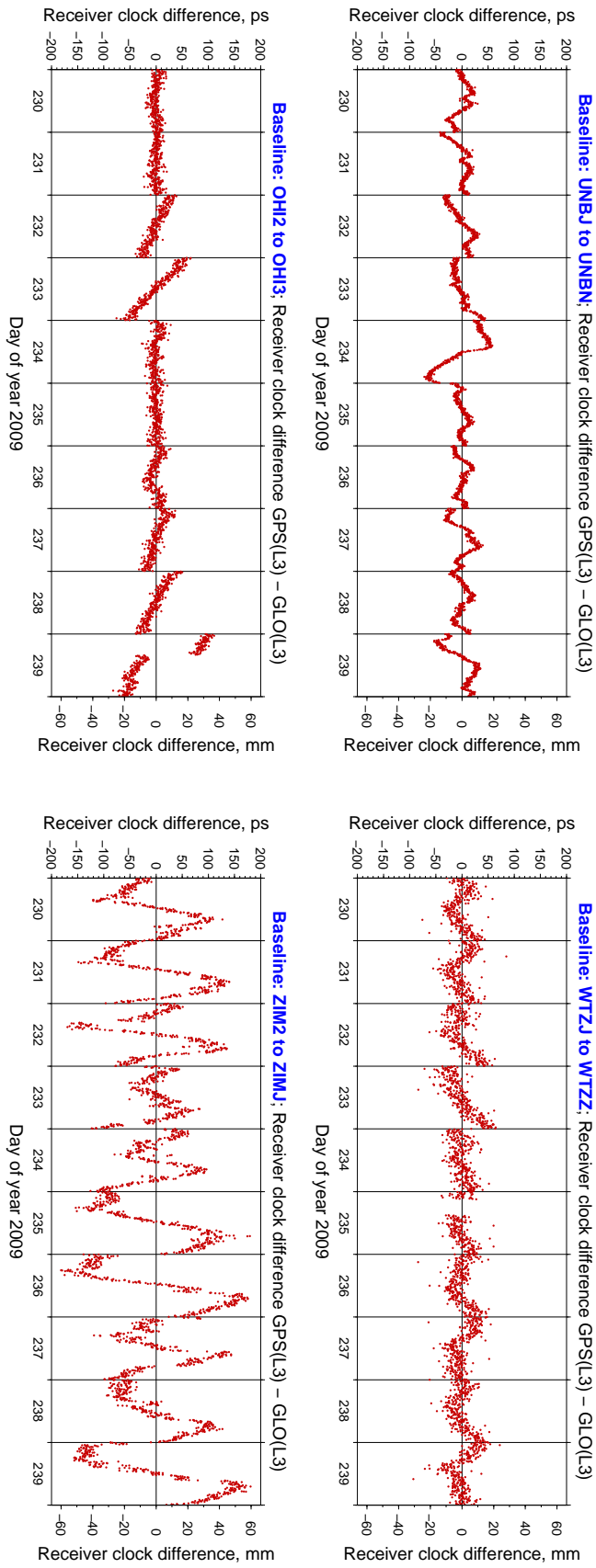


**Figure 5.3:** Differences between the receiver clock corrections computed using the ionosphere-free linear combination (L3) from GPS and GLONASS.

It is also interesting to study the differences between the GPS and GLONASS observations in the ionosphere-free linear combination (L3) to get a situation, comparable to regional or global multi-GNSS analyses. The results for more baselines are provided in Fig. 5.3 indicating significant variations in time for the ISB. Even the baseline in O'Higgins shows a drift of 20 to 40 mm per day in the ISB for some of the days. In Fredericton the biggest variations seems to be introduced by UNBT (TPS NET-G3 receiver) whereas in Wettzell WTZR (LEICA GRX1200GGPRO, not shown in this figure) shows a bigger variation relative to the other two stations. We conclude that the time dependency in the ISB has to be taken into account for these short baseline/small network solutions.

Because of the small number of receiver combinations only the inconsistencies can be observed. It is impossible to say which receiver types definitively introduce these time variations of the ISB.

### 5.3.2 Inter-system bias in the RMS of the post-fit residuals

The differences between the GPS- and GLONASS-derived receiver clock differences in the ionosphere-free linear combination in Fig. 5.3 let us expect a clear impact on the RMS of the observations, if the variation in time of the ISB is not properly considered in the data processing. Four solutions have been generated for the ten days to verify this expectation:

**GNSS-spec. clocks:** Independent receiver clock corrections for each GNSS are estimated. There are no requirements concerning the stability of the ISB, but *288 additional parameters* have to be solved for (for each station and each day with independent reference clock conditions for each GNSS).

**Constant ISB:** One constant ISB is set up per day. This approach assumes that the ISB is stable during the day on the level of the phase noise resulting in only *one additional parameter* per station.

**Hourly ISB:** This strategy represents a compromise between the two above GNSS-combination strategies. The ISB is introduced by piece-wise linear parameters with an hourly resolution (*25 additional parameters* and a zero-mean condition). This approach allows for a certain variation of the ISB in time.

**GPS+GLONASS:** As a reference, the GPS and GLONASS observations have been processed separately. The RMS of the residuals for the single-GNSS solutions allow to compute an expected RMS of the residuals in a multi-GNSS solution ( $RMS_{GNSS}$ ) by:

$$RMS_{GNSS} = \sqrt{\frac{nObs_{GPS} \cdot RMS_{GPS}^2 + nObs_{GLO} \cdot RMS_{GLO}^2}{nObs_{GPS} + nObs_{GLO}}}$$

$nObs$  and  $RMS$  are the number of observations and the RMS of the residuals for each GNSS ( $GPS$ ,  $GLO$ ).

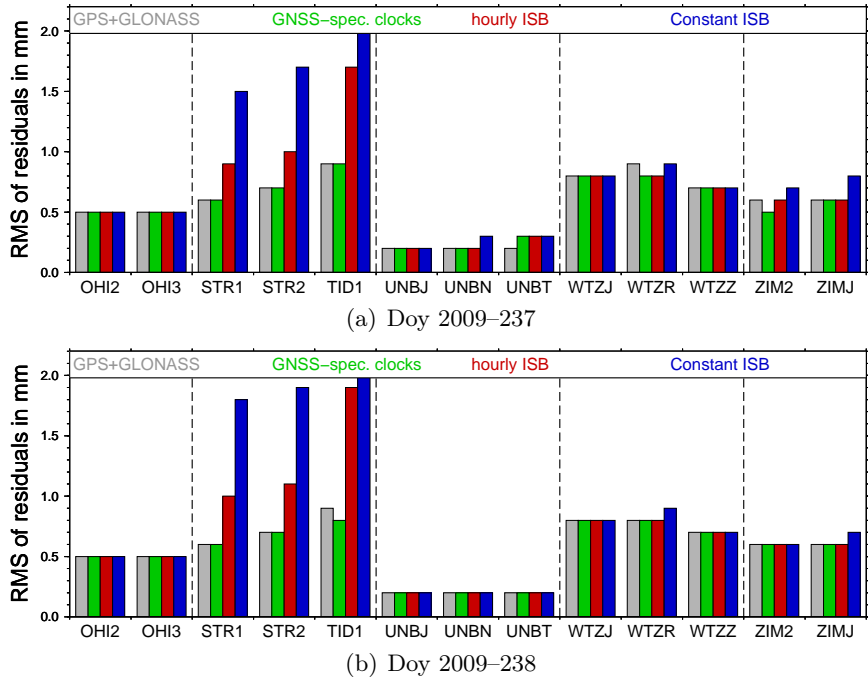


**Figure 5.4:** RMS of the post-fit residuals with different combination strategies for the measurements from GPS and GLONASS

The results of these four strategies are presented for two days in Fig. 5.4.

The reference value (GPS+GLONASS, gray bars) is obtained for all examples in the case of independent receiver clocks for each GNSS (*GNSS-spec. clocks*, green bars), because there are no requirements concerning the synchronization between the internal GPS and GLONASS receiver clocks. This strategy is safe from the parametrization point of view — but is it really necessary to introduce so many additional parameters to process the data from two GNSS together?

The variations of the ISB in Fig. 5.3 suggest a RMS on the order of 2 to 5 mm if only a constant ISB is assumed (*constant ISB*, blue bars). The results for different stations in Fig. 5.4 indicate that only the groups of Canberra and Zimmerwald have systematically larger RMS values.

If we assume a drift of 20 mm over one day in the ISB the relation of 1:2 for the number of GLONASS and GPS observations implies that  $\approx 14$  mm discrepancy of the ignored ISB have to be absorbed by the GLONASS and  $\approx 7$  mm by the GPS residuals. A corresponding increase of the residuals cannot be observed (a drift of 14 or 7 mm over 288 observation epochs results to an increase of the RMS of 1.82 or 1.25 mm, respectively). The hardware delay of the receiver clock is correlated to 100% with the mean carrier phase ambiguities in a phase-only zero-difference solution (and cancels out in a double difference solution). The phase ambiguity parameters are thus able to absorb a moderate variation of the ISB.

Assuming the ambiguities to cover an interval of 6 hours (e.g., one full satellite pass) they refer to 25% of the ignored trend in the ISB discrepancies assumed for one day: about 2 or 1 mm for GLONASS and GPS, respectively. If the ambiguities are freely estimated the RMS of the residuals is only increased by this small amount mainly at the two ends of the path. Here also the observations with low elevation can be found which are usually down-weighted because of the uncertainty of the troposphere model or the expected influence of potential multipath effects.

This is why we can observe an increase of the RMS in Fig. 5.4 only in two examples where the differences between the GPS(L3) and GLONASS(L3) receiver clock estimates also show extreme values (ZIM2/ZIMJ and for TID1 exceeding the scale used in Fig. 5.3).

### 5.3.3 Influence of inter-system bias on station coordinate solutions

The **mean station coordinate** in the Up, North, and East components computed from the ten days are listed in Tab. 5.2. Because the true coordinates are unknown the solution *GNSS-spec. clocks* serves as reference, i.e., the differences of the individual solutions from this reference is provided.

The coordinates between the multi-GNSS solution with independent receiver clocks for each GNSS (*GNSS-spec. clocks*) and hourly estimated ISB (*hourly ISB*) agree on the tenth of a millimeter with the reference solution. The only exception is the station TID1 with big and irregular variation of the ISB (see the RMS in Fig. 5.4).

**Table 5.2:** Comparison of the coordinate solutions in mm. Solution *GNSS-spec. clocks* is used as reference because the true coordinate solution is unknown.

(a) Baselines from L1-solutions:

Baseline	num	GPS-only			GLONASS-only			GNSS-spec. clocks			Hourly ISB			Constant ISB		
		up	north	east	up	north	east	up	north	east	up	north	east	up	north	east
OHI2 –OHI3	10	0.6	0.1	-0.7	-0.8	-0.1	0.7	0.0	0.0	0.0	-0.0	-0.0	0.0	-0.0	0.0	-0.0
STR1 –STR2	9	-0.4	0.2	0.1	0.9	-0.3	-0.2	0.0	0.0	0.0	-0.0	-0.0	0.0	-0.1	-0.0	0.0
STR1 –TID1	9	0.2	0.4	-1.6	-0.4	-0.7	2.2	0.0	0.0	0.0	0.0	0.0	-0.0	0.2	0.2	-0.7
UNBJ –UNBN	9	-0.0	-0.0	0.1	0.0	0.0	-0.0	0.0	0.0	0.0	0.0	0.0	-0.0	-0.0	0.0	0.0
UNBJ –UNBT	9	-0.0	-0.0	0.0	0.1	0.0	-0.0	0.0	0.0	0.0	0.0	0.0	-0.0	0.1	-0.0	-0.1
WTZJ –WTZR	10	-0.7	0.5	0.6	1.2	-0.9	-0.8	0.0	0.0	0.0	-0.0	0.0	-0.0	0.1	-0.1	-0.1
WTZJ –WTZZ	10	-0.5	0.5	0.2	0.9	-0.8	-0.2	0.0	0.0	0.0	0.0	0.0	0.0	0.0	-0.0	0.0
ZIM2 –ZIMJ	10	0.1	-0.2	-0.3	-0.2	0.3	0.4	0.0	0.0	0.0	-0.0	0.0	-0.0	-0.1	0.2	-0.5

(b) Baselines from L2-solutions:

Baseline	num	GPS-only			GLONASS-only			GNSS-spec. clocks			Hourly ISB			Constant ISB		
		up	north	east	up	north	east	up	north	east	up	north	east	up	north	east
OHI2 –OHI3	10	-0.0	-0.1	-0.3	0.0	0.2	0.3	0.0	0.0	0.0	0.0	0.0	0.0	0.0	0.0	0.0
STR1 –STR2	9	-0.9	0.2	0.5	1.9	-0.4	-0.6	0.0	0.0	0.0	0.0	0.0	0.0	0.1	0.0	-0.5
STR1 –TID1	9	0.2	0.5	-1.3	-0.2	-1.1	2.4	0.0	0.0	0.0	-0.3	0.1	0.0	1.7	-0.5	-1.2
UNBJ –UNBN	9	0.0	-0.0	-0.1	-0.1	0.1	0.0	0.0	0.0	0.0	0.0	0.0	0.0	0.0	0.0	-0.0
UNBJ –UNBT	9	0.1	-0.0	0.5	-0.2	0.0	-0.7	0.0	0.0	0.0	0.0	0.0	0.0	0.1	-0.0	-0.2
WTZJ –WTZR	10	-0.1	0.6	0.6	0.2	-0.9	-0.8	0.0	0.0	0.0	-0.0	0.0	0.0	-0.1	0.1	-0.1
WTZJ –WTZZ	10	-0.5	0.2	-0.3	1.0	-0.3	0.4	0.0	0.0	0.0	0.0	0.0	0.0	-0.0	-0.0	0.2
ZIM2 –ZIMJ	10	-0.1	-0.1	-0.3	0.2	0.1	0.4	0.0	0.0	0.0	0.0	0.0	0.0	0.2	-0.3	0.7

**Table 5.3:** Repeatability of the coordinate series in mm. The solution with the best over-all components repeatability is indicated.

(a) Baselines from L1-solutions:

Baseline	num	GPS-only			GLONASS-only			GNSS-spec. clocks			Hourly ISB			Constant ISB		
		up	north	east	up	north	east	up	north	east	up	north	east	up	north	east
OHI2 –OHI3	10	0.5	0.5	0.8	0.6	0.5	0.4	0.5	0.5	0.4	<b>0.5</b>	<b>0.5</b>	<b>0.4</b>	0.5	0.5	0.4
STR1 –STR2	9	0.7	0.3	0.6	0.7	0.5	0.6	<b>0.6</b>	<b>0.3</b>	<b>0.5</b>	0.6	0.4	0.5	0.6	0.4	0.5
STR1 –TID1	9	6.2	1.7	5.4	6.5	1.4	4.0	6.1	1.4	4.4	6.1	1.4	4.4	<b>5.7</b>	<b>1.2</b>	<b>4.7</b>
UNBJ –UNBN	9	0.2	0.1	0.3	0.3	0.2	0.4	0.2	0.1	0.3	<b>0.2</b>	<b>0.1</b>	<b>0.3</b>	0.2	0.1	0.4
UNBJ –UNBT	9	0.3	0.1	0.4	0.3	0.1	0.3	<b>0.3</b>	<b>0.1</b>	<b>0.3</b>	0.3	0.1	0.4	0.2	0.1	0.4
WTZJ –WTZR	10	0.3	0.2	0.3	0.5	0.2	0.5	0.4	0.2	0.3	0.4	0.2	0.3	<b>0.4</b>	<b>0.2</b>	<b>0.2</b>
WTZJ –WTZZ	10	0.1	0.1	0.2	0.4	0.2	0.4	0.2	0.1	0.2	0.2	0.1	0.2	<b>0.2</b>	<b>0.1</b>	<b>0.2</b>
ZIM2 –ZIMJ	10	0.7	0.2	0.5	0.6	0.3	0.8	0.6	0.2	0.6	<b>0.5</b>	<b>0.2</b>	<b>0.5</b>	0.6	0.2	0.6

(b) Baselines from L2-solutions:

Baseline	num	GPS-only			GLONASS-only			GNSS-spec. clocks			Hourly ISB			Constant ISB		
		up	north	east	up	north	east	up	north	east	up	north	east	up	north	east
OHI2 –OHI3	10	0.6	0.5	0.7	0.7	0.4	0.6	0.6	0.5	0.5	<b>0.6</b>	<b>0.4</b>	<b>0.5</b>	0.6	0.5	0.5
STR1 –STR2	9	1.1	0.3	0.6	0.7	0.5	0.7	0.9	0.4	0.6	<b>0.9</b>	<b>0.3</b>	<b>0.6</b>	0.7	0.4	1.0
STR1 –TID1	9	6.1	1.6	5.8	6.9	2.1	4.1	6.0	1.5	4.8	<b>6.2</b>	<b>1.5</b>	<b>4.5</b>	8.5	4.0	13.0
UNBJ –UNBN	9	0.2	0.2	0.5	0.3	0.1	0.3	0.2	0.2	0.4	0.2	0.2	0.4	<b>0.2</b>	<b>0.2</b>	<b>0.4</b>
UNBJ –UNBT	9	0.3	0.1	0.5	0.2	0.1	0.4	0.2	0.0	0.4	<b>0.2</b>	<b>0.0</b>	<b>0.4</b>	0.3	0.1	0.4
WTZJ –WTZR	10	0.2	0.2	0.2	0.5	0.2	0.6	0.3	0.2	0.2	0.3	0.2	0.2	<b>0.3</b>	<b>0.2</b>	<b>0.2</b>
WTZJ –WTZZ	10	0.2	0.2	0.3	0.5	0.2	0.3	0.2	0.2	0.2	<b>0.2</b>	<b>0.2</b>	<b>0.2</b>	0.2	0.2	0.3
ZIM2 –ZIMJ	10	0.9	0.1	0.6	0.9	0.3	0.7	0.9	0.2	0.5	<b>0.9</b>	<b>0.2</b>	<b>0.5</b>	0.9	0.3	0.5

Disregarding the two stations with the increased RMS of the residuals if only a constant ISB has been considered (Canberra and Zimmerwald) the coordinates agree within half of a millimeter, if no variation of the ISB during the day is considered in the data processing (*constant ISB*).

The GPS-only and the GLONASS-only solutions differ by up to 3 mm. All combined multi-GNSS coordinates lie, as expected, between the two system-specific solutions.

Usually the **repeatability of the daily station coordinates** is taken as an indicator of the quality of a GNSS-solution: Even if a repeatability computed from only ten days needs to be read with utmost care we have included them in Tab. 5.3. The solution with the best repeatability over all three coordinate components is marked in bold font.

It is at first right noteworthy that all multi-GNSS solutions show better repeatability values than single GNSS solutions. This does, however, only indicate the benefit that may be expected from adding the observations of an alternative GNSS in a combined processing of the data.

Only in two cases the independent receiver clock estimation for each GNSS gives the best results. In most other cases the hourly piece-wise linear ISB show the best repeatability for the multi-GNSS station coordinates.

Even though the differences in the repeatability between the three strategies to handle the ISB are small, the hourly piece-wise linear parametrization seems to be a promising compromise between the two extreme strategies.

### 5.3.4 Influence of inter-system bias on rapid-static positioning

In the experiments of this section one endpoint of a baseline or one of the stations in the small network was kept fixed and the remaining station/stations are estimated with one set of coordinates per epoch (sampling 5 min.). Series of kinematic solutions are generated in this way and their sensitivity caused by time variations of the ISB is checked.

From these kinematic position time series, rapid-static solutions with different interval lengths  $\tau = 10 \text{ min} \dots 10 \text{ h}$  are generated. The arithmetic mean of all  $n$  positions within the interval  $\tau_i$

$$\bar{x}(\tau_i) = \frac{1}{n} \sum_{j=1}^n x_j(t) \quad \text{with } t \in \tau_i$$

is assumed to be the rapid-static coordinate solution for this particular interval. The standard deviation of this arithmetic mean may also be computed from the kinematic positions of the interval

$$s(\tau_i) = \sqrt{\frac{1}{n(n-1)} \sum_{j=1}^n (x_j(t) - \bar{x}(\tau_i))^2} \quad \text{with } t \in \tau_i$$

usable as a measure of the uncertainty of the interval's rapid-static solution. By computing the arithmetic mean of all  $s(\tau_i)$  belonging to the same interval length  $\tau$  a typical measure of the uncertainty of a rapid-static solution with a certain length of assumed measurement intervals is derived. These values are provided in Fig. 5.5.

Note that all multi-GNSS solutions are better than the GPS-only solutions (magenta curves). This confirms the benefit from the additional GLONASS measurements in the rapid-static solution. In O'Higgins and Wettzell (but also to a minor extent in Fredericton) the green curve (*GNSS-spec. clock*) is above the red one (*hourly ISB*) and the blue one (*constant ISB*) for short intervals. The reduced number of parameters with only 25 or 1 ISB per day obviously help to stabilize the rapid-static solutions for short intervals. With the exception of Zimmerwald the three curves using different strategies to handle the ISB come together indicating that a constant ISB seems to be sufficient. For Zimmerwald the hourly estimates of the ISB are necessary to generate the best solutions, in particular over long intervals.

## 5.4 Impact of the inter-system bias on ambiguity resolution

In Sect. 5.3.2 we saw that part of the variations in the ISB may be absorbed by the (real-valued) phase ambiguity parameters. This mechanism cannot work (at least not to the same extent), if the ambiguities are resolved to their integer values.

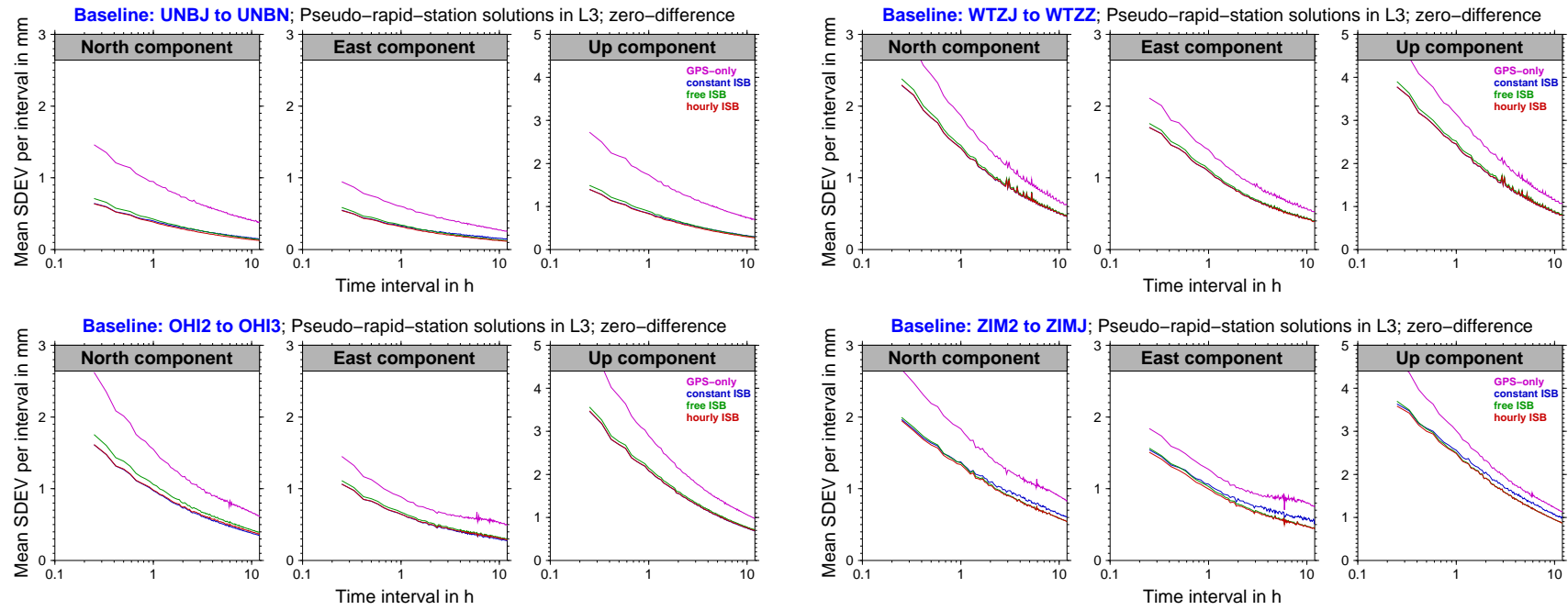


**Figure 5.5:** Standard deviation of a mean coordinate computed from a certain time interval (extracted from a kinematic positioning with a sampling of 5 minutes).

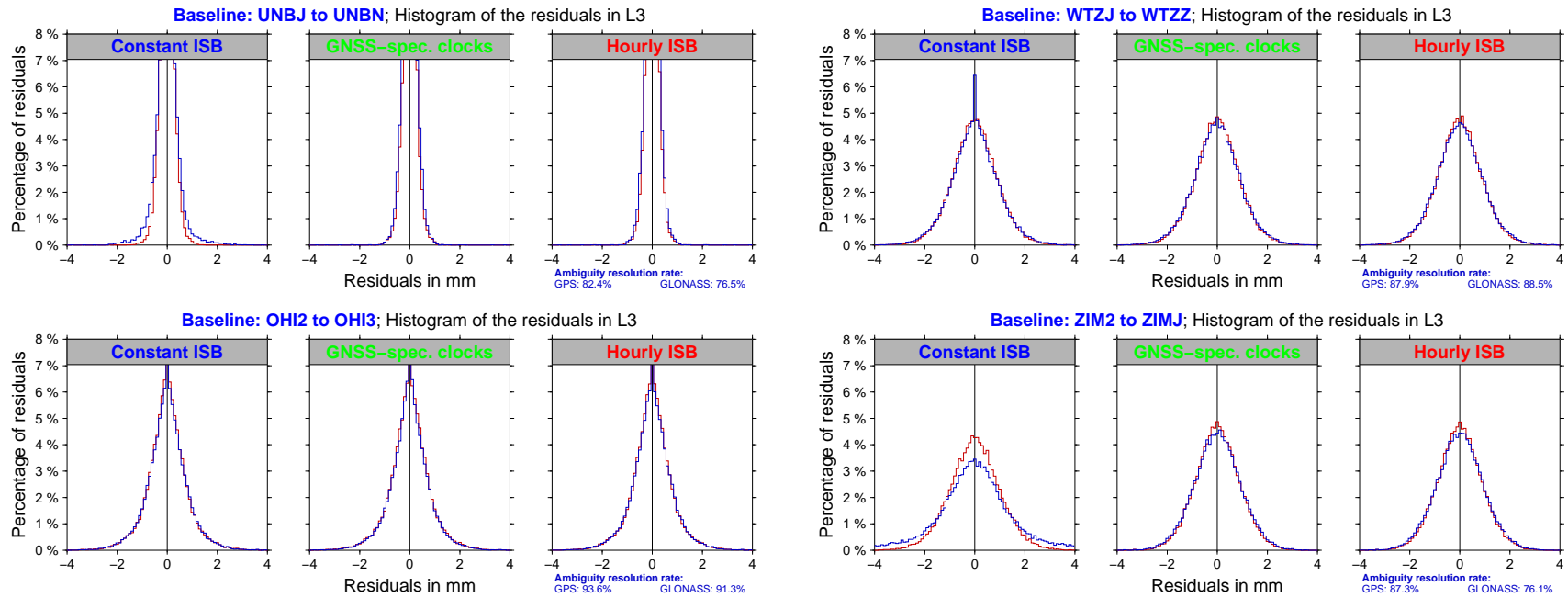


**Figure 5.6:** Histogram of the residuals from baseline solutions where the ambiguities are freely estimated (red curves) or their integer values are introduced (blue curves).

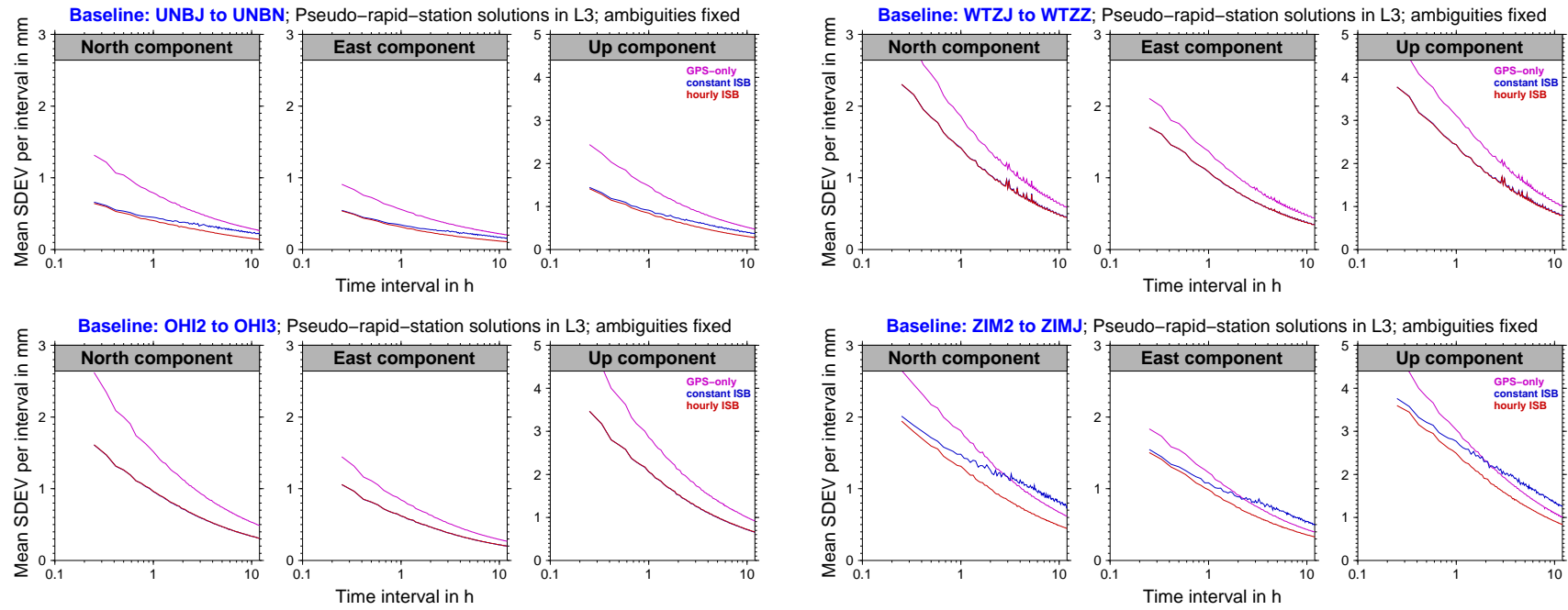


**Figure 5.7:** Standard deviation of a mean coordinate computed from a certain time interval (extracted from a kinematic positioning with a sampling of 5 minutes), computed with resolved ambiguity parameters.

To check the impact the ambiguities are resolved separately for GPS and GLONASS. No inter-system double-difference ambiguity was resolved to allow the system to compensate for the ISB. Because the baselines are short the direct ambiguity resolution approach for L1 and L2 was used. We refer to Dach et al. (2007) for more details on ambiguity resolution strategies implemented in the Bernese Software.

The histograms of the residuals related to the solutions before (red curves) and after (blue curves) ambiguity resolution are given in Fig. 5.6. It is expected that the distribution of the residuals does not change due to ambiguity resolution (if already the real-valued ambiguity estimates are very close to integer values). This is the case for the baselines in Wettzell and O’Higgins for all three strategies to handle the ISB.

The baseline in Zimmerwald shows a significant deviation when the ISB is assumed to be constant for each day. Increased residuals for the solution with resolved ambiguities expand the histogram (blue curve) with respect to the histogram of the residual with freely estimated, real valued ambiguities (red curve). The other two versions for handling the ISB (*GNSS-spec. clocks* and *hourly ISB*) show the same distribution of residual with and without ambiguity resolution. The fourth example (Fredericton) shows a similar pattern as Zimmerwald but on a smaller magnitude.

A new set of kinematic solutions introducing the resolved integer ambiguities was generated. The quality of a set of assumed rapid-static solutions with different interval lengths is computed as in Sect. 5.3.4, the results are provided in Fig. 5.7.

The results confirm the histograms of the residuals. In Wettzell and O’Higgins the quality of all multi-GNSS solutions are equivalent, independent of the strategy of ISB handling. In Fredericton the solutions with constant ISB are worst for longer intervals. Nevertheless, even for 10 h interval length all versions of multi-GNSS solutions perform better than the GPS-only solution.

This is not the case for Zimmerwald. The variations of the ISB in time are so big that the solution with a constant ISB is worse in quality than the GPS-only solution for intervals longer than two hours. This degradation of the multi-GNSS with respect to the GPS-only solution is caused by the fact that the ambiguity parameter cannot absorb the variations of the ISB in time if there are not enough ISB parameters estimated — as in the case of the *hourly ISB*. This solution type provides better results than the GPS-only solutions also over 10 hours — even for Zimmerwald.

## 5.5 Summary

When combining the measurements of different GNSS the inter-system bias (ISB) needs a special attention. The data of five groups of two or three multi-GNSS stations in the IGS network have been analyzed for 10 days in August 2009.

It is important to check the time stability of the ISB of the receivers. The stability of the ISB of the pseudorange data is already well documented. Because of the much lower noise level of the carrier phase measurements, the stability requirements of the ISB are more demanding for phase observations.

It may be necessary to model the ISB in the data analysis by more than one parameters. A piece-wise linear ISB parametrization with a resolution of one hour seems to be sufficient for all cases in this study. This is a compromise between the two extreme strategies:

- to introduce a constant ISB for the entire processing interval (e.g., one day) because it can absorb a certain variation in time. This is in particular important if the ambiguities are resolved to their integer numbers.
- to estimate GNSS-specific receiver clock corrections for each station and epoch to allow for a freely running ISB. The big number of additional parameters weakens the solutions.

Piece-wise linear ISB with a spacing of about one hour seems to provide the best results when combining GPS and GLONASS phase measurements in a multi-GNSS analysis.

## 5.6 References

- Böhm, J., A. Niell, P. Tregoning, and H. Schuh (2006). Global Mapping Function (GMF): A new empirical mapping function based on numerical weather model data. *Geophysical Research Letters* 33:L07304, DOI 10.1029/2005GL025546.
- Dach, R., U. Hugentobler, P. Fridez, and M. Meindl (editors, 2007). *Bernese GPS Software, Version 5.0*. User Manual, Astronomical Institute, University of Bern, Switzerland.
- Dach, R., E. Brockmann, S. Schaer, G. Beutler, M. Meindl, L. Prange, H. Bock, A. Jäggi, and L. Ostini (2009). GNSS processing at CODE: status report. *Journal of Geodesy*, 83(3–4):353–365, DOI 10.1007/s00190-008-0281-2.
- Dach, R., S. Schaer, H. Bock, S. Lutz, and G. Beutler (2010). CODE’s new combined GPS/GLONASS clock product. In: *International GNSS Service: Analysis Center Workshop*, June 28–July 2, 2010, Newcastle upon Tyne, United Kingdom.
- Dow, J., R. Neilan, C. Rizos (2009). The International GNSS Service in a changing landscape of Global Navigation Satellite Systems. *Journal of Geodesy*, 83(3–4):191–198, DOI 10.1007/s00190-008-0300-3.
- Schaer, S., E. Brockmann, and D. Ineichen (2009). Inclusion of GLONASS for EPN Analysis at CODE/swisstopo. In Torres, J., J. Ihde. and H. Hornik, editors, *EU-REF Publication, No. 17*, EUREF Symposium, June 04–06, 2007, London, United Kingdom, Mitteilungen des BKG, volume 42:86–94, ISBN 978-3-89888-916-2.
- Springer, T. and R. Dach (2010). GPS, GLONASS, and more. *GPS World*, 21(6):48–58.

# 6 Evaluation of the Impact of Atmospheric Pressure Loading Modeling on GNSS Data Analysis

Rolf Dach<sup>1</sup>, Johannes Böhm<sup>2</sup>, Simon Lutz<sup>1</sup>, Peter Steigenberger<sup>3</sup>,  
Gerhard Beutler<sup>1</sup>

<sup>1</sup> Astronomical Institute, University of Bern  
Sidlerstrasse 5, 3012 Bern; Switzerland

<sup>2</sup> Institute of Geodesy and Geophysics, Vienna University of Technology  
Gusshausstraße 27–29, 1040 Wien; Austria

<sup>3</sup> Institut für Astronomische und Physikalische Geodäsie, Technische Universität München  
Arcisstraße 21, 80333 München; Germany

Published in *Journal of Geodesy*, DOI 10.1007/s00190-010-0417-z

Received: 29 March 2010 / Accepted: 02 October 2010

## Abstract

*In recent years, several studies have demonstrated the sensitivity of Global Navigation Satellite System (GNSS) station time series to displacements caused by atmospheric pressure loading (APL). Different methods to take the APL effect into account are used in these studies: applying the corrections from a geophysical model on weekly mean estimates of station coordinates, using observation-level corrections during data analysis, or solving for regression factors between the station displacement and the local pressure.*

*The Center for Orbit Determination in Europe (CODE) is one of the global analysis centers of the International GNSS Service (IGS). The current quality of the IGS products urgently asks to consider this effect in the regular processing scheme. However, the resulting requirements for an APL model are demanding with respect to quality, latency, and — regarding the reprocessing activities — availability over a long time interval (at least from 1994 onward). The APL model of Petrov and Boy (2004) is widely used within the VLBI community, and is evaluated in this study with respect to these criteria.*

*The reprocessing effort of CODE provides the basis for validating the APL model. The data set is used to solve for scaling factors for each station to evaluate the geophysical atmospheric non-tidal loading model. A consistent long-term validation of the model over 15 years, from 1994 to 2008, is thus possible. The time series of 15 years allows to study seasonal variations of the scaling factors using the dense GNSS tracking network of the IGS.*

*By interpreting the scaling factors for the stations of the IGS network, the model by Petrov and Boy (2004) is shown to meet the expectations concerning the order of magnitude of the effect at individual stations within the uncertainty given by the GNSS data processing and within the limitations due to the model itself. The repeatability of station coordinates improves by 20% when applying the effect directly in the data analysis and by 10% when applying a post-processing correction to the resulting weekly coordinates compared to a solution without taking APL into account.*

## 6.1 Introduction

The station coordinates established by the space-geodetic techniques are affected by many effects resulting in geometrical site displacements at different time scales and magnitudes. When analyzing observations of the Global Navigation Satellite Systems (GNSS) it has become widely accepted practice to apply solid Earth tides and ocean tidal loading effects using the latest models for these displacements (McCarthy and Petit, 2004), thus removing the largest effects with magnitudes bigger than a few centimeters. The repeatability and consistency of weekly time series of station coordinates (e.g., within the International GNSS Service, IGS, Dow et al., 2009) are therefore well below the centimeter level — even for the vertical component (Ferland and Piraszewski, 2009). Several other geophysical effects are currently not taken into account by the IGS for GNSS data processing — even if the expected effects amount to more than one centimeter. Depending on the location of the station these effects are crustal deformations due to, e.g., atmospheric pressure loading, ocean-induced non-tidal loading, or continental water mass surface loading in the neighborhood of the stations.

Subsequently we focus on atmospheric pressure loading (APL). Several studies successfully assessed APL for space-geodetic data including the validation of geophysical APL models (Tregoning and van Dam, 2005; Steigenberger et al., 2009a; Tesmer et al., 2008; MacMillan and Gipson, 1994; van Dam and Herring, 1994; Böhm et al., 2009; Bock et al., 2005, and many others). Tregoning and Watson (2009) have investigated the impact of ignoring APL in the frequency domain of station coordinates time series. Here we use the model developed by Petrov and Boy (2004) — a model widely used within the VLBI-community (VLBI: Very Long Baseline Interferometry).

The Center for Orbit Determination in Europe (CODE) is interested to improve the quality of the GNSS data processing. For that reason the impact of applying APL

corrections<sup>1</sup> on relevant parameters is evaluated in this paper. Because CODE acts as one of the global analysis centers (AC) of the IGS some additional requirements need to be considered to cover also the operational aspects of this service:

- A consistent set of corrections is necessary for the reprocessing activities at least back to 1994.
- The final products are generated with a latency of only three days. Consequently the APL corrections are (reliably) needed with the same latency at least.
- If the ACs of the IGS start using APL corrections to generate their products, the users of the IGS products will ask for such corrections (e.g., to keep the consistency of a Precise Point Positioning, PPP, Zumberge et al., 1997), as well.
- Because of the substantial number of GNSS sites (in particular outside the IGS) an open access of the APL model in grids with a sufficient spatial resolution is required. Providing corrections as time series for individual stations (as it is done, e.g., for VLBI) is not feasible.

These requirements were considered, e.g., when selecting the APL model and its representation.

The set of GNSS stations included in the CODE reprocessing effort (details are provided in Sect. 6.2.1) is used here for validating APL corrections, to compare different methods to consider the APL effect in the GNSS data analysis, and to assess the impact of APL on some selected parameters of the GNSS data processing. The density and the global distribution of the GNSS sites in combination with the nearly continuously available observations make this material an ideal data set to study APL. The APL model by Petrov and Boy (2004) is described in Sect. 6.2.2.

The weekly GNSS solutions are compared to weekly mean values emerging from the APL model in Sect. 6.3.1. In a second step the corrections from the APL model are directly applied to the individual observations in the parameter estimation process. To assess the quality of the corrections, scaling factors for the APL corrections from the model are estimated as additional parameters. The results are discussed in Sect. 6.3.2.

As an alternative to introducing a geophysically–derived APL model one may estimate regression factors between the local pressure and the station displacement; this approach is discussed in Sect. 6.4. The study is concluded in Sect. 6.5 by comparing the repeatabilities of the coordinate time series based on the different strategies of applying the APL corrections. Because these results are derived from processing a global and dense GNSS network, the impact of correcting or not correcting for the APL effect on global parameters (datum definition and GNSS satellite orbits) is discussed in Sect. 6.6.

---

<sup>1</sup>For GNSS measurements only corrections for the vertical and horizontal site displacement as provided by an APL model are relevant. Therefore we use the term APL “corrections” subsequently without stating each time that these are the displacement corrections.

## 6.2 Data sets

### 6.2.1 GNSS solution

CODE is a joint venture of the Astronomical Institute of the University of Bern (AIUB, Bern, Switzerland), the Swiss Federal Office of Topography (swisstopo, Wabern, Switzerland), the Federal Agency for Cartography and Geodesy (BKG, Frankfurt am Main, Germany), and the Institut für Astronomische und Physikalische Geodäsie of the Technische Universität München (IAPG/TUM, Munich, Germany). All operational computations related to the IGS are performed at the AIUB using the latest development version of the Bernese GPS Software (Dach et al., 2007).

CODE participated in the first reprocessing effort of the IGS. The corresponding computations were performed at IAPG/TUM between summer 2008 and spring 2009 (Steigenberger et al., 2009b). The cleaned observation files, including the resolved integer carrier phase ambiguities, were used to generate a new set of daily solutions by making use of the latest CODE processing models and strategies (Schaer et al., 2008): satellite orbit parameters<sup>2</sup> only for GPS, Earth rotation parameters (with daily time resolution), station coordinates, and troposphere parameters are set up and estimated from the data. Because it is the usual practice in the IGS (but also for the other space-geodetic services) we derive weekly solutions by stacking the daily normal equation systems and by solving the resulting normal equation system. The procedure results in 783 weekly normal equation systems covering the time interval between GPS weeks 0729 (January 1994) and 1511 (December 2008).

The weekly solutions are subsequently stacked to generate a cumulative solution. Outliers and discontinuities are automatically detected in this solution using the program FODITS (acronym for “find outliers and discontinuities in time series”, Ostini et al., 2008), a new component of the Bernese GPS Software. Linear station motion is taken into account by this program. The datum definition is realized by minimum constraints strategy by applying no-network-rotation conditions with respect to the IGS05 (an IGS-specific realization of ITRF2005, Altamimi et al., 2007) on a set of reference stations verified by inspecting the residuals of a Helmert transformation. For all solutions in this study the same outliers and discontinuities were identified and removed, and the same reference sites were used.

According to Steigenberger et al. (2009a) parts of the APL deformation may be absorbed by the troposphere modeling in the GNSS data processing. In contrast to the operational processing at CODE we use, therefore, the Vienna Mapping Function 1 (VMF1, Böhm et al., 2006b) and a priori hydrostatic zenith path delays derived from the European Centre for Medium-Range Weather Forecasts (ECMWF), provided as

---

<sup>2</sup>Six initial osculating elements and nine empirical parameters are set up for each satellite arc. The empirical parameters consist of three constant and six once-per-revolution parameters in the Sun-oriented coordinate system according to the orbit model described in Beutler et al. (1994). Four of the periodic parameters (the  $D$ -components pointing from the satellite to the Sun and the  $Y$ -components going along the solar panel axis of the satellite) are heavily constrained to zero. Empirical velocity changes (so-called pseudo-stochastic pulses) are set up in three orthogonal directions, constrained, and solved for at 12 hour intervals.

a component of the VMF1. These coefficients are interpolated from the grid files ( $2.0^\circ \times 2.5^\circ$  every six hours) and corrected for the actual station height according to Kouba (2008).

### 6.2.2 Time series of atmospheric pressure loading corrections

The variation of the mass distribution in the atmosphere is causing changes in the loading deformation of the Earth surface, where the mass distribution can be expressed by the distribution of the surface pressure  $p(\varphi, \lambda, t)$  as, e.g., provided by global weather models. The permanent deformation caused by the long-term mean pressure field  $\bar{p}(\varphi, \lambda)$  is included in the station coordinates of the reference frame. For that reasons only the deviation  $\Delta p(\varphi, \lambda, t) = p(\varphi, \lambda, t) - \bar{p}(\varphi, \lambda)$  needs to be considered for the loading computation. The relation between the pressure variations  $\Delta p(\varphi, \lambda, t)$  and the vertical deformation  $\zeta_{up}(\varphi, \lambda, t)$  is given by the so called Green's Function  $\mathfrak{G}_r(\cos \beta)$  characterizing the deformability of the Earth (load love numbers  $h'_n$ ) and considering the angular distance  $\beta$  of the mass from the point of deformation by a development of Legendre polynomials of  $\mathfrak{P}_n(\cos \beta)$ :

$$\zeta_{up}(\varphi, \lambda, t) = \int_A \frac{\Delta p(\varphi', \lambda', t)}{g} \cdot \mathfrak{G}_r(\cos \beta) dA \quad (6.1)$$

$$\mathfrak{G}_r(\cos \beta) = \frac{G \cdot R}{g} \sum_{n=1}^{\infty} h'_n \cdot \mathfrak{P}_n(\cos \beta) \quad (6.2)$$

where  $G$  is the constant of gravitation,  $R$  the mean radius of the Earth, and  $g$  the mean surface gravity according to the used Earth model.  $(\varphi', \lambda')$  denotes the location of the surface element  $dA$ . Analogue loading functions exist for the horizontal components (see, e.g., Farrell, 1972).

The time series of displacements caused by the APL provided by the Service of the Atmospheric Pressure Loading run by NASA GSFC (<http://gemini.gsfc.nasa.gov/aplo>, Petrov and Boy, 2004) were extracted from a global grid representation with a spatial resolution of  $2.5^\circ \times 2.5^\circ$  and a time resolution of six hours. They are provided in the center of mass (CM) frame (Blewitt, 2003). The corresponding  $S_1$  and  $S_2$  constituents of the displacements caused by the APL computed by Petrov and Boy (2004)<sup>3</sup> have been applied at the observation level.

By introducing geophysical models into the GNSS data processing their impact on the reference frame realization needs to be investigated. This seems to be in particular necessary, because the time interval used for this solution differs from the interval used by Petrov and Boy (2004) to compute the reference pressure field  $\bar{p}(\varphi, \lambda)$ . The time-averaged corrections from the APL model are computed for all 240 stations, which are included into the GNSS processing over the entire interval. These mean values

<sup>3</sup>According to Petrov and Boy (2004) four parameters have been estimated for each grid point from the surface pressure fields over the time period from 1980 to 2002: a mean pressure to realize a reference pressure field  $\bar{p}(\varphi, \lambda)$ , sine and cosine amplitude of the  $S_1$  and cosine for  $S_2$  constituent to extract the atmospheric tidal signal.

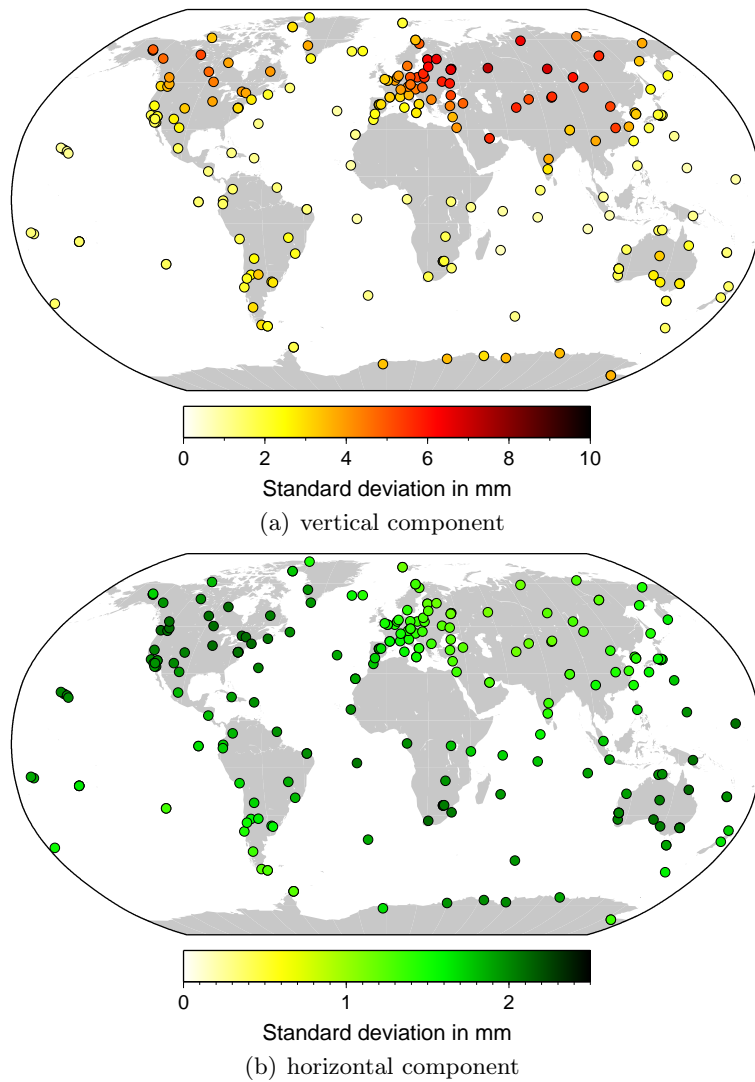


**Figure 6.1:** Standard deviation of the APL corrections from the Petrov and Boy (2004) model over 15 years (January 1994 to December 2008) for the 240 stations included in the GNSS solution.

are below 0.1 mm indicating that the reference pressure field in the background of the APL model is sufficiently accurate to avoid a negative impact on the reference frame realization.

The next step consists of evaluating the order of magnitude of the APL corrections for the stations of the network. The RMS of the APL corrections for the stations of the GNSS solution over the 15 year interval is shown in Fig. 6.1. The figure confirms that the vertical deformations (Fig. 6.1(a)) are small for stations close to the coast line and larger for in-land stations. On the other hand, the horizontal deformations ( $\sqrt{dn_i^2 + de_i^2}$ , Fig. 6.1(b)) are a magnitude smaller than the vertical deformations. The biggest horizontal deformations can in general be found for stations located at the coasts of the big continents. This behavior is a consequence of the inverse barometer hypothesis used in the APL model by Petrov and Boy (2004). As expected, pressure variations are larger at higher latitudes than at the equator.

Fig. 6.1(a) also shows that the size of the vertical corrections is substantially different for the Northern and Southern hemispheres, a consequence of the different ratio between continental and oceanic areas in the two hemispheres; but also the magnitude of the horizontal deformations in Fig. 6.1(b) is not equally distributed. This fact implies that the mean vertical and horizontal corrections over the grid of the APL model can be translated into a variation of the geocenter coordinates (GCC). To assess this effect the corrections for the deformations in the North, East, and Up direction ( $dn_i, de_i, du_i$ ) from all grid points  $i$  (located at the latitude  $\varphi_i$  and longitude  $\lambda_i$ ) are converted into cartesian geocentric coordinates ( $dx_i, dy_i, dz_i$ ) and summed up over all  $m$  grid points for each epoch  $t_n$ :

$$\begin{pmatrix} dX_i(t_n) \\ dY_i(t_n) \\ dZ_i(t_n) \end{pmatrix} = \mathfrak{R}(\varphi_i, \lambda_i) \cdot \begin{pmatrix} dn_i(t_n) \\ de_i(t_n) \\ du_i(t_n) \end{pmatrix} \quad (6.3)$$

$$\begin{pmatrix} dX(t_n) \\ dY(t_n) \\ dZ(t_n) \end{pmatrix} = \frac{1}{m} \sum_{i=1}^m \begin{pmatrix} dX_i(t_n) \\ dY_i(t_n) \\ dZ_i(t_n) \end{pmatrix} \quad (6.4)$$

with the rotation matrix

$$\mathfrak{R}(\varphi_i, \lambda_i) = \begin{pmatrix} -\sin(\varphi_i) \cos(\lambda_i) & -\sin(\lambda_i) & \cos(\varphi_i) \cos(\lambda_i) \\ -\sin(\varphi_i) \sin(\lambda_i) & \cos(\lambda_i) & \cos(\varphi_i) \sin(\lambda_i) \\ \cos(\varphi_i) & 0 & \sin(\varphi_i) \end{pmatrix}$$

The result — the times series of  $dX(t), dY(t), dZ(t)$  — is provided in Fig. 6.2, which shows a variation of almost 5 mm in magnitude in the  $Z$ -component. The  $Y$ -component shows a clear annual variation as well, but only with an amplitude of about 2 mm. The effect for the  $Y$ -component is in turn larger in size than the effect for the  $X$ -component (which is below 1 mm).

As most of the sites in our solution (as most of the space-geodetic tracking sites) are located on the Northern hemisphere, the variations of the GCC induced by the APL effect are amplified when ignoring APL in the data analysis. It is the basic assumption of the GNSS data processing that the center of mass as it is realized by the satellite

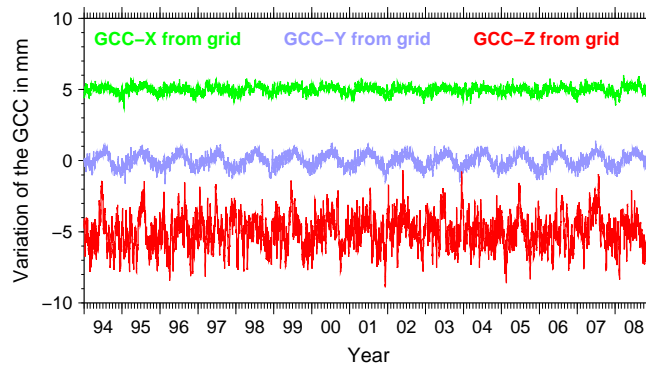


**Figure 6.2:** APL corrections from the  $2.5^\circ \times 2.5^\circ$  grid, translated into variations of the GCC. Individual components were shifted by 5 mm.

orbits and the origin of the terrestrial reference frame (as realized by the coordinates of the ground stations) coincide. Otherwise the obtained satellite orbits may be effected. This aspect will be discussed in Sect. 6.6.2.

## 6.3 Atmospheric pressure loading and coordinate time series

### 6.3.1 Comparisons based on weekly GNSS solutions

A simple way of validating the APL model consists of estimating correlation factors given by the slope of a linear regression between the variation of the station heights in the weekly GNSS solutions and in the weekly mean vertical APL corrections derived from the model. The results are provided in Fig. 6.3. The colors indicate the size of the APL effect as provided by the RMS of the corrections (see Fig. 6.1(a)). Only stations with large APL corrections ( $\text{RMS} \geq 4$  mm) and with at least 300 weekly solutions have been included.

Figure 6.3 shows that most of the correlation factors are between 0.5 and 0.9 and that they are on the average about 0.8 (instead of 1.0 as expected for a perfect model). Note that a 20% deviation from 1.0 corresponds on average to a change of about 1 mm in the vertical station coordinate. It is therefore difficult to decide whether the APL model has deficiencies or whether the deviations have to be attributed to the GNSS analysis (e.g., receiver and satellite antenna calibration, Schmid et al., 2007). It is also possible that the neglected APL corrections are distributed to other sites due to the datum definition of the weekly solutions (see Böhm et al., 2009, and Fig. 6.2).

One should also keep in mind that this method is based on weekly mean coordinate sets derived from GNSS, which are compared to weekly mean APL corrections. The APL correction is computed without applying epoch-specific weights. When calculating the APL corrections it is therefore assumed that the number of GNSS observations is constant throughout the entire week. In the case of GNSS analysis based on real data

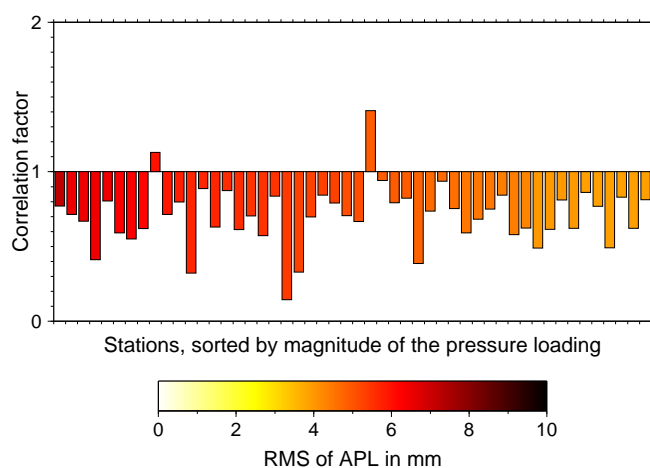


**Figure 6.3:** Correlation factors between the time series of weekly height variations of the GNSS solution and weekly mean APL corrections from the Petrov and Boy (2004) model. The colors indicate the size of the APL effect for the stations (in units of the RMS of the corrections from the model over 15 years).

this is clearly not true because of temporal data outages. In addition, the number of satellites tracked by the stations varies roughly between 8 and 12 satellites throughout a day in the current GPS constellation for mid-latitude sites.

Böhm et al. (2009) state that the variation of the APL effect within 24 hours may be significant compared to the magnitude of the effect itself. It is therefore necessary to check the impact of our simplifying assumption resulting from the weekly processing schedules of the space-geodetic services. These results are presented in Sect. 6.3.2. There are, however, also possible advantages of the simplified procedure as they are discussed, e.g., by Collilieux et al. (2010): The GNSS solution itself does not contain any APL model. (1) Solutions based on the same space-geodetic technique or (2) solutions based on different techniques may be corrected after data analysis and before combination in a consistent way using identical values. This aspect may be important for the rigid processing scheme applied within the IGS, because a dependency on the external generation of the APL corrections may be introduced due to different latencies of the APL and GNSS products. If, e.g., the final solution is running three or four days behind real time, the latency of the APL corrections available at <http://gemini.gsfc.nasa.gov/aplo/> is not sufficient (APL latencies of more than one week occur occasionally). For a GNSS reprocessing effort such latencies are, of course, no issue.

### 6.3.2 Comparisons by direct estimation of scaling factors

The APL corrections are directly applied to the observations in the GNSS analysis in this section and scaling factors for the vertical and the horizontal components are estimated for each station. The corresponding additional parameters are stacked when combining the daily and weekly solutions to the long-term GNSS solution as

described in Sect. 6.2.1. Note that these scaling factors are considered as constants for a station, even if a discontinuity had to be introduced in the coordinate time series.

The resulting scaling factors are provided in Fig. 6.4 and the colors are related to the RMS of the APL correction over the time interval of 15 years. Only sites available in at least 300 weekly solutions and with a minimum RMS in the APL of 4 mm are included. The ordering of the stations is the same as in Fig. 6.3. The deviation from the expected scaling factor of 1.0 is in general below 30%. For stations with big APL effects deviations between 10 and 20% are typical. In view of the expected uncertainties of the model (15%, Petrov and Boy, 2004) and the GNSS solutions (week-to-week repeatability for the vertical component of about 1.5 mm for the best stations, Schaer et al., 2008) the APL model may be considered as “confirmed” by the GNSS solution.

The scaling factors displayed in Fig. 6.4 (estimated from the GNSS data when applying the APL corrections directly to the observations) confirm the APL model whereas this is not the case for the correlation factors in Fig. 6.3 (based on weekly mean station deformations and APL corrections). This implies that directly correcting the observations for APL is preferable to applying only weekly mean APL corrections to weekly coordinate solutions.

The direct APL correction on the observation level removed the systematic offset of the correlation factors obtained when correcting only weekly mean coordinate solutions. The relative station-to-station relation seen in the two figures is rather similar for most of the stations, which implies that part of the APL effect has been absorbed by other parameters (or even the NNR-condition) when ignoring the effect in the analysis. When correcting the weekly solutions by weekly mean APL values an “over-correction” of the effect takes place. This phenomenon is comparable to what Böhm

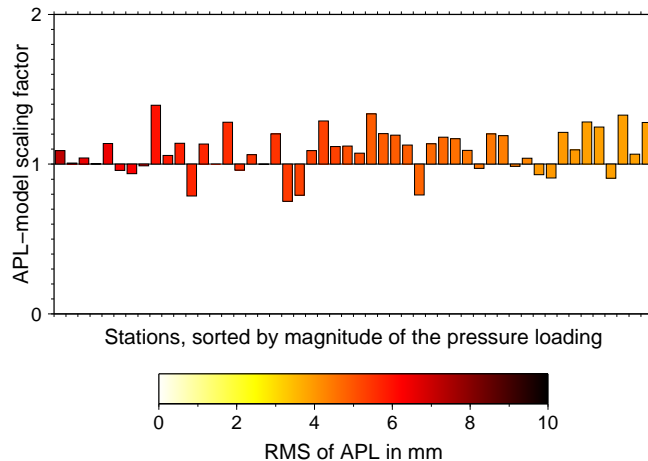


**Figure 6.4:** Scaling factors for the APL corrections from the Petrov and Boy (2004) model computed from 15 years of GNSS processing. The colors indicate the size of the APL effect for the stations (in units of the RMS of the corrections from the model over 15 years).

et al. (2009) showed: In the VLBI analysis the neglected APL corrections are distributed to the other stations in the network. Even if our GNSS analysis includes many more stations with a better global distribution, about two thirds of the stations are located in the Northern hemisphere — and roughly 20% of all included sites are in Europe.

Among the stations contributing to Fig. 6.4 there are two receivers, both located at Kirkkonummi, Finland, namely METS and METZ<sup>4</sup>. In the global network solution both sites have been treated as independent (the observations are used with the ionosphere-free linear combination with individual troposphere parameters). Nevertheless, “the same” results concerning APL are expected because of the closeness of the two receivers. The correlation factors associated with the weekly GNSS solutions and the weekly mean APL values from the model are 0.55 and 0.59, respectively. The values indicate that the APL corrections stemming from the model are about twice the size of the effect seen by the GNSS analysis. In contrast to that, the estimated scaling factors for the APL model as established on the observation level are 0.94 and 0.96, respectively, for the two receivers and agree even better than the results obtained with the weekly mean APL corrections. Nevertheless, both pairs of correlation factors and scaling factors agree within the statistical expectation.

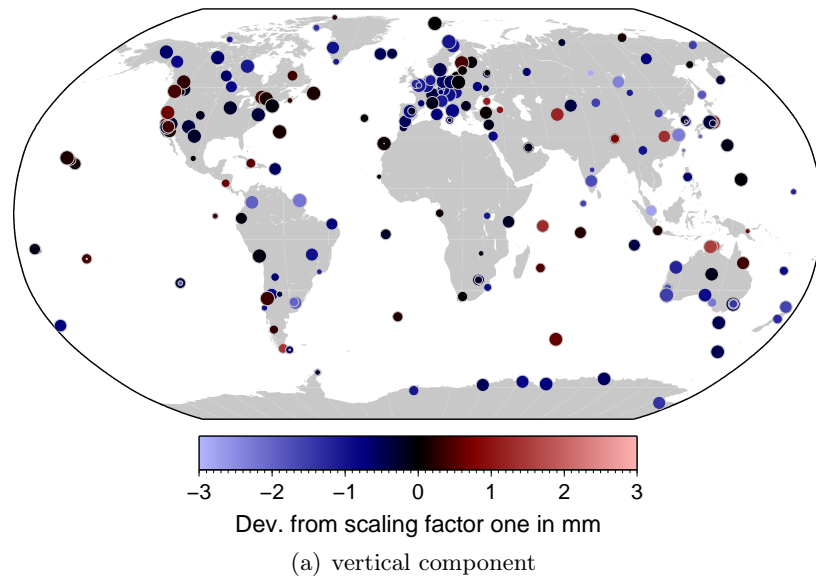
Figure 6.5 gives a complete overview of the resulting scaling factors. The deviations of the scaling factors from 1.0 are scaled by the RMS of the APL corrections for each of the three components from the model (see, e.g., Fig. 6.1(a) for the vertical component) to take into account the sizes of the APL effects at the individual stations. Different occupation times for the IGS stations are characterized by different sizes of the symbols — larger circles indicate a more reliable scaling factors because of the length of the time series.

Figure 6.5(a) shows black or very dark dots for nearly all stations, indicating that the APL model agrees on the 1 mm level with the GNSS solution. On the one hand, no systematic deficiencies for the APL model values, e.g., in particular regions, could be found. On the other hand, some stations in the GNSS solution contribute only with a limited number of weeks to this validation, which is indicated by smaller circles.

Figures 6.5(b) and 6.5(c) show the analogue results for the horizontal components: a general confirmation for the APL model. Black or dark symbols are related to deviations of about 0.5 mm from a scaling factor of 1.0. In the North–South component bigger exceptional points (symbols with light colors, north Canada and Kourou) are found than for the East–West component. Negative scaling factors dominate for stations in South America for the East–West component whereas positive scaling factors are found in Australia. This fact indicates deficiencies in the reference frame realization due to the inhomogeneous station distribution in the network, in particular the extremely high concentration of stations in Europe. This effect is amplified by the

---

<sup>4</sup>There are more examples for groups of GNSS receivers at the same location in the processed network, but either the magnitude of the APL effect is much smaller at these locations or fewer than 300 weekly solutions are available suggesting a higher uncertainty for the obtained scaling factors.



Scaling factors derived from:  
 ○ 15 years of data   ○ 12 years of data   ○ 9 years of data   ○ 6 years of data

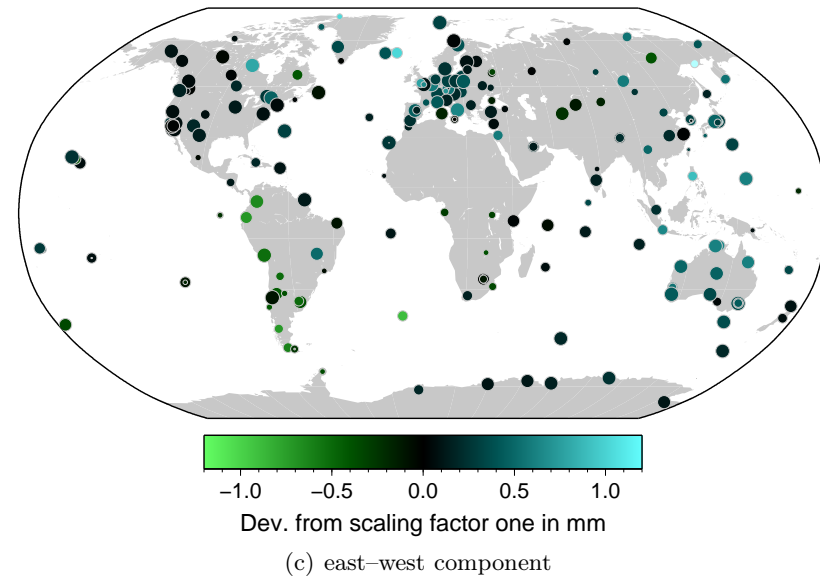
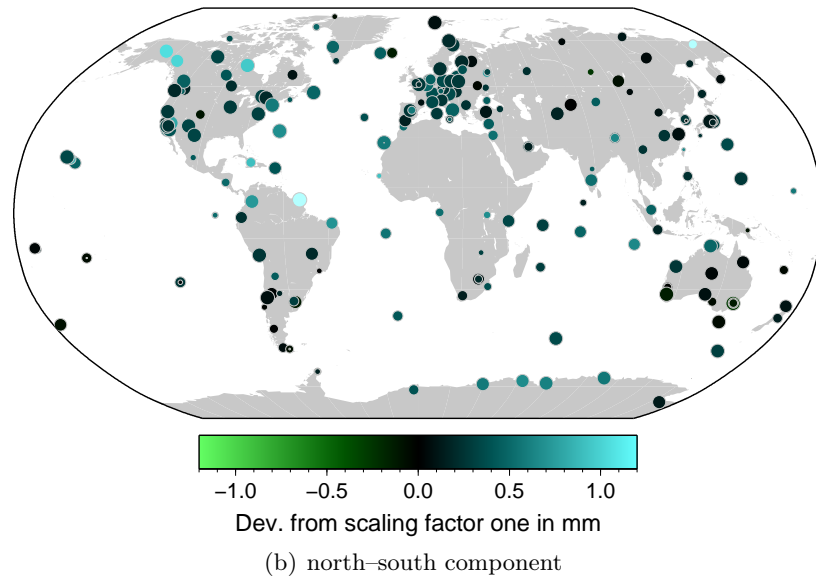
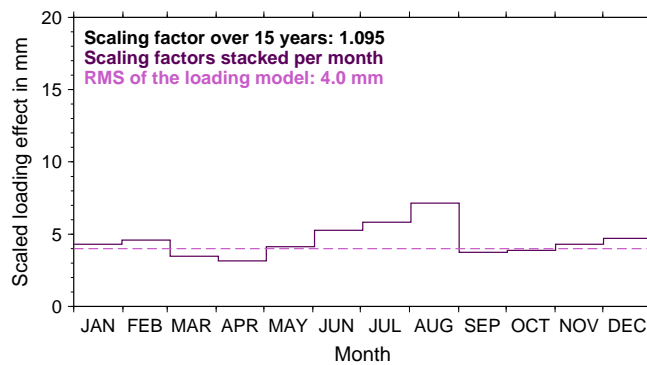


**Figure 6.5:** Deviation of the scaling factors from 1.0 for the APL corrections emerging from the Petrov and Boy (2004) model established by the analysis of 15 years of GNSS data scaled by the size of the APL correction for the station (in units of the RMS of the corrections from the model over 15 years).

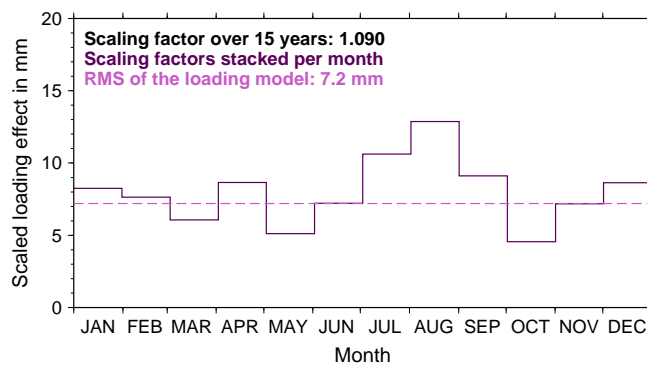
simultaneous estimation of the three APL model scaling factors per station (if the APL values do not vary in time it is a one-to-one correlation).

In summary, more than 80% of the stations show a deviation of less than 0.5 mm for the rescaled scaling factors in the horizontal components (as displayed in Fig. 6.5), if only stations with a minimum data interval of 300 weeks are considered. In the case of the vertical component a deviation of less than 1 mm is detected for 75% of the sites.

The scaling factors are available for each station in weekly normal equations, allowing it to stack all weekly scaling factors belonging to a particular month. This results in 12 scaling factors per station referring to each month of the year. These values can be used to decide whether the APL model values agree on the same quality level for all months of the year with the corresponding estimated values. The coordinates and velocities of the cumulative solution covering 15 years with one scaling factor for the entire interval are introduced as known. This procedure prevents the estimated



(a) Station Zimmerwald, Switzerland



(b) station Arti, Russia

**Figure 6.6:** Scaled loading effect per month computed by stacking the weekly scaling factors of each month over all the years to obtain twelve scaling factors per station (in units of the RMS of the APL corrections from the model over 15 years). The dashed line indicates the RMS of APL corrections — it refers to the scaling factor of 1.0.

station coordinates and velocities to absorb parts of the annual variations of the scaling factors.

Figure 6.6(a) shows the result for the Zimmerwald site in Switzerland as a typical European station with a moderate APL effect. Figure 6.6(b) shows the results for Arti, Russia, which is the station with the largest APL effect in the GNSS solution.

Large deviations from the expected scaling factor of 1.0 and also from the mean scaling factor over 15 years occur in particular for the summer months. It is very unlikely that the APL model is of lesser quality during this period than in the remaining months of the year. It is more likely that other effects of the same size as APL (e.g., ocean-induced non-tidal or continental water mass surface load) not taken into account in the GNSS analysis, are responsible for this deviation.

## 6.4 Atmospheric pressure loading corrections based on local pressure time series

The APL effect on vertical station displacements is fully described in Eqs. (6.1) and (6.2). The Green's function does quickly decrease with increasing angular distance implying that the loading deformation mainly depends on the masses located close to the point for which the deformation is computed. Considering this fact, approximations have been suggested to simplify the computation of APL. Rabbel and Zschau (1985) have proposed to consider only the distribution of the atmospheric pressure in a distance of up to 2000 km around the point where the deformation shall be computed. But even with this approach, for each of the big numbers of GNSS tracking stations a separate loading computation is necessary before the processing of the GNSS measurements can be started. There is a number of studies (Tesmer et al., 2008; Kaniuth and Vetter, 2006, and others), which solve for regression factors between the time series of local pressure and vertical station displacement to take the APL effects into account. Some of these studies introduce annual variations for the regression factors (e.g., Manabe et al., 1991).

It is clearly only an approximation taking only the vertical component into account and ignoring the pressure distribution around the tracking station. It has the advantage that the dependency on externally generated APL models is avoided. The local pressure values at the observing stations are a component of the troposphere delay model. They are available for the GNSS data processing, if local atmosphere values are considered for the a priori troposphere model (e.g., the hydrostatic zenith path delay as provided by Böhm et al., 2006b, which is derived from the ECMWF weather model).

By introducing time series of local pressure instead of the APL model one can also generate a comparable solution for the 240 stations of the CODE reprocessing solution. Local pressure as a function of time is extracted from the grids of VMF1 coefficients. The mean pressure for each grid point over the 15 years considered here is computed to obtain a reference pressure field. The deviation from this mean pressure field for

each individual grid file is the pressure anomaly used for the estimation of regression factors in the following analysis.

#### 6.4.1 Comparison of APL corrections with local pressure data

Before analyzing the GNSS-derived regression factors the regression factors between the APL corrections of the Petrov and Boy (2004) model and the local pressure field are studied. A small inconsistency occurs, because the APL corrections are computed from data of the NCEP (National Centers for Environmental Prediction) whereas the local pressure values are extracted from the ECMWF. According to van Dam et al. (2003) the differences between the two models are small enough not to have a significant impact on the APL modeling.

At each grid point of the APL model a regression factor relative to the local pressure is computed from the 15 year period between 1994 and 2008. The result is shown in Fig. 6.7(a), the corresponding formal uncertainty of the regression factors in Fig. 6.7(b). The regression factors lie between  $-0.3$  and  $-0.5$  mm/hPa for most of the continental regions. They are larger (up to  $-1.0$  mm/hPa) for central Asia. The Himalaya region, where the regression factors are even positive, is an exception. This regional anomaly currently cannot be explained, but it might be related to the realization of the reference pressure and the topography in the area. Surprisingly, the regression factors are not zero over the ocean areas close to the equator — but the formal uncertainties of the regression factors in these regions are up to ten times larger than elsewhere. These features are, however, related to the inverted barometer hypothesis realized over the oceans and need not be discussed further.

The formal uncertainty of the regression factors mainly depends on the magnitude of the variation of local pressure as a function of time. The larger the variation of local pressure values, the better the regression factors can be established. Therefore, the RMS values of local pressure of the global grid are provided in Fig. 6.8, which explains the regions of higher uncertainty of the regression factors in Fig. 6.7.

Because seasonal variations of the scaling factors for the APL model were detected in the GNSS data at the end of Sect. 6.3.2, the regression factors between the APL model and the local pressure were also computed on a monthly basis using 15 years of data. The twelve maps in Fig. 6.9 reflect the monthly mean regression factors as established over the 15 years time interval<sup>5</sup>. The largest variations occur in Africa, Central Asia, and close to the Himalaya region. At least a part of these variations may be explained by the uncertainty of the regression parameters corresponding to Figs. 6.7 and 6.8.

---

<sup>5</sup>The mean pressure field used as basis for the local pressure values has been computed as arithmetic mean over the full interval of 15 years for each grid point. Seasonal variations are not considered. For that reason for each monthly map not only a slope (regression factor) but also an offset has been computed.

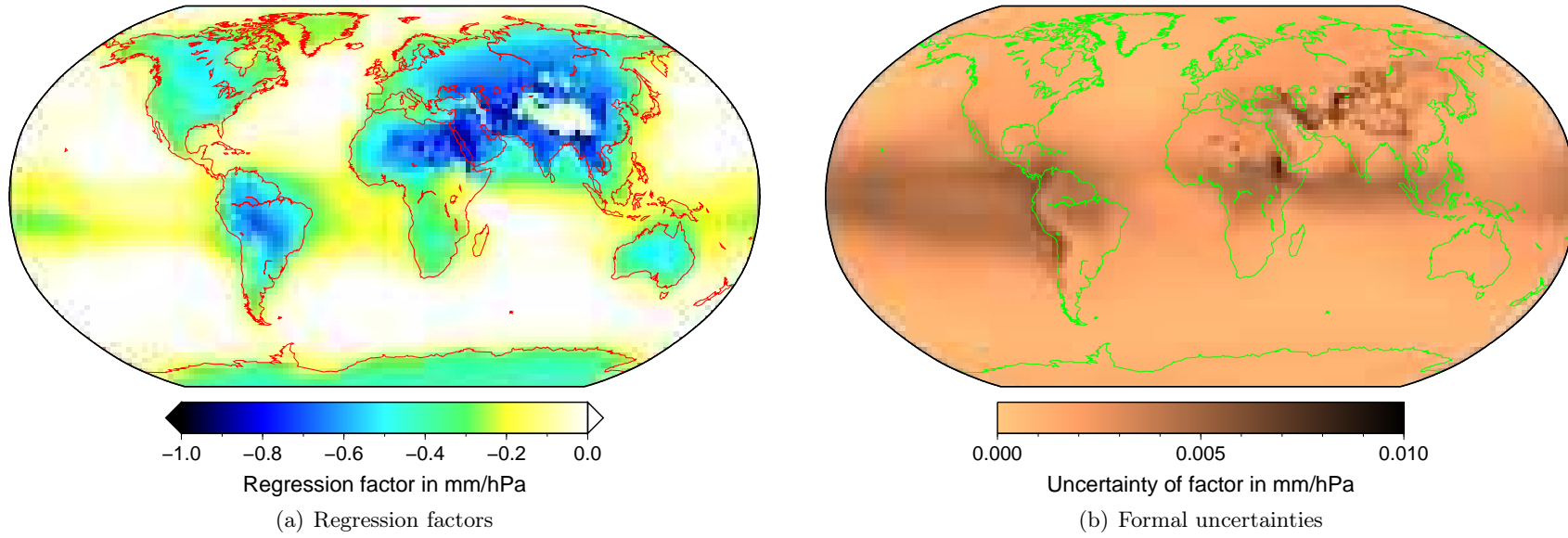


**Figure 6.7:** Regression factors between the time series of local pressure and APL model from Petrov and Boy (2004) (top) over 15 years with their formal uncertainty (bottom).

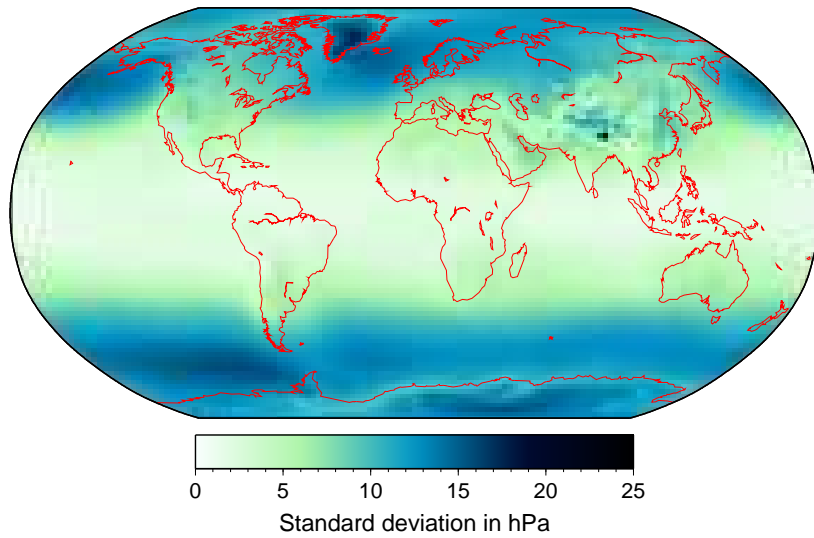


**Figure 6.8:** Standard deviation of the local pressure over 15 years (January 1994 to December 2008).

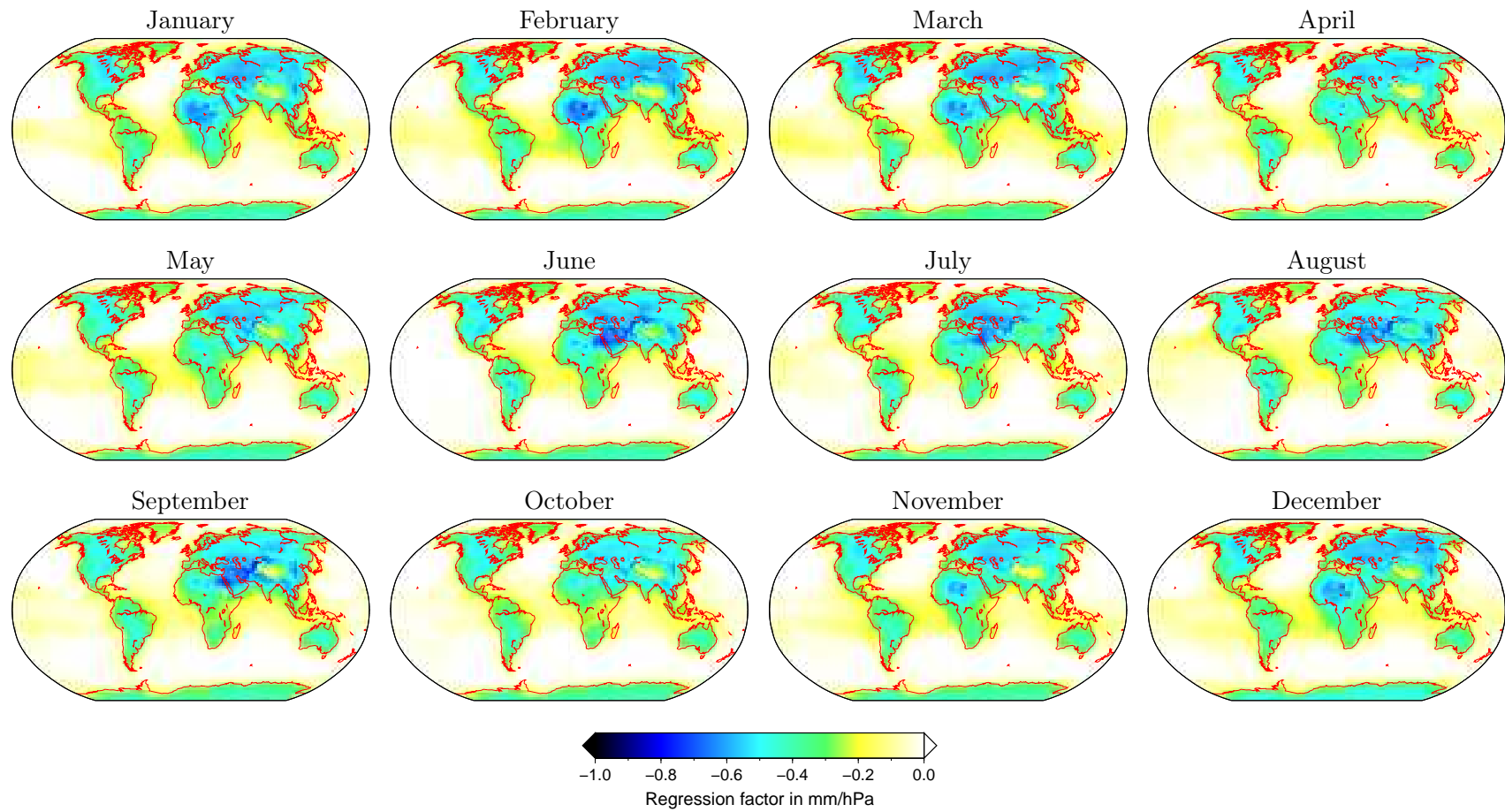


**Figure 6.9:** Mean monthly regression factors over 15 years between the time series of local pressure and the APL model from Petrov and Boy (2004).

Real monthly variations of the regression factors cannot be explained in this experiment: it is a comparison between the local pressure and the APL model with the global pressure field as the main input parameter (apart from the coastal lines and the Green's function which are both constant in time). Possibly, the treatment of the inverse-barometer effect and the mean seasonal pressure distribution may lead to this effect.

#### 6.4.2 Regression factors from GNSS data analysis

The grids containing local pressure are interpolated for the coordinates of the GNSS tracking stations and introduced to compute the regression factors starting from the observation level. The resulting regression factors between the time series of local pressure and vertical displacement for all 240 stations are provided in Fig. 6.10.

In the regions with big APL effects the regression factors are in the expected range between  $-0.3$  and  $-0.6$  mm/hPa. In general these values agree well with results of studies using the same method. Our regression factors are usually in good agreement with the map in Fig. 6.7(a). The size of the circles indicates the different occupation intervals for the IGS stations.

If the regression factors for each particular station and month of the year are considered as common parameters in the weekly normal equation systems of the 15 year time period one obtains twelve parameters per station characterizing the mean annual variation of the station-specific factors. The values for Zimmerwald and Arti are provided in Fig. 6.11. The dashed line shows the monthly regression factors between the local pressure and the APL model. The latter ones are solely based on geophysical

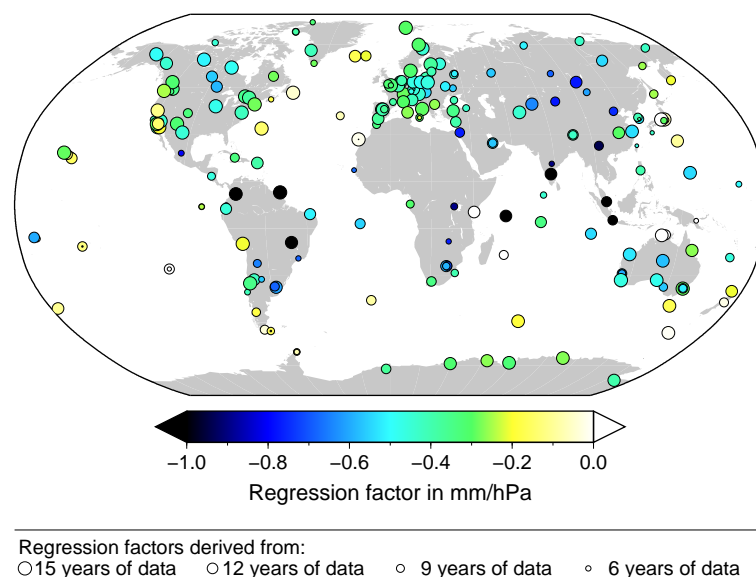
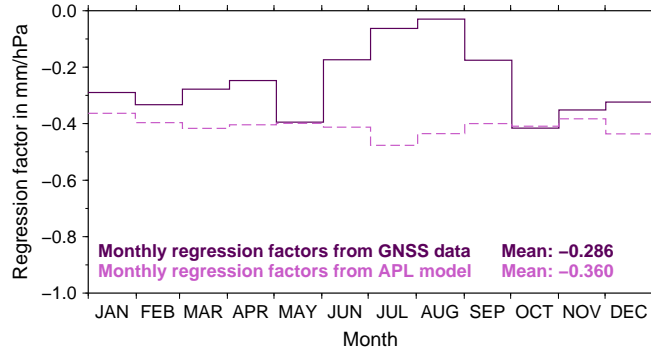
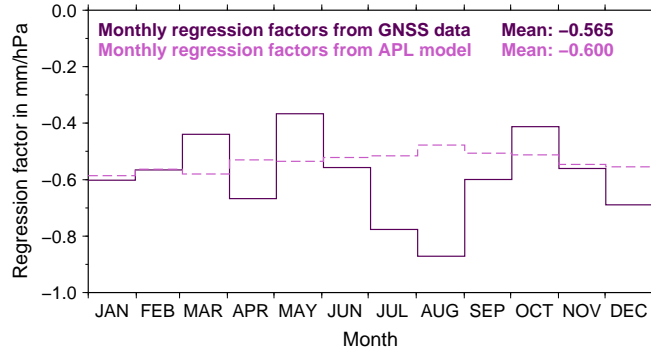


**Figure 6.10:** Regression factors between the time series of local pressure and vertical site displacement from 15 years of data.



(a) station Zimmerwald, Switzerland



(b) station Arti, Russia

**Figure 6.11:** Regression factors between local pressure and vertical station displacement for each month of the year(s) computed by stacking the weekly regression factors of each month to obtain twelve regression factors per station.

models. They are much smoother than the results stemming from the GNSS data. Therefore, these variations are related to other effects than APL (as already suggested in Sect. 6.3).

In Fig. 6.10 there are a few coastal stations with high regression factors of almost  $-1$  mm/hPa. These sites are located close to the equator. The APL effect, as emerging from the model, is very small, see Fig. 6.1. The RMS values are for Kourou (French Guyana, IGS-station ID: KOUR) 1.3 mm, for Bogota (Colombia, BOGT) 1.5 mm, and for La Misere (Seychelles, SEY1) 0.9 mm. The variation of the weekly station positions is, on the other hand, rather high (but can be mostly explained by almost annual signals). The RMS of the weekly station heights for Kourou is 10.1 mm, for Bogota 10.6 mm, for La Misere 10.3 mm.

Figure 6.8 also shows very small variations of the local pressure for these sites (RMS value for Kourou is 1.7 hPa, for Bogota 1.5 hPa, for La Misere 1.9 hPa). The estimation of regression factors is therefore not very reliable for these sites — the formal errors are five to ten times larger than for other sites. The estimated coefficients seem to reflect, as a matter of fact, other unmodeled effects (e.g., due to ocean non-tidal loading effect or site displacements due to continental water mass surface load, which is, e.g., very pronounced in the Amazon area, see van Dam et al.,

2001, or even introduced by the GNSS data acquisition or processing). This conclusion is supported by a pronounced variation of the monthly regression factors:

Kourou	minimum in June:	-2.3 mm/hPa	
	maximum in April:	+0.7 mm/hPa	
Bogota	minimum in July:	-4.6 mm/hPa	It should also be noted that these
	maximum in January:	+0.8 mm/hPa	
La Misere	minimum in December:	-3.6 mm/hPa	
	maximum in March:	+0.6 mm/hPa	

three stations do not belong to the best performing stations in the IGS network. This increases of course the uncertainty the GNSS solution. Nevertheless, the stacking of the weekly solutions for the individual months over several years helps to smooth out this influence.

## 6.5 Effects seen in the repeatability of station coordinates

The repeatability (RMS of the residuals) of the weekly coordinate solutions is a good indicator to assess the benefit of a model for GNSS analysis. Without considering the APL effect it is between 4 and 6 mm for most of the sites — but it may reach or slightly exceed 10 mm for some of the stations. With a few exceptions an improvement of the repeatability of the weekly station coordinate time series between 1 and 2 mm can be found by taking APL into account. These are small numbers, but with respect to the repeatability of the original series without taking the APL effect into account we end up with an improvement of up to 20%.

Figure 6.12 shows the change of the repeatability for the station heights with the largest variation in the APL considering the APL effect by the methods discussed above:

- *blue*: Weekly station coordinate time series are computed without considering APL but corrected by the weekly mean values from the APL model.
- *red*: Corrections from the APL model are directly applied to the observations during the data processing.
- *violet*: APL-corrections are again applied on the observation level but the estimated scaling factor for the APL model for the station is used to rescale the APL model.
- *green*: APL is considered by estimating regression factors between the station height and the local pressure for each station.

In agreement to the findings in Tregoning and van Dam (2005) the improvement of the repeatability is better if the corrections are applied directly to the observations during the data processing (red bars) than obtained when correcting the weekly coordinate solutions for mean APL values (blue bars). In some cases the original APL corrections are worse (red bars) than the rescaled APL corrections (violet bars).

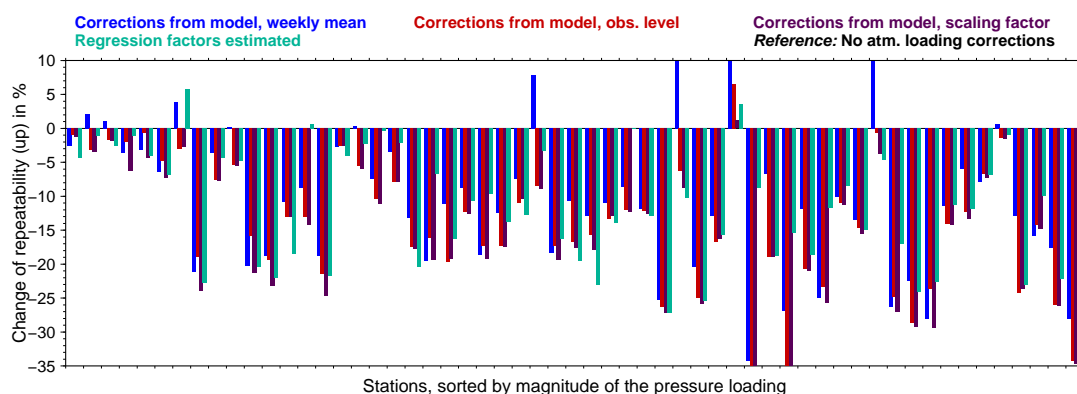


**Figure 6.12:** Improvement/degradation of the repeatability of the station heights (RMS of residuals) as derived from the weekly solutions over the 15 years considering the APL effect in different ways with respect to the solution ignoring APL. Stations with a RMS of larger than 4 mm in the APL corrections in the Petrov and Boy (2004) model over 15 years are given in descending order of the size of the APL-induced effect

For many stations the direct application of the APL corrections is more effective than the use of regression factors between time series of the local pressure and the vertical site displacement (green bars). This result is related to the fact that not only the pressure at the location of the station but also in the surrounding area has an important impact on the APL for a site. Even if the horizontal component of APL is completely ignored by this strategy, there is a marginal improvement on the station repeatability also for North and East component (up to 0.1 mm).

In summary over all about 50 stations in Fig. 6.12 we find only one case where an ignored APL effect gives the best result (all bars in the positive range) and only three examples, where the repeatability favors correcting the APL by mean corrections on the estimated weekly coordinates (blue bars). For eleven stations the best repeatability is achieved by solving for regression factors instead of applying the corrections from the APL model (green bars). For most of the stations the use of the APL model corrections on the observation level thus provides the best repeatability (red or violet bars). In 36 cases (about two thirds of the stations) both versions of the APL corrections on the observation level (the original APL model and the rescaled APL model) are slightly better than applying the APL via regression factors (the green above the red and violet bars).

If the rescaled APL corrections (violet bars) are significantly better for some of the stations than the direct APL corrections (red bars) — in particular if only the violet bars are below the green bars (eleven stations) — should not let us conclude that it is better to apply the rescaled APL corrections for a routine data processing, in particular for deriving a reference frame. Because the scaling factors were estimated station-by-station their influence on the global parameters is unclear. These results should motivate a more detailed investigation of the stations-specific time series, including:

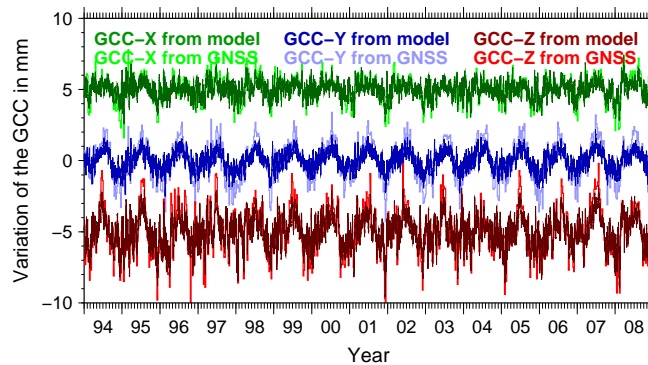


**Figure 6.13:** Variations of the GCC from stacking the APL corrections from the APL model at the locations of the GNSS-tracking stations (light curves) and the difference of the translations in the datum definition of the weekly solutions between a solution corrected for APL and another without correcting APL (dark curves). Individual components are shifted by 5 mm.

- the review whether the GNSS data processing has any deficiencies, e.g., in handling multipath effects,
- the check whether several stations in the same region are affected similarly to review the quality of the input data for the APL computation, or
- the check whether the APL effect is correlated with other geophysically induced crustal deformations (e.g., due to ocean non-tidal loading).

The repeatability of the horizontal components in the weekly solutions without applying any APL correction is on the order of 2 to 3 mm (up to 5 mm for a small number of stations). The repeatability is only changed by a tenth of a millimeter or even less when correcting for APL displacements. This implies that the APL corrections have no significant impact on the repeatability. Nevertheless, it is worth mentioning that applying APL corrections on the basis of weekly mean values degrade the repeatability for nearly all stations, whereas it is slightly improved for all other methods to consider APL. There are only 15 out of 50 stations where the repeatability has been improved by at least 5%. On the other hand, the repeatability for the horizontal component has not been degraded if the corrections from the APL model have been applied on the observation level, what can also be interpreted as a confirmation of the APL model.

## 6.6 Influence of APL on Global Parameters

### 6.6.1 Influence on Geodetic Datum Definition

The two series of weekly coordinates with APL corrections from the Petrov and Boy (2004) model and time series without APL corrections may be compared by a seven-parameter Helmert transformation. The translations should be comparable to the

variations of the GCC derived from the APL corrections. Both time series are provided in Fig. 6.13. For the purpose of comparison the variations of the GCC are computed from the APL model corrections at the locations of the GNSS stations. This reference time series therefore is noisier than the one computed using all grid points (see Fig. 6.2).

The two curves are in good agreement even though the GNSS-derived variations of the GCC show larger variations in the  $Y$ - and  $Z$ -components than the time series derived from the APL model. This finding implies that the APL effect is not absorbed by other parameters than station coordinates. The full APL effect remains in the station coordinate parameters or can be absorbed by the datum parameters when not correcting the data for APL. According to Steigenberger et al. (2009a), the use of ECMWF-derived a priori troposphere delays together with the VMF1 prevented a compensation of the APL effect by the troposphere modeling in the GNSS analysis as it has been observed by the use of the Global Pressure and Temperature model (GPT, Böhm et al., 2007) together with the Global Mapping Function (GMF, Böhm et al., 2006a).

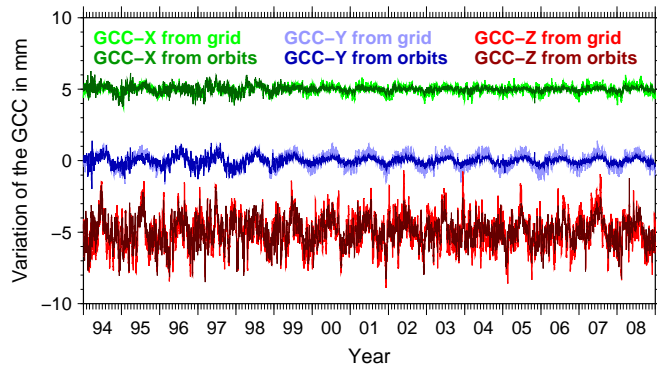
### 6.6.2 Influence on GNSS-Satellite Orbits

The variations in the GCC discussed in Sect. 6.6.1 can be compensated by additional no-network-translation conditions for the minimum constraints datum definition to generate fully consistent realizations of the terrestrial reference frame for series of daily solutions one without and the other one with APL corrections on observation level. If the GNSS satellite orbits of these two solutions, are given by discrete positions of the satellites every 15 minutes in the Earth-fixed frame, they are fully consistent to the coordinate sets of the station coordinates. The two sets of satellite positions computed with and without APL corrections are consequently forced to be in the same reference frame.

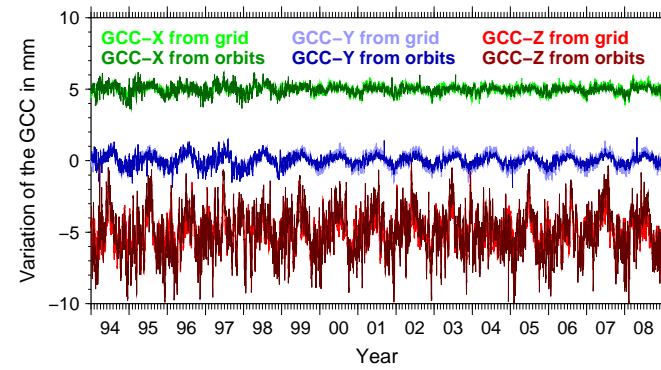
The orbits of two consecutive days,  $i-1$  and  $i$  are expected to have identical positions for each satellite for the midnight epoch  $t_i$ :  $r_{i-1}^{\vec{r}}(t_i) = r_i^{\vec{r}}(t_i)$ . The resulting discontinuities  $|r_i^{\vec{r}}(t_i) - r_{i-1}^{\vec{r}}(t_i)|$  may serve as a quality indicator. The sum of discontinuities over all days  $\sum |r_i^{\vec{r}}(t_i) - r_{i-1}^{\vec{r}}(t_i)|$  do not show any significant effect whether the APL corrections are applied or not.

Applying the APL corrections on the observation level or ignoring APL results in differences in the satellite positions of 3 to 4 mm RMS on average. At least a part of these differences may be explained by daily computed translation between the sets of satellite positions (1 mm in  $Y$ - and 4 mm in the  $Z$ -component). This seems to be in contradiction to the fully consistent station coordinate sets from both solutions which are both computed with the same datum realization and show no systematic differences in terms of transformation parameters (even no translations because of the no-network-translation conditions).

Figure 6.14(a) shows the translation parameters between the two sets of GNSS satellite positions (dark curves). They are compared to the variation of the GCC (light curves) that have already been introduced in Fig. 6.2. At least for the interval after the year

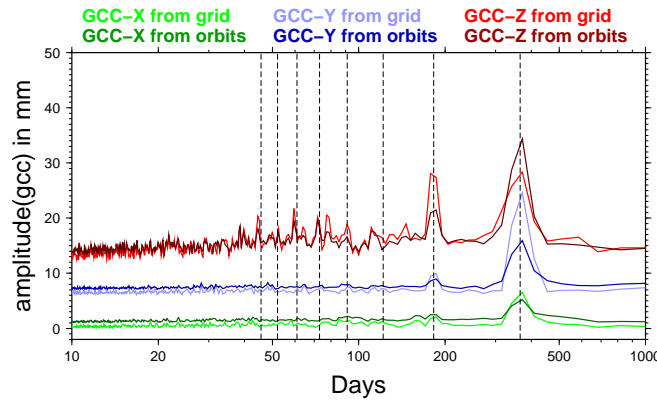


(a) Default orbit determination scheme with constraints to the once-per-revolution terms

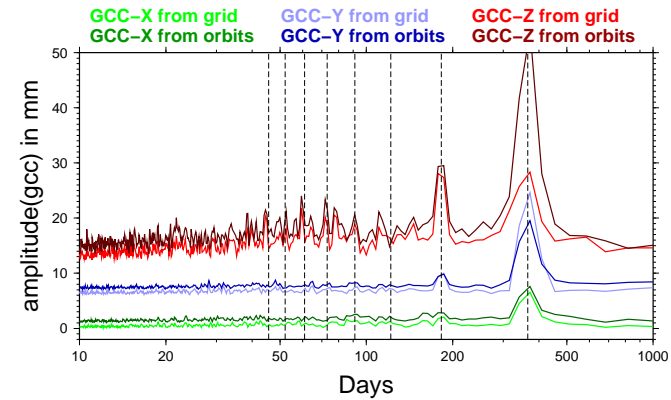


(b) Alternative orbit determination scheme without any constraints to the once-per-revolution terms

**Figure 6.14:** Translations between the satellite positions computed with and without correcting for the APL effect in the Earth fixed coordinate system (dark curves). For comparison, the curves from Fig. 6.2 reflecting the variation of the GCC by the APL corrections are repeated (light curves). Individual components are shifted by 5 mm.



(a) Default orbit determination scheme with constraints to the once-per-revolution terms



(b) Alternative orbit determination scheme without any constraints to the once-per-revolution terms

**Figure 6.15:** Amplitude spectra of the results from Fig. 6.14. Individual components are shifted by 6 mm. The dashed lines indicate the period of one year (365.25 days) and its harmonics.

2000 the  $X$ - and  $Y$ -translation components are in phase but smaller than the APL corrections translated to the GCC. This is supported by the spectra of the time series provided in Fig. 6.15(a).

Dach et al. (2008) have shown that the realization of the origin depends on the parametrization and on the constraining of the once-per-revolution orbit parameters for the GNSS data processing. Assuming that this mechanism works in both directions, the APL induced variation of the GCC may translate into the satellite orbits if the once-per-revolution terms are not sufficiently constrained.

This can easily be verified by inspecting another pair of solution series where the once-per-revolution terms of the orbit model are estimated without applying any constraints. The effect of the APL corrections on this solution with the alternative orbit determination scheme is shown in Figs. 6.14(b) and 6.15(b) respectively. Nearly the full variation of the GCC introduced by the APL effect is absorbed by these orbit parameters. The influence of the alternative results of these terms is reflected by the translations computed between the two sets of satellite positions, with and without APL corrections at the observations during the data processing.

The experiment performed in this section demonstrates that ignoring the APL during the GNSS data processing may affect the GNSS satellite orbits, depending on the orbit model and orbit parameter constraining. Even if the orbit model as it is applied at CODE seems robust for variations of the GCC generated by APL there are other ACs in the IGS that apply other or even no constraints to the once-per-revolution terms. Because the GNSS orbits cannot be corrected on the basis of weekly mean station coordinates (satellite orbits are not included in the weekly SINEX files of the IGS) these results are another important argument for applying the APL correction directly to the observations during the data processing.

## 6.7 Summary

The effect of APL is clearly visible in GNSS-derived coordinate time series. Because of the time variation in the APL effect a direct correction to the observations seems to be the right choice, in particular for weekly solutions. This direct correction is justified in particular because the real GNSS observation scenario (with data outages or the variation of the number of measurements per epoch, e.g., due to the satellite visibility) is not unambiguously recoverable from weekly or daily solutions exchanged between the analysis centers. In addition, once-per-revolution orbit parameters may also be affected by the APL effect depending on the used orbit model and the orbit parameter constraining. Information considering the APL corrections has to be documented for further use, e.g., for the combination of results (as it is done today, e.g., for correcting the ocean tidal loading effect).

The application of APL corrections on the observation level improves the repeatability of weekly station heights between 10 and 20% on the average. Correcting weekly solutions for APL only on the basis of weekly mean values from the same model reduces the gain roughly by a factor of two. The application of APL via regression

factors between the time series of local pressure and vertical site displacement is also less beneficial than the application of APL on the observation level, because the distribution of the pressure in the vicinity of the station has a significant impact on the APL of the station and the effect in the horizontal components is completely ignored.

Because observation-level corrections for the APL effect cannot be removed from the solutions, the particular model needs to be carefully checked before making use of the corrections. For this purpose scaling factors for the model of Petrov and Boy (2004) were directly estimated during the GNSS processing of the 15 years of data considered here. The Petrov and Boy (2004) model agrees within the expected uncertainty level of the model with the GNSS analysis. By stacking the scaling factors of the same months within the year(s) in the entire 15 year interval a seasonal variation of the scaling factors was derived. When comparing monthly regression factors between an APL model and the local pressure field the variation is much smaller. Other effects of the same order of magnitude as APL (e.g., ocean non-tidal or continental water mass surface load) and currently not taken into account in the GNSS analysis are most likely responsible for this result.

## 6.8 References

- Altamimi, Z., X. Collilieux, J. Legrand, B. Garayt, and C. Boucher (2007). ITRF2005: A new release of the International Terrestrial Reference Frame based on time series of station positions and Earth orientation parameters. *Journal of Geophysical Research*, 112(B9):401–419, DOI 10.1029/2007JB004949.
- Beutler, G., E. Brockmann, W. Gurtner, U. Hugentobler, L. Mervart, M. Rothacher, and A. Verdun (1994). Extended Orbit Modeling Techniques at the CODE Processing Center of the International GPS Service for Geodynamics (IGS): Theory and Initial Results. *Manuscripta Geodetica*, 19(6):367–386.
- Blewitt G (2003) Self-consistency in reference frames, geocenter definition, and surface loading of the solid earth. *Journal of Geophysical Research*, 108(B2):2103, DOI 10.1029/2002JB002082.
- Bock, D., R. Noomen, and H. G. Scherneck (2005). Atmospheric pressure loading displacement of SLR stations. *Journal of Geodynamics*, 39(3):247–266, DOI 10.1016/j.jog.2004.11.004.
- Böhm, J., A. Niell, P. Tregoning, and H. Schuh (2006a). Global Mapping Function (GMF): A new empirical mapping function based on numerical weather model data. *Geophysical Research Letters* 33:L07304, DOI 10.1029/2005GL025546.
- Böhm, J., B. Werl, and H. Schuh (2006b). Troposphere mapping functions for GPS and VLBI from ECMWF operational analysis data. *Journal of Geophysical Research*, 111:B02406, DOI 10.1029/2005JB003629.

- Böhm, J., R. Heinkelmann, and H. Schuh (2007). Short note: A global model of pressure and temperature for geodetic applications *Journal of Geodesy*, 81(10):679–683, DOI 10.1007/s00190-007-0135-3.
- Böhm, J., R. Heinkelmann, P.J.M. Cervera, A. Pany, and H. Schuh (2009). Atmospheric loading corrections at the observation level in VLBI analysis. *Journal of Geodesy*, 83(11):1107–1113, DOI 10.1007/s00190-009-0329-y.
- Collilieux, X., Z. Altamimi, D. Coulot, T. van Dam, and J. Ray (2010). Impact of loading effects on determination of the International Terrestrial Reference Frame. *Advances in Space Research*, 45(1):144–154, DOI 10.1016/j.asr.2009.08.024
- Dach, R., U. Hugentobler, P. Fridez, and M. Meindl (editors, 2007). *Bernese GPS Software, Version 5.0*. User Manual, Astronomical Institute, University of Bern, Switzerland.
- Dach, R., T. Springer, and Z. Altamimi (2008). Experiment on impact of constrained orbit parameters on station coordinates. In: *International GNSS Service: Analysis Center Workshop*, June 2–6, 2008, Miami Beach, Florida, USA.
- Dow, J., R. Neilan, C. Rizos (2009). The International GNSS Service in a changing landscape of Global Navigation Satellite Systems. *Journal of Geodesy*, 83(3–4):191–198, DOI 10.1007/s00190-008-0300-3.
- Farrell, W.E. (1972). Deformation of the Earth by Surface Loads. *Reviews of Geophysics and Space Physics*, 10:761–797, DOI 10.1029/RG010i003p00761.
- Ferland, R., M. Piraszewski (2009). The IGS-combined station coordinates, Earth rotation parameters and apparent geocenter. *Journal of Geodesy*, 83(3–4):385–392, DOI 10.1007/s00190-008-0295-9.
- Kaniuth, K. and S. Vetter (2006). Estimating atmospheric pressure loading regression coefficients from GPS observations. *GPS Solutions*, 10(2):126–134, DOI 10.007/s10291-005-0014-4.
- Kouba, J. (2008). Implementation and testing of the gridded Vienna Mapping Function 1 (VMF1). *Journal of Geodesy*, 82(4–5):193–205, DOI 10.1007/s00190-007-0170-0.
- MacMillan, D.S. and J.M. Gipson (1994). Atmospheric pressure loading parameters from Very Long Baseline Interferometry observations. *Journal of Geophysical Research*, 99(B9):18,081–18,087, DOI 10.1029/94JB01190.
- Manabe, S., T. Sato, S. Sakai, and K. Yokoyama (1991). Atmospheric Loading Effect on VLBI Observations. In: *AGU Chapman Conference on Geodetic VLBI: Monitoring Global Change*, NOAA Technical Report NOS 137, NGS 49, U.S. Department of Commerce, NOAA/NOS, Rockville, MD, pp 111–122.
- McCarthy, D. and G. Petit (editors, 2004). IERS Conventions (2003). IERS Technical Note 32, Bundesamt für Kartographie und Geodäsie, Frankfurt am Main.

- Ostini, L., R. Dach, M. Meindl, S. Schaer, and U. Hugentobler (2008). FODITS: a new tool of the Bernese GPS Software. In Ihde, J. and H. Hornik, editors, *EUREF Publication, No. 18*, EUREF Symposium, June 18–20, 2008, Brussels, Belgium. in press.
- Petrov, L. and J.P. Boy (2004). Study of the atmospheric pressure loading signal in Very Long Baseline Interferometry observations. *Journal of Geophysical Research*, 109:B03405, DOI 10.1029/2003JB002500.
- Rabbell, W. and J. Zschau (1985). Static deformations and gravity changes at the Earth's surface due to atmospheric loading. *Journal of Geophysics*, 56:81–99.
- Schaer, S., R. Dach, and M. Meindl (2008). CODE Analysis Strategy Summary. URL <http://www.aiub.unibe.ch/download/CODE/CODE.ACN>.
- Schmid, R., P. Steigenberger, G. Gendt, M. Ge, and M. Rothacher (2007). Generation of a consistent absolute phase center correction model for GPS receiver and satellite antennas. *Journal of Geodesy*, 81(12):781–798, DOI 10.1007/s00190-007-0148-y.
- Steigenberger, P., J. Böhm, and V. Tesmer (2009a). Comparison of GMF/GPT with VMF1/ECMWF and implications for atmospheric loading. *Journal of Geodesy*, 83(10):943–951, DOI 10.1007/s00190-009-0311-8.
- Steigenberger, P., S. Schaer, S. Lutz, R. Dach, L. Ostini, U. Hugentobler, H. Bock, A. Jäggi, M. Meindl, and D. Thaller (2009b). CODE contribution to IGS reprocessing: status and perspectives. In: EGU General Assembly, April 19–24, 2009, Vienna, Austria.
- Tesmer, V., J. Böhm, B. Meisel, M. Rothacher, and P. Steigenberger (2008). Atmospheric loading coefficients determined from homogeneously reprocessed GPS and VLBI height time series. In: Finkelstein, A. and D. Behrend (editors) *Measuring the future*, Proceedings of the 5<sup>th</sup> IVS General Meeting, pp 307–313
- Tregoning, P. and T. van Dam (2005). Atmospheric pressure loading corrections applied to GPS data at the observation level. *Geophysical Research Letters*, 32:L22310, DOI 10.1029/2005GL024104.
- Tregoning, P. and C. Watson (2009). Atmospheric effects and spurious signals in GPS analyses. *Journal of Geophysical Research*, 114:B09403, DOI 10.1029/2009JB006344.
- van Dam, T. and T.A. Herring (1994). Detection of atmospheric pressure loading using Very Long Baseline Interferometry measurements. *Journal of Geophysical Research*, 99(B3):4505–4517, DOI 10.1029/93JB02658.
- van Dam, T., J. Wahr, P.C.D. Milly, A.B. Shmakin, G. Blewitt, D. Lavalee, and K. Larson (2001). Crustal displacements due to continental water loading. *Geophysical Research Letters*, 28(4):651–654, DOI 10.1029/2000GL012120.
- van Dam, T., H.P. Plag, O. Francis, and P. Gegout (2003). GGFC Special Bureau for Loading: Current status and plans. In: Richter, B., W. Schwegmann,

and W.R. Dick (editors) *Proceedings of the IERS Workshop on Combination Research and Global Geophysical Fluids*, Verlag des Bundesamts für Kartographie und Geodäsie, Frankfurt am Main, no. 30 in IERS Technical Note, pp 180–198.

Zumberge, J. F., M. B. Heflin, D. C. Jefferson, M. M. Watkins, and F. H. Webb (1994). Precise point positioning for the efficient and robust analysis of GPS data from large networks. *Journal of Geophysical Research*, 102(B3):5005–5017, DOI 10.1029/96JB03860.



# 7 Continuous Geodetic Time Transfer Analysis Methods

Rolf Dach<sup>1</sup>, Thomas Schildknecht<sup>1</sup>, Urs Hugentobler<sup>1,2</sup>, Laurent-Guy Bernier<sup>3</sup>, and Gregor Duddle<sup>3</sup>

<sup>1</sup> Astronomical Institute, University of Bern  
Sidlerstrasse 5, 3012 Bern; Switzerland

<sup>2</sup> now at Forschungseinrichtung Satellitengeodäsie,  
Institut für Astronomische und Physikalische Geodäsie, Technische Universität München  
Arcisstraße 21, 80333 München; Germany

<sup>3</sup> METAS Swiss Federal Office of Metrology and Accreditation  
Lindenweg 50, 3003 Wabern, Switzerland

Published in *IEEE Transactions on Ultrasonics, ferroelectrics, and frequency transfer*,  
vol. 53(7), pp. 1250–1259

Received: 09 September 2004 / Accepted: 21 December 2005

## Abstract

*We address two issues that limit the quality of time and frequency transfer by GPS Carrier Phase. The first issue is related to inconsistencies between code and phase observations. We describe and classify several types of events that can cause inconsistencies and observe that some of them are related to the internal clock of the GPS receiver. Strategies to detect and overcome time-code inconsistencies have been developed and implemented into the Bernese GPS Software package. For the moment only inconsistencies larger than the 20 ns code measurement noise level can be detected automatically.*

*The second issue is related to discontinuities at the day boundaries that stem from the processing of the data in daily batches. Two new methods are discussed: clock hand-over and ambiguity stacking. The two approaches are tested on data obtained from a network of stations and the results are compared with an independent time transfer method. Both methods improve the stability of the transfer for short averaging times, while there is no benefit for averaging times longer than 8 days. We show that continuous solutions are sufficiently robust against modeling and preprocessing errors to prevent the solution from accumulating a permanent bias.*

## 7.1 Introduction

The geodetic method for GPS time and frequency transfer (GPS CP: GPS Carrier Phase) is now a widely accepted method for high accuracy applications. The method makes use of both carrier phase measurements and pseudorange observations. It is a global method providing the precise differences between a number of clocks (entire network, not only one baseline) in a consistent way with a high sampling rate (see, e.g., Schildknecht et al., 1990; Larson et al., 2000). Therefore, not only the long-term stability of clocks but also the short-term behavior may be compared. Another advantage of the geodetic method is the fact that GPS receivers connected to external clocks are inexpensive to operate as compared to other precise time and frequency transfer techniques. After the submission the data the International GNSS Service (IGS)<sup>1</sup> provides high quality results at low cost to the timing community (see, e.g., Ray, 2000; Senior et al., 2004; Hugentobler et al., 2008).

For the purpose of geodetic analysis, four simultaneous measurements are required (code and phase measured at both carrier frequencies) for each satellite observed. Most geodetic receivers are designed strictly for geodetic applications without consideration for the specific requirements of time and frequency transfer. This may cause problems when interpreting the relationship between an external clock driving the GPS receiver and the estimated receiver clock values.

The Swiss Federal Office of Metrology and Accreditation (METAS) has built a Geodetic Time Transfer terminal (GeTT-terminal, description see Dudle et al., 1998) whereas the Astronomical Institute of the University of Bern (AIUB) has implemented the time transfer capability into the Bernese GPS Software package (Hugentobler et al., 2001). In a collaboration of these two institutions the potential and the problems of the method were investigated. In summer 2003 a new phase of the collaboration between METAS and AIUB was started. The aim is mainly

- to install an IGS station at METAS,
- to use the GeTT terminals for comparison of the primary frequency standard FOCS-1 (Joyet et al., 2002) via GPS CP with similar devices of other timing laboratories,
- to improve the routines for time and frequency transfer within the Bernese GPS Software, and
- to compute non-standard solutions.

The present paper focuses on a special solution computed

- to test a new preprocessing capability for the detection of inconsistencies in the code and phase measurements (see Section 7.3), and
- to get experience with two new developments in the Bernese GPS Software to generate continuous time transfer solutions without discontinuities at the day boundaries (see Section 7.4).

---

<sup>1</sup>In March 2005 the translation of the acronym IGS was redefined from *International GPS Service* to *International GNSS Service* to denote that the activity of the IGS has been resp. will be extended from GPS to other Global Navigation Satellite Systems (GNSS), e.g., GLONASS or GALILEO.

The solution covers a period of 150 days at the beginning of the year 2003. The preprocessing was started with 70 IGS stations. For each day a subset of about 40 globally distributed stations was selected after the preprocessing step. Twelve stations equipped with H-masers or located at time laboratories were included in the 40 station subset whenever possible. All solutions discussed in this paper are based on the same set of observations obtained from the 40 station subset. For all computations presented here, the additional input information (e.g., satellite orbits, Earth orientation parameters, station coordinates, and troposphere parameter) are the contributions to the IGS final products of the Center for Orbit Determination in Europe (CODE) located at AIUB. Consequently, the only differences between the presented results are the analysis methods.

## 7.2 Theoretical Background

The parameter estimation in the Bernese GPS Software is based on the standard least squares adjustment method as it is described, e.g., in Koch (1988). While processing the observations a normal equation system is set up. It has to be solved to get estimates for the parameters of interest. Combining the normal equations by stacking of common parameters is a very efficient method to produce, e.g., multi-day solutions. Other GPS analysis software also uses a Kalman filter approach instead.

The basic GPS observation equation for code and phase measurements have the following form:

$$P_i^k = \left| \vec{x}^k - \vec{x}_i \right| + \Delta_{trop} + \Delta_{ion} + \delta m_i^k + c\delta_i - c\delta^k + \epsilon_i^k \quad (7.1)$$

$$L_i^k = \left| \vec{x}^k - \vec{x}_i \right| + \Delta_{trop} - \Delta_{ion} + dm_i^k + c\delta_i - c\delta^k + \lambda N_i^k + e_i^k \quad (7.2)$$

where

$P_i^k, L_i^k$	Code/phase observation of station $i$ to satellite $k$
$\vec{x}_i, \vec{x}^k$	Position vector of station $i$ and satellite $k$ , respectively
$\Delta_{trop}$	Signal delay in the troposphere
$\Delta_{ion}$	Signal delay in the ionosphere
$\delta m_i^k, dm_i^k$	Influence of multipath effects on the code/phase observation of station $i$ to satellite $k$
$\delta_i, \delta^k$	Clock correction of the receiver at the station $i$ , and transmitter of satellite $k$ with respect to GPS time
$c$	Speed of light
$N_i^k$	Phase ambiguity
$\lambda$	Wavelength of the carrier phase
$\epsilon_i^k, e_i^k$	Measurement noise for the code/phase observation of station $i$ to satellite $k$

As the phase measurements are much more precise than the code observations, it is preferable to use the carrier phase data for time and frequency transfer. However,

the main difficulty that arises when using the phases observations to estimate the clock parameters can be seen in Eq. 7.2 where, there is a one-to-one, correlation between the clock parameters and the phase ambiguities coming from the fact that the partial derivatives with respect to these two parameters are proportional to each other. But, while the clock parameters vary from epoch to epoch, the ambiguity parameters are constant over a certain time interval (e.g., for one satellite pass). Because the individual satellites are ascending at different epochs the phase ambiguity parameters do overlap. This allows to compute a frequency transfer solution for a time interval connected by overlapping ambiguity parameters with the high precision of the phase data. An epoch where the ambiguities for all satellites are lost (e.g., because of splitting the data into independent daily computation batches) cannot be bridged by a phase-only frequency transfer solution.

On the other hand, the clock parameters can be computed from the code measurements (see Eq. 7.1) which, however, have a higher noise level than the phase measurements. Combining both observation types together into one parameter adjustment process — applying appropriate weighting for the different observation types — one can benefit from the high precision of the phase measurements also for time transfer. The high precision of a phase-only frequency transfer may be obtained also for the time transfer solution as long as the epochs are connected by ambiguity parameters.

Because of the low weight to the code measurements, the length of the time interval connected by overlapping phase ambiguities mainly defines the precision of the time transfer solution. If the ambiguity parameters are lost for all satellites, then the time and frequency transfer solution is disrupted. The solutions before and after the disruption are independent and the consequence is a discontinuity in the time transfer series. The magnitude of these discontinuities depends on the noise of the code observations. Assuming daily independent time transfer solutions discontinuities up to a magnitude of 1 ns can be found (see, e.g., Ray and Senior, 2003). This value could be decreased if the time interval connected by phase ambiguities can be increased (e.g., by computing 3 day solutions).

The geodetic time transfer method can deliver the high precision associated with the low noise level of the phase observations only within the time interval covered by one processing batch. On the other hand the batch to batch discontinuities in the time transfer are determined by the noise level of the code observations, a fact which is reflected by the day boundary discontinuities. In addition, the uncertainty of the estimated phase ambiguities at the beginning and the end of a day is slightly higher than in the middle of the day because less observations contribute to these parameters. This may directly affect the clock estimates because of the one-by-one correlation between ambiguity and clock parameters.

The idea of the continuous geodetic time transfer methods is to extend the time interval connected by phase ambiguities as much as possible. This results in a solution adequately reflecting the continuous characteristics of the clocks. The high accuracy reachable in a daily solution can be extended over several days keeping the advantage that the geodetic time transfer method makes no assumption on the the physical

behavior of the clocks. In addition, a frequency transfer solution is no longer limited by the day boundary discontinuities.

## 7.3 Preprocessing: code and phase consistency

In this section the results from the preprocessing concerning inconsistencies between the code and phase observations are summarized. Such inconsistencies are, in fact an issue for the geodetic time and frequency transfer in general because the measurements are processed together. In the context of a continuous geodetic time transfer analysis the occurrence of data inconsistency events is even more harmful than in the case of daily batches processing because the effects of the inconsistencies propagate over a processing interval that spans over several days. An investigation of the receiver algorithms and of the environmental mechanisms that could be at the origin of the reported data inconsistency events is out of the scope of this paper.

### 7.3.1 Detection and Corrective Action

The observation equations associated with code and phase measurements, Eqs. 7.1 and 7.2, are almost identical apart from the additional phase ambiguity term  $\lambda N_i^k$  and the opposite sign of the ionospheric delay  $\Delta_{ion}$ . The main effect of the ionospheric delay can be eliminated by forming a linear combination of the observations associated with both carrier frequencies (labelled  $P_{3i}^k$  and  $L_{3i}^k$  respectively). As long as the ambiguity parameter remains constant between epoch  $t_n$  and  $t_{n+1}$  the difference

$$\Delta\delta_i^k(t_n) = \left[ P_{3i}^k(t_{n+1}) - P_{3i}^k(t_n) \right] - \left[ L_{3i}^k(t_{n+1}) - L_{3i}^k(t_n) \right] \quad (7.3)$$

is expected to be zero for all satellites within an uncertainty margin mainly determined by the noise level of the code data. This requires that the influence of the multipath for each observation type is constant too ( $\delta m_i^k(t_n) = \delta m_i^k(t_{n+1})$  and  $dm_i^k(t_n) = dm_i^k(t_{n+1})$ ). In the case of an outlier or of a cycle slip, the difference is non-zero only for a particular observation while the difference stays zero for all other observations made at the same epoch on other satellites.

In some cases the differences  $\Delta\delta_i^k(t_n)$  are non-zero and are the same for all satellites in view from the station  $i$ . This means that the phase clock terms ( $\delta_i$  in Equations 7.1) and the code clock terms ( $\delta_i$  in Equations 7.2) have changed by a different amount between epoch  $t_n$  and epoch  $t_{n+1}$ . We call this type of phase-code inconsistency an internal receiver clock event because all the observations made at a given epoch are affected by the same amount of time inconsistency exactly as if the receiver internal clock had made a step. This is to be distinguished from an event of the external clock driving the GPS receiver that would affect both the phase and code time parameters by the same amount.

After each disruption of the consistency in the phase-code time parameter series, i.e. after each receiver clock event, a new set of phase ambiguity parameters has to

be introduced for all satellites. This constitutes a loss of the continuity in the phase ambiguity parameters that is equivalent to a day boundary interruption, with the same consequences on the time transfer accuracy (see Section 7.2).

### 7.3.2 Multipath Effects

Multipath and related effects affect code and phase observations with a different magnitude. For phase observations the multipath is limited to one fourth of the wavelength (5 cm) whereas for code measurements it can typically reach values of up to 5 m (e.g., Seeber, 1993). Consequently, the change of multipath conditions can also lead to inconsistencies between code and phase observations.

On the other hand, as long as the multipath effects do not corrupt the code resp. phase observations from all satellites of an epoch with the same magnitude, there are good chances to detect the affected data in the preprocessing by screening the post-fit residuals. The remaining part of the multipath may cause a pattern in the estimated receiver clock correction results that usually repeats every day with the repeating satellite configuration (if the multipath conditions are constant from day to day).

Observations that pass the screening algorithm based on Eq. 7.3 can only be affected by multipath that does not change significantly between two consecutive epochs (usually 30 seconds). If the multipath changes slowly the noise level for the detection of the inconsistency events may increase. The algorithm does interpret, however, an abrupt change of the multipath conditions for all measurements of an epoch by the same magnitude (e.g., the change of an electric field in the surrounding of the antenna or the antenna cable that interferes with the GPS signal) as an inconsistency between code and phase data, i.e., as an event that we have called internal receiver clock event. This naming may not correctly describe the actual source of the inconsistency in this particular case but it does not matter because in this paper we do not investigate the source of the inconsistencies but their impact on the geodetic time transfer processing.

### 7.3.3 Classification and Example

Any algorithm based on Equation 7.3 used to detect inconsistencies between the code and phase data is limited by the noise level of the code measurements. Depending on the antenna environment and the receiver type, only events with a magnitude above 15...20 ns can be detected automatically and handled with the current preprocessing tools of the Bernese GPS Software. For smaller receiver clock events it is presently impossible to distinguish reliably between an inconsistency event and multipath.

The receiver clock events leading to inconsistencies between the code and phase data for the period covered by this study are summarized in Dach et al. (2004). The events with a magnitude above 20 ns that are automatically detected during the data

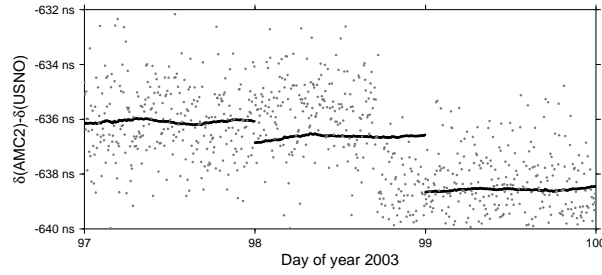


**Figure 7.1:** GPS receiver clock solution for IGS stations at USNO and AMC2 for the days 97 to 99 in year 2003. The dark line is the result of daily independent solutions using code and phase measurements in a common analysis. The dots are the result from a code-only solution for the clocks.

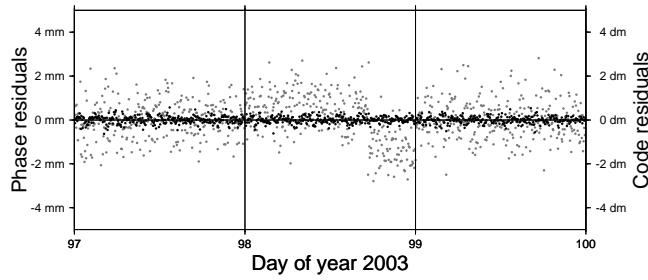


**Figure 7.2:** Code (gray dots) and phase (dark dots) residuals for the IGS site USNO for the days 97 to 99 of the year 2003. The mean residuals of each epoch for all observed satellites are plotted.

preprocessing from the 70 IGS stations selected for this solution can be grouped into three categories:

1. *Millisecond-jumps:* The mean values of  $\Delta\delta_i^k(t_n)$  for all observed satellites is an integer multiple of 1 ms. Since the exact size of the event is known from the characteristics of some receivers, the phase data can be corrected and no setup of additional phase ambiguities is necessary.
2. *Receiver specific jumps:* ASHTECH receivers may show events that are analogous to the millisecond-jumps but the mean difference  $\Delta\delta_i^k(t_n)$  is either  $\pm 28.75$  ms or  $\pm 57.50$  ms. From the events found in the campaign a mean value of 28,750,503.1 ns with an uncertainty of 2.7 ns can be estimated. Because of the uncertainty the phase data were not corrected and new phase ambiguities were introduced.
3. *Tracking problems:* There are also a number of other events with an arbitrary magnitude. Many of them are found in time intervals where the receivers do not track all satellites in view for unknown reasons.

Some of the receivers showing such events are connected to external clocks, others are not. Because of the magnitude of the events (up to about 500...700 ns) they cannot be explained by multipath.

However, inconsistency events smaller than 20 ns exist and affect the time transfer solution, too. Figure 7.1 shows the time transfer results between the IGS stations at USNO (Washington, D.C., U.S.A.) and AMC2 (Colorado Springs, U.S.A.) for three days from the entire solution time series of 150 days. The combined code/phase solution shows a day boundary discontinuity between the days 098 and 099 of about 2 ns which is more than generally expected. A code-only clock solution was added to the figure which is, of course, much more noisy. Nevertheless, at epoch 17:10 of day 098 of year 2003 a jump in the code-only solution of about 2...3 ns can be found whereas the combined code/phase clock solution shows no discontinuity at this particular epoch. Looking at the code and phase residuals for station USNO from the clock solution using code and phase measurements in a common analysis an inconsistency between the code and phase data for the specific epoch is evident (see Fig. 7.2).

Analyzing the data of the IGS station USN1 (another receiver at the US Naval Observatory near to the receiver USNO) for the same time interval reveals no discontinuity, neither in the code-only solution nor in the code and phase combined results. The two receivers are connected to two different clocks but a discontinuity in the steering clocks can be ruled out since no anomaly can be found in published differences of the clocks (URL:<ftp://tycho.usno.navy.mil/pub/usnodc-amc.gpscp/mc2-mc3.rtcrr.cal>). This confirms that the GPS station USNO must be responsible for the jump *and not the clock driving the GPS receiver*.

In addition, the day boundary discontinuities for the station USNO obtained from the generation of the continuous IGS time scale (results and residuals are provided at URL:<https://goby.nrl.navy.mil/IGStime/IGST/1213/USNO.timeplot.ps>) are consistent with those found in the daily independent solution using the code and phase measurements in Fig. 7.1. This independently confirms that the station USNO caused this inconsistency.

### 7.3.4 Consequences for GPS CP Time and Frequency Transfer

These inconsistencies between code and phase data have consequences for the time and frequency transfer using GPS CP:

- A calibration constant for time transfer (e.g., Petit et al., 2001) determined before the event will not be valid after the event.
- The time transfer results for a clock cannot be used for frequency transfer across a receiver clock event if they are based on code and phase data processed in a combined analysis.
- Frequency transfer using a phase-only solution is possible across this particular epoch assuming that the receiver clock event does not have any impact on the phase observations.

A second receiver connected to the same clock may be used to overcome such inconsistency events. Of course, this increases the maintenance and the data flow. The analysis of these additional measurements is only necessary if a receiver clock event has been detected. Results from such experiments may help to find out the circumstances under which the receiver clock events occur.

It is obvious that all these receiver clock events have to be detected during the data analysis to make results useful for time and frequency transfer. From the example given above it is clear that inconsistencies are easier to detect in the middle of an analysis batch. For events taking place close to midnight a continuous solution is preferable from this point of view. On the other hand, in a continuous time transfer series any event that was not detected and handled in the data analysis has an impact on the entire solution whereas in a daily independent processing scheme only the results of the particular day are affected. In the next section methods for continuous time transfer series are discussed.

## 7.4 Methods for Continuous Time Transfer Series

An easy way to overcome the discontinuities at the day boundaries is to analyze the data of a particular time interval twice in overlapping computation batches (e.g., Bruyninx and Defraigne, 1999). After the GPS data analysis, offsets for each baseline can be computed to concatenate the independent time transfer solutions. A demonstration of this method for a long time interval is given in Dach et al. (2002).

The advantage of this approach is that it can use the results from any processing software capable of computing time transfer series without any modifications. The results of the daily solutions may be independently connected with a stand-alone program. The disadvantage is that correlations between the clock parameters of an epoch cannot be considered since this postprocessing step is done baseline by baseline. As a consequence the consistency of the results from the entire network, one of the major advantages of the GPS CP time and frequency transfer is lost. Other methods to overcome the day boundary discontinuities are, therefore, preferable.

A filter approach for the GPS data analysis as proposed in Senior et al. (1999) allows to generate a continuous geodetic time transfer solution. A forward and backward filtering is required and parameters (e.g., phase ambiguities) need to be kept in the system also over the day boundaries. The analogous algorithm for the least squares adjustment used in the Bernese GPS Software consists in a first step in the generation of independent, e.g., daily solutions. In a second step common parameters from the daily solutions are stacked to produce a multi-day solution. To obtain a continuous geodetic time transfer solution either the clock parameters at midnight — easier to implement — or the phase ambiguity parameters from continuously observed satellite arcs — more correctly representing the measurement process — may be stacked. The

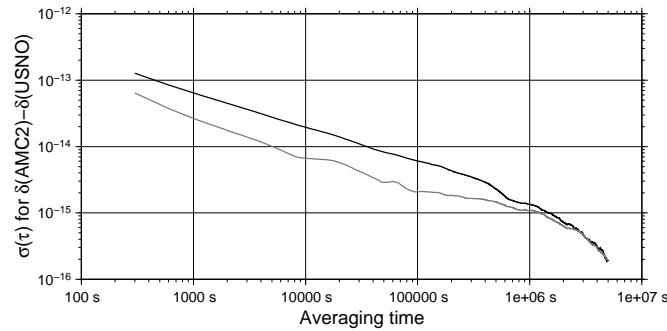


**Figure 7.3:** Allan deviation for the comparison of the receiver clocks of the IGS sites USNO and AMC2 for 150 days of year 2003 (dark line: daily independent solutions, gray line: continuous time transfer series obtained from three-day solutions generated with clock hand-over).

technical realization, the advantages and disadvantages of these two possibilities are discussed in this section.

#### 7.4.1 Clock Hand-over

A procedure to take care of the day boundary discontinuities already in the data analysis step would consist in handing over the clock parameters at midnight. If the computation intervals span from midnight to midnight one epoch is common to both consecutive daily solutions. The clock parameters for the midnight epoch of the previous day may be introduced to connect the daily solutions. The station coordinates, satellite orbits, Earth orientation parameters, and the troposphere estimates have of course to be continuously modeled (only very small discontinuities can be accepted).

A continuous time transfer solution may be produced by using the midnight epoch for a clock hand-over but the initialization still depends only on the first day of the time series. A multi-day solution can be generated when the clock parameters of the midnight epoch from consecutive days are stacked together on normal equation level. In this way the information from the code and phase measurements of  $n$  days can be collected in one normal equation system. To compute, e.g., a three-day solution the normal equations of three consecutive days are connected by the corresponding clock parameters at midnight and all other relevant parameters. The clock solution is computed for the middle day, whereas the clock estimates from the previous step are introduced for the first day of this triple. With this algorithm it is possible to move on with the processing day by day.

Because of the large number of parameters in the normal equation system (one per station and satellite clock for each epoch, ambiguity parameters, and others) such a multi-day solution is generated in several parameter-prelimination and parameter-resubstitution steps. This is a standard procedure which is implemented in the Bernese GPS Software for several parameter types.

To present the results of the time transfer solutions the IGS stations at USNO (Washington, D.C., U.S.A.) and AMC2 (Colorado Springs, U.S.A.) are selected as an example from the global network. Both sites are equipped with ASHTECH Z-XII3T receivers and are connected to H-masers. Common data from both stations are not available for all days within the 150 days analyzed for this study. For this reason, continuous solutions can only be generated for five periods covering about two weeks and one period covering 50 days.

In Fig. 7.3 the Allan deviations for the daily independent solution (dark line) and for a continuous time transfer solution using the clock hand-over method (gray line) are compared. The discontinuities at the day boundaries affecting the daily independent solution vanish. As a result the continuous time transfer solution becomes smoother.

It must be mentioned that Fig. 7.3 is based on a three-day solution. The three-day solution is the optimum span to get a continuous time transfer series with the clock hand-over method. The clock solution of the day  $n$  to be computed is fixed on the results for the previous day  $n - 1$ . In the next step it will be introduced as known for the clock estimation for day  $n + 1$ . Therefore, the continuous time transfer series becomes smoother if the data from day  $n + 1$  are added while computing the clock solution for day  $n$ . The time transfer series cannot be improved by connecting more than three days with the clock hand-over method. The observations from days after  $n + 1$  have no significant impact on the clock estimates for day  $n$  since the results for the clocks from the day  $n - 1$  were kept fixed.

The standard deviation for a single clock difference is 0.9 ns for the daily independent solution resp. 0.8 ns for the continuous solution generated with the clock hand-over method. If only the 50 day interval without data gaps is considered the noise of the clock solution decreases from 0.8 ns to 0.5 ns when applying the clock hand-over method instead of generating daily independent solutions. These values contain of course also the uncertainty on the synchronization between both clocks.

This example demonstrates that the clock hand-over method works well to generate continuous time transfer series. More baselines from the network solution could be added with similar results. The method is efficient because the continuous time series results during the data analysis and the number of parameters to get the continuous solution is limited to one per station resp. satellite. The disadvantage of this approach is that only the midnight epoch (or any other epoch) connects the independent solutions. It is essential that this particular epoch is recorded and that the observations of the epoch are not removed during the preprocessing procedure. The midnight epoch is, e.g., unfortunately not recorded by some receivers (e.g., IGS station NPLD, Teddington, United Kingdom) and as a result, the time transfer series cannot be connected for these stations.

### 7.4.2 Ambiguity Stacking

As stated in Section 7.2 the length of the time interval connected by the phase ambiguities has to be increased to decrease the magnitude of the discontinuities at the day boundaries in the time transfer series. On the other hand, there are technical reasons that limit the time interval of data that can be analyzed together to compute a solution where all epochs are connected by the phase ambiguities (as far as there are no other reasons to lose the connection by the ambiguity parameters, e.g., total loss of the signal by the receiver or receiver clock events leading to an inconsistency between the code and phase measurements).

The way around is simple and it is already applied for many other parameter types in the GPS analysis today: the result of the data analysis of each independent computing batch (usually one day) is a normal equation system containing, among other parameters, also the phase ambiguity parameters. Independent (e.g., daily) solutions can be connected by stacking the corresponding ambiguity parameters at the day boundary together to generate a multi-day solution on normal equation level. This is more efficient than analyzing each observation several times for independent overlapping multi-day solutions and it is a method to overcome the technical limitations for the number of days to be added to a multi-day solution.

This is in principle very simple, but it needs a very involved book keeping in the analysis software. It is not sufficient to assign pairs of ambiguities for stacking by the epoch, the station, the satellite, the frequency, and the wavelength-factor. In addition, the parameters must be initialized identically for all analysis parts (including all relevant corrections, like phase windup — see Wu et al., 1993).

If the preprocessing for the observation files takes place independently for each computation interval, at least one initial phase ambiguity has to be setup for each satellite and station. Whether stacking of the ambiguity parameters is possible depends on the conditions encountered for the corresponding ambiguity parameters of consecutive normal equation systems. They may be classified as follows:

- The GPS receiver worked without any disturbing events across the epoch of the boundaries of the normal equations — the ambiguity stacking is possible.
- A cycle slip took place at the epoch of the boundaries of the normal equations — the ambiguity stacking is not possible.
- An inconsistency between code and phase data due to an internal receiver clock event occurred at the epoch of the boundaries between the normal equations — no ambiguity stacking for all satellites is allowed.
- No data are available for some epochs around the boundaries of the normal equations for any reasons (e.g., deleted in the preprocessing). In this case the stacking is still possible if neither a cycle slip nor a receiver clock event is detected.

It is therefore crucial to check carefully if the conditions for ambiguity stacking are fulfilled before combining the normal equations. At first all pairs of ambiguities to be connected have to be identified. The applied algorithm requires that the differences

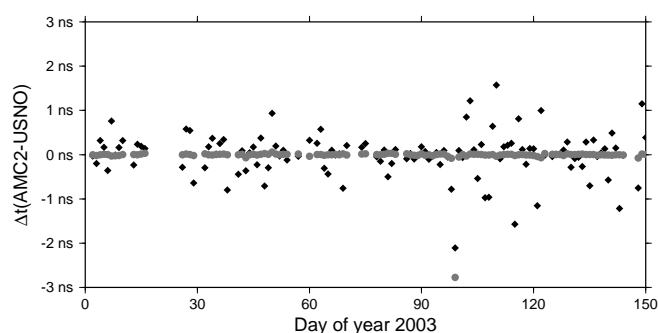


**Figure 7.4:** Day boundary discontinuities — differences of the clock solution for the mid-night epoch obtained in consecutive daily solutions — for the comparison of the receiver clocks of the IGS sites USNO and AMC2 (dark diamonds: daily independent solutions, gray dots: continuous time transfer solution generated with ambiguity stacking).

between the corresponding pairs of ambiguities have to be identical within the phase noise for each station and have to be zero within the code noise assuming a common analysis of the code and phase data. In the case of a cycle slip, the corresponding difference of ambiguities exceeds the phase noise criteria. The code noise condition is intended to detect internal receiver clock events causing an inconsistency between the code and phase measurements.

To compute the clock solution for day  $n$  the normal equations of the days  $n - 1$  and  $n$  are used. All relevant parameters — including the phase ambiguities — are stacked together to generate a two-day solution. To get a continuous time series of the solution the estimated phase ambiguities for the day  $n - 1$  are introduced as known. The ambiguity parameters that are connected across the midnight epoch of days  $n - 1$  and  $n$  are estimated together with the other parameters. This procedure is shifted from one day to the next to generate a continuous solution.

The ambiguity stacking algorithm does not impose directly that the estimated clock values at the day boundaries become identical. The method restores the continuity of the phase ambiguity parameters over the day boundaries that is lost by analyzing daily independent data sets. The magnitude of the remaining day boundary discontinuities corresponds to the noise level of the solution within each day and is, therefore, mainly given by the small noise of the phase measurements.

Figure 7.4 shows the day boundary discontinuities for the receiver clock solutions for the IGS sites USNO and AMC2. For the daily independent solutions (dark diamonds) the discontinuities have a magnitude of up to 1 ns. Applying ambiguity stacking, the steps at the day boundaries are close to zero (gray dots) — a continuous time transfer solution has been generated. The only exception is day 099 of year 2003 where the ambiguities were not connected because of the internal receiver clock event for station USNO discussed in Section 7.3. The magnitude of the corresponding day boundary discontinuity is slightly less than 3 ns. This value is very close to 2.87 ns

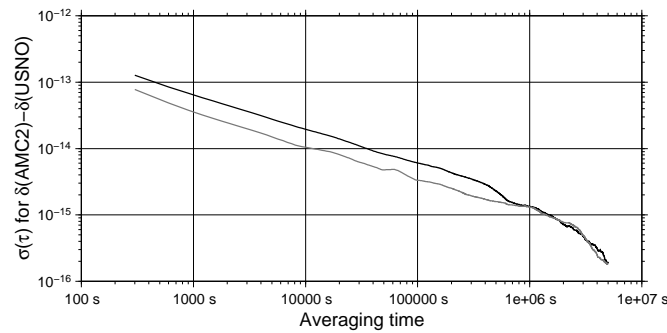


**Figure 7.5:** Allan deviation for the comparison of the receiver clocks of the IGS sites USNO and AMC2 for 150 days of year 2003 (dark line: daily independent solutions, gray line: continuous time transfer solution generated with ambiguity stacking).

which corresponds to the wavelength of the Melbourne–Wübbena linear combination of  $86 \text{ cm}^2$ .

The Allan deviation for the time transfer series of the baseline AMC2–USNO shown in Fig. 7.5 confirms the improvement due to the continuity of the resulting clock solution. The effect of the day boundary discontinuities on the Allan deviation can be seen very clearly. Both curves converge for an averaging time of about 8 days — the effect of the day boundary discontinuities has an impact on the time transfer solutions for shorter averaging time.

A three-day solution may be generated by adding the day  $n + 1$  to the procedure for computing the clock solution for day  $n$ . This extension does not improve the results for the continuous time transfer series as long as the estimates for ambiguity parameters connecting the days  $n$  and  $n + 1$  over the midnight epoch are not introduced as known for processing the next day. Even in that case, no significant improvement is expected unless all ambiguities are lost close to the midnight epoch for day  $n$ . The reason for this is the overlapping of the validity time intervals of the ambiguity parameters, mainly corresponding to the satellite visibility.

### 7.4.3 Comparison

When connecting daily independent solutions over a long time span the modeling of all effects becomes more important since their influences can accumulate in the continuous time series (see Dach et al., 2003). Any data problem that has not been detected and handled in the preprocessing affects not only the solution of one day but the entire resulting time series. This is independent of the method used to generate the continuous time transfer series.

<sup>2</sup>The Melbourne–Wübbena combination is a linear combination of both, phase and code observables as described by Wübbena (1985) and Melbourne et al. (1985). This combination eliminates the effect of the ionosphere, the geometry, the clocks, and the troposphere. Therefore, it is, e.g., useful to check GPS observations for cycle slips or to analyse the noise of the observations — a procedure that may be applied by the receiver software.

**Table 7.1:** Arithmetic mean and its standard deviation for the difference between the time transfer solutions for the first 150 days of year 2003 and values provided in the Circular T for an exemplary set of baselines. The values are given in nanoseconds.

Baseline		Daily independent	Clock hand-over	Ambiguity stacking
USNO	BRUS	$-55.7 \pm 1.8$	$-55.8 \pm 1.7$	$-55.9 \pm 1.7$
USNO	NPLD	$-8715.0 \pm 1.3$		$-8714.8 \pm 1.1$
USNO	PTBB	$-80.6 \pm 2.2$	$-80.8 \pm 2.1$	$-80.8 \pm 2.2$

To confirm the long term stability of the continuous time series, one needs an independent method of time transfer. Circular T publishes on a monthly basis the differences between the coordinated timescale UTC and all local representations  $UTC(i)$ . Among the stations selected for the 40 station network under study, several participate in UTC and their offset is thus announced periodically. If the difference between  $UTC(i)$  and the clock driving the GPS CP equipment is known for all epochs of interest, it is for specific baselines possible to compare the results obtained by GPS CP to those gained from Circular T.

Table 7.1 shows the mean value of the difference between the time transfer based on GPS CP and the time transfer based on Circular T with its corresponding uncertainty. The fact that these differences are not zero indicates that no calibration constant has been applied to the GPS CP method. Nevertheless, the estimates for the calibration constant from this 150 day solution are identical within a few nanoseconds to the corresponding values published in Senior et al. (2004). They are derived from the combined final IGS clock products. Several independent analysis groups contributed to this solution which is based on a more stable network represented by more than 40 stations. Furthermore a longer time interval was analyzed.

There are, however, two points to be mentioned with respect to the uncertainties. The fact that they are small is a direct consequence of the long term stability of the GPS CP method. Indeed, if any modeling or preprocessing problem would accumulate, leading to a drift between the GPS CP result and the Circular T, the uncertainties would be significantly higher. The uncertainty values are identical to the values in Tab. 7.1 — and not smaller — if a linear function instead of an offset is used to model the differences between the geodetic time transfer solutions and the Circular T. Of course these uncertainty values do not only reflect the uncertainty of the geodetic time transfer methods but also the uncertainty of the Circular T values. Second, it is worthwhile noting that neither the clock hand-over nor the ambiguity stacking yields uncertainties smaller than the daily independent solution. This observation is confirmed by the Allan deviation shown in Fig. 7.5. As compared to the daily independent solution, the continuous time transfer improves the stability of the frequency transfer for averaging intervals up to 8 days, while on longer averaging intervals the methods yield the same frequency stability as measured by the Allan deviation.

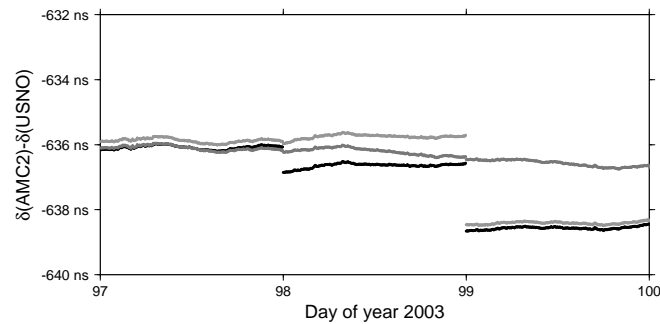


**Figure 7.6:** GPS receiver clock solution for IGS stations at USNO and AMC2 for the days 97 to 99 in year 2003. (dark line: daily independent solutions, gray line: continuous time transfer series obtained from three-day solutions generated with clock hand-over, light gray line: continuous time transfer solution generated by ambiguity stacking).

It is also an important issue to compare how the different methods deal with inconsistencies such as those observed in Sect. 7.3 (see Figs. 7.1 and 7.2). Figure 7.6 displays the receiver clock differences between USNO and AMC2 for the daily independent solution (dark line), the solution obtained with the clock hand-over (gray line), and the solution generated by ambiguity stacking (light gray line) for this particular time interval.

Two methods (daily independent and ambiguity stacking) lead to a discontinuity at midnight of day 099 of year 2003. There is only an offset for each day between both time transfer time series. This is the expected behavior since the time transfer result should be dominated by the frequency precisely obtained from the phase data. In contrast, the continuous time transfer series derived from the clock hand-over algorithm is smooth also for the midnight epoch of day 099 of year 2003. But it shows that the code measurements affect the frequency transfer time series, too. This is caused by a large discrepancy between the code and phase data induced by the receiver clock event.

By construction, the clock hand-over has one clock parameter for the midnight epoch of day 099 of year 2003 whereas the other two methods are allowed to introduce a discontinuity at this particular epoch, thereby compensating for the receiver clock event at 17:10 of day 098. As a result, only six hours of the entire time transfer series are affected by the event whereas the clock hand-over methods needs several days to recover. This demonstrates that the smoothest time transfer solution, i.e. with the smallest Allan deviations, see Fig. 7.3, is not necessarily the most accurate solution.

The example of Fig. 7.6 shows that the ambiguity stacking method is superior to the clock hand-over method when it comes to confine the propagation of errors caused by model or preprocessing problems. This is due to the fact that in the clock hand-over method all parameters are concatenated without imposing further conditions whereas in the ambiguity stacking method statistical checks are performed. The price to pay is an implementation in the software which is much more complex. In addition more parameters have to be managed for the connection of the daily independent

solutions. The benefit is a higher flexibility in the analysis which makes possible steps in the direction of real-time analysis such as switching from daily solutions to subdaily solutions.

For all three solutions the discontinuity in Fig. 7.6 should be located at 17:10 of day 098 when the inconsistency event took place — and not at midnight as found by the daily independent solution and by for the continuous solution generated with ambiguity stacking. Because of the small magnitude of the event it was not detected during the preprocessing. This affects not only the continuous geodetic time transfer solutions but also the daily independently generated results.

For any event that was identified in the preprocessing the phase ambiguities for all satellites are interrupted and the discontinuity in the resulting time transfer series appears at the correct epoch. If this epoch is close to midnight (e.g., within one hour) the uncertainty of the time transfer solution may be increased because only a short time interval is connected by phase ambiguities (see Sect. 7.2). Adding the data of the subsequent day in a continuous geodetic time transfer solution reduces this problem because the time interval connected by phase ambiguities can be increased.

If the preprocessing algorithms can be improved in order to identify all receiver clock events (even such small events as in the example of Fig. 7.6) the continuous geodetic time transfer solutions from the clock hand-over as well as from the ambiguity stacking method will become identical. In addition, for daily independent solutions the day boundary discontinuities will not indicate such events by an abnormal magnitude anymore.

## 7.5 Summary and Conclusions

Two methods to overcome the day boundary discontinuities of the GPS CP time and frequency transfer are presented in this paper. Both methods are implemented in the Bernese GPS Software and extensively tested with real data.

*The clock hand-over method* uses the observations from midnight to midnight of each day to assure that one epoch is common to two consecutive days. The clock solution of the day currently processed is connected to the results from the previous day using the clock parameters at midnight. The procedure is easy to understand and easy to use. The number of parameters necessary for the concatenation is limited to one per station clock and per satellite clock. The disadvantages are that observations of the midnight epoch must be available and that modeling and preprocessing problems may affect the solution of several days.

*The ambiguity stacking method* reconnects the ambiguity parameters at the day boundaries that are cut due to the daily independent data analysis scheme. This is done on normal equation level. The procedure may be applied to generate multi-day solutions as well as to obtain the results closer to real-time if time intervals shorter than one day are analyzed in each processing step. The disadvantage of the method is that a huge number of ambiguity parameters have to be managed for connecting the daily

independent solutions on normal equation level and that for each ambiguity stacking step a check for cycle slips has to be performed. The benefit from this implementation effort is that the continuity is not depending on the availability of one single epoch and that the propagation of modeling and preprocessing problems through the solution is limited by applying the statistical test necessary to detect potential cycle slips between the consecutive normal equations. In addition, this implementation allows to compute a continuous frequency transfer solution over several days (or even longer) without using the code data at all.

Both methods improve the short term ( $\tau < 8$  days) stability of the frequency transfer as compared to the daily independent solutions. Over longer averaging intervals the frequency stability of all methods is the same.

Independently from the method applied to generate a continuous time transfer series the check of the consistency of the two observation types (code and phase measurements) that have to be analyzed together for time transfer is an important issue. Unfortunately this consistency may be disturbed by what we have defined as internal receiver clock events. After such an event the code and phase data no longer refer to the same internal receiver clock. This effect may be compensated by the introduction of new ambiguity parameters for all satellites at the epoch at the epoch of the inconsistency event. It is necessary to detect such events in the preprocessing of the data to make the results reliable. The continuous solutions with one of the described methods help also to detect such events that took place close to a boundary of the time interval analyzed together in one processing step (e.g., midnight for a daily processing scheme).

## Acknowledgment

The AIUB hosts the Center for Orbit Determination in Europe (CODE), which is a collaboration between the Astronomical Institute of the University of Bern (AIUB), the Federal Office of Topography (Swisstopo, Switzerland), the Federal Agency for Cartography and Geodesy (BKG, Germany), and the Institut Géographique National (IGN, France). The results presented in this paper benefit from the work of the IGS analysis centre CODE.

## 7.6 References

- Bruyninx, C. and P. Defraigne (1999). Frequency Transfer Using GPS Code and Phases: Short- and Long-Term Stability. In *Proceedings 31<sup>st</sup> Precise Time and Time Interval (PTTI) Systems and Applications Meeting*, Dana Point, California, December 7–9, 1999.
- Dach, R., T. Schildknecht, T. Springer, G. Duddle, and L. Prost (2002). Continuous Time Transfer Using GPS Carrier Phase. *IEEE Transactions on Ultrasonics, Ferroelectrics, and Frequency Control*, 49(11):1480–1490, DOI 10.1109/TUFFC.2002.1049729.

- Dach, R., G. Beutler, U. Hugentobler, S. Schaer, T. Schildknecht, T. Springer, G. Duddle, and L. Prost (2003). Time transfer using GPS carrier phase: error propagation and results. *Journal of Geodesy*, 77(1–2):1–14, DOI 10.1007/s00190-002-0296-z.
- Dach, R., G. Duddle, T. Schildknecht, and U. Hugentobler (2004). Status Report of the AIUB–METAS Geodetic Time Transfer. In *Proceedings 18<sup>th</sup> European Frequency and Time Forum (EFTF)*, Guildford, United Kingdom, April 4–7, 2004.
- Duddle, G., F. Overney, L. Prost, T. Schildknecht, and T. Springer, (1998). First Results on a Transatlantic Time and Frequency Transfer by GPS Carrier Phase. In *Proceedings 30<sup>th</sup> Precise Time and Time Interval (PTTI) Systems and Applications Meeting*, Reston, Virginia, December 1–3, 1998.
- Hugentobler, U., M. Meindl, G. Beutler, H. Bock, R. Dach, A. Jäggi, C. Urschl, L. Mervart, M. Rothacher, S. Schaer, E. Brockmann, D. Ineichen, A. Wiget, U. Wild, G. Weber, H. Habrich, and C. Boucher (2008). CODE IGS Analysis Center Technical Report 2003/2004. In Gowey, K., R. Neilan, and A. Moore, editors, *IGS 2003–2004 Technical Reports*, Jet Propulsion Laboratory, Pasadena, California, USA, pp. 40–50, IGS Central Bureau. URL [http://www.igs.org/igscb/resource/pubs/2003-2004\\_IGS\\_Annual\\_Report.pdf](http://www.igs.org/igscb/resource/pubs/2003-2004_IGS_Annual_Report.pdf).
- Hugentobler, U., S. Schaer, and P. Fridez (editors, 2001). *Bernese GPS Software, Version 4.2*. User Manual, Astronomical Institute, University of Bern, Switzerland.
- Joyet, A., G. Miletì, P. Thomann, and G. Duddle, (2002). Continuous Fountain Cs Standard: Stability and Accuracy Issues. In Gill, P., editor, *Proc. 6th Symposium on Frequency Standards and Metrology*, pp. 273–280.
- Koch, K.R. (1988). *Parameter estimation and hypothesis testing in linear models*. Springer, Berlin Heidelberg New York, ISBN: 978-3-540-65257-1.
- Larson, K., J. Levine, L. Nelson, and T. Parker (2000). newblockAssessment of GPS Carrier–Phase Stability for Time–Transfer Applications, *IEEE Transactions on Ultrasonics, Ferroelectrics, and Frequency Control*, 47(2):484–494, DOI 10.1109/58.827441.
- Melbourne, W. G. (1985). The Case for Ranging in GPS Based Geodetic Systems. In , Goad, C., editor, *Proceedings 1st International Symposium on Precise Positioning with the Global Positioning System*, pp.373–386, U.S. Department of Commerce, Rockville, Maryland.
- Petit, G., Z. Jiang, J. White, R. Beard, and E. Powers, (2001). Absolute Calibration of an Ashtech Z12–T GPS receiver. *GPS Solutions*, 4(4):41–46, DOI 10.1007/PL00012865.
- Ray, J. (2000). The IGS/BIPM time and frequency pilot project. In *the IGS 2000 Annual Report*, Pasadena, CA: Jet Propulsion Laboratory, pp. 28–30.
- Ray, J. and K. Senior (2003). IGS/BIPM pilot project: GPS carrier phase for time/frequency transfer and timescale formation. *Metrologica*, 40:270–288.

- Schildknecht, T., G. Beutler, W. Gurtner, and M. Rothacher (1990). Towards Sub-nanosecond GPS Time Transfer using Geodetic Processing Techniques. In *Proceedings of the 4<sup>th</sup> European Frequency and Time Forum (EFTF)*, Neuchâtel, Switzerland, pp. 335–346, 1990.
- Seeber, G. (1993). *Satellite Geodesy – Foundations, Methods, and Applications*. Walter de Gruyter, Berlin New York, ISBN 3-11-017549-5.
- Senior, K., E. Powers, and D. Matsakis (1999). Attenuating Day-Boundary Discontinuities in GPS Carrier-Phase Time Transfer. In *Proceedings 31<sup>st</sup> Precise Time and Time Interval (PTTI) Systems and Applications Meeting*, Dana Point, California, December 7–9, 1999
- Senior, K., G. Petit, and J. Ray (2004). Comparison of instrumental and empirical station timing biases for a set of Ashtech Z12T GPS receivers. In *Proceedings 18<sup>th</sup> European Frequency and Time Forum (EFTF)*, Guildford, United Kingdom, April 4–7, 2004.
- Wu, J. T., C. Wu, G. A. Hajj, W. I. Bertiger, and S. M. Lichten (1993). Effects of antenna orientation on GPS carrier phase. *Manuscripta Geodaetica*, 18:91–98.
- Wübbena, G. (1985). Software Developments for Geodetic Positioning with GPS Using TI 4100 Code and Carrier Measurements. In Goas, C., editor, *Proceedings 1st International Symposium on Precise Positioning with the Global Positioning System*, pp. 403–412, U.S. Department of Commerce, Rockville, Maryland.